MATERIALS CHEMISTRY FRONTIERS

REVIEW

View Article Online
View Journal | View Issue

Cite this: *Mater. Chem. Front.*, 2023, **7**, 5693

Recent progress in metal–organic frameworks for the separation of gaseous hydrocarbons

Jing-Hong Li, Jun-Xian Chen, Rui-Biao Lin * and Xiao-Ming Chen *

Received 23rd April 2023,
Accepted 21st August 2023

DOI: 10.1039/d3qm00430a

rsc.li/frontiers-materials

The separation of gaseous hydrocarbons is involved in many important industrial processes for manufacturing chemicals, polymers, plastics, and fuels, and is performed through cryogenic distillation, which is heavily energy-intensive. Adsorption-based gas separation technology by using adsorbent materials can potentially fulfill a much energy-efficient gas separation. As a new generation of adsorbent materials, metal–organic frameworks (MOFs) have been demonstrated to have great potential in addressing important gas separations of hydrocarbons. In this review, we outline the uniqueness of MOF adsorbents for their separation application for gaseous hydrocarbons. A variety of microporous MOFs have been developed for separating gaseous hydrocarbons, which have been achieved by fine-tuning their pore sizes for high molecular sieving effects and/or immobilizing binding sites on their pore surfaces for their specific recognition of small molecules. Herein, we highlight recent important progress in this very important topic, focusing on the purification of ethylene, propylene, and butadiene.

1. Introduction

Gaseous hydrocarbons involve not only essential fuels for modern society but also are applied as important feedstocks in the chemical industry. Hydrocarbons usually are volatile, invisible, and flammable, and tend to be highly dispersed, easily contain mixtures of low concentration, and thus are difficult to handle. The separation and purification of hydrocarbons are critical industrial chemical processes to produce bulk commodities for fuels, polymers, and plastics. Some of these separation processes are carried out on a very large industrial scale. For example, olefin/paraffin separation produces light olefins of over 200 million tonnes.[1] The huge markets of hydrocarbon products make a large contribution (thousands of billions of US dollars) to the annual revenues of the oil and gas industry. Most of the industrial separations of hydrocarbons traditionally rely on thermal-driven technologies, mainly fractional distillation involving numerous evaporation–condensation cycles, which are a high energy-intensity process. In particular, to separate mixed hydrocarbons of similar volatilities for high purity, relevant industrial processes are operated in complicated facilities and under harsh conditions. For the separation and purification of industrial commodities, it is believed that energy-intensive processes, such as distillation consume 10–15% of the world's energy production. Adsorptive separation based on porous adsorbents is a promising technology to lower relevant separation

Key Laboratory of Bioinorganic and Synthetic Chemistry of Ministry of Education, School of Chemistry, IGCME, Sun Yat-Sen University, Guangzhou 510275, China. E-mail: linruibiao@mail.sysu.edu.cn, cxm@mail.sysu.edu.cn

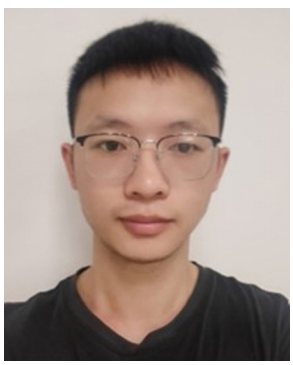

Jing-Hong Li

Jing-Hong Li obtained his BS degree from Gannan Normal University in 2017, and MS from Shantou University in 2020. Currently, he is a PhD scholar in Sun Yat-sen University. His main interests includes the design and fabrication of porous coordination polymers (PCPs), hydrogen-bonded organic frameworks (HOFs), and their functions.

Jun-Xian Chen

Jun-Xian Chen obtained her BS degree in Chemical Engineering and Technology from Sun Yat-sen University in 2021. She is currently a PhD scholar in Chemistry in Sun Yat-sen University under the supervision of Prof. Xiao-Ming Chen. Her current research interest includes the design and fabrication of functional porous coordination polymers for gas separation.

energy use. For example, alternative technologies, such as adsorptive separation and/or membrane-based technologies, can be up to 10 times more energy-efficient than the traditional distillation methods, which have not been fully realized.[1] These nonthermal technologies can separate hydrocarbon molecules according to their chemical affinities or sizes rather than differences in boiling points, and thus can be carried out under mild conditions, hence greatly reducing the energy inputs.[2] The core of these candidate technologies is the separation performance of solid porous media or permeable membranes, which are often made of porous materials with nanosized voids and desired internal pore features.

Metal–organic frameworks (MOFs, also known as porous coordination polymers) are an emerging type of crystalline porous solids, which are assembled by metal-containing nodes and organic linkers or struts through coordination bonds to have pore space. MOFs are unique owing to their exceptional porosity, diverse structures, tunable pore size, and ease of functionality.[3–6] After two decades of intensive practices, MOF materials are well demonstrated for their exceptional capability for pore adjustment and interior modification. Today, about 100 000 of MOFs have been synthesized. MOFs can show ultrahigh porosity with the largest pore surface area of over 7000 $m^2\ g^{-1}$, or with pore sizes ranging from 3 to 100 Å, the highest thermal stability of over 600 °C, or exceptional chemical stability in concentrated acidic/basic solutions.[3,7,8] The high modularity of MOFs enables us to construct their isostructural analogues of different pore sizes/shapes and surfaces (such as functional organic groups, metal open sites, *etc.*) with the same coordination networks. The key design element for MOFs is thus to functionalize their pore surface with binding sites and/or adjust their pore size/shape for molecular separation. In this context, MOFs have shown great promise that is superior to conventional porous materials (activated carbon and zeolites) in addressing important separations of gaseous hydrocarbons.[9–19]

For separation processes in physical adsorbents, their separation mechanism can be roughly categorized into either equilibrium or non-equilibrium adsorption. Equilibrium adsorption processes are thermodynamic and are mainly driven by binding affinity differences dominated by those functional sites (*i.e.*, binding sites) through supramolecular interactions. Pore functionalization with strong binding sites can significantly boost such type of separation performance. For non-equilibrium adsorption processes,[20] including kinetic separation and molecular sieving, the separation is achieved by differing the diffusivity, which is highly affected by the pore sizes and flexibility of adsorbents. The kinetic separation can be amplified after narrowing the pores of adsorbents. There are also cases that the separation is achieved by a combination of both thermodynamic and kinetic processes. In addition, there are gas separation processes that are usually performed with the collaboration of framework flexibility and structural transformation, namely, gate-opening or pore opening. Considering all aspects, it is very important to systematically control the pore size, pore surface and even the flexibility of adsorbents.

On the other hand, hydrocarbons are composed of the same elements with different carbon bonds and carbon/hydrogen ratios. Their physical properties and even chemical properties can be very similar (Table 1). The adsorptive separation by differing their molecular shapes or adsorption affinities in physical adsorbents is thus required to perform with high accuracy, which can be achieved by MOFs.[13] For example, compared with the mixture counterpart propane, propylene, as one major petrochemical product, differs by just two hydrogen atoms, and there is around a 5 K difference in their boiling points. It has been demonstrated that MOFs with embedded binding sites (ranging from open metal sites to polar functional groups, such as anionic fluoride, hydroxyl and amino) can effectively separate olefins/paraffins owing to the difference in thermodynamic affinity. Another applicable approach is to adjust the pore sizes of MOFs

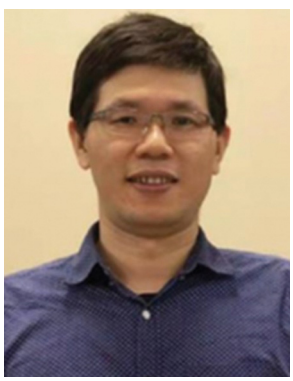

Rui-Biao Lin

Rui-Biao Lin obtained his BSc in Chemistry from Sun Yat-Sen University (SYSU) in 2009. He obtained his PhD in 2014 (SYSU). During 2016–2020, he worked at the University of Texas at San Antonio as a postdoctoral fellow. Since 2021, he has been working as a full professor in SYSU, where he is working on multifunctional porous materials, including metal–organic frameworks and hydrogen-bonded organic frameworks.

Xiao-Ming Chen

Xiao-Ming Chen received his BS (1983) and MS (1986) degrees from Sun Yat-Sen University and PhD from the Chinese University of Hong Kong in 1992. He is an Academician of the Chinese Academy of Sciences, and Academician of The World Academy of Sciences for the advancement of science in developing countries (TWAS). He is a professor in the School of Chemistry at Sun Yat-Sen University and director of the Institute of Green Chemistry and Molecular Engineering. His current research interest includes the design, synthesis, and crystal engineering of functional metal–organic/hybrid materials, including coordination polymers, metal–organic frameworks, and their applications (such as adsorption/separation, catalysis, and electric/magnetic properties).

Table 1 Physical parameters of selected gas and vapor hydrocarbons[12]

Adsorbate	Normal boiling point/K	Density/g L^{-1} (101.325 kPa, 273.15 K)	Kinetic diameter/Å	Polarizability × 10^{25}/cm^3	Dipole moment × 10^{18}/esu cm	Quadruple moment × 10^{26}/esu cm^2
CH_4	111.66	0.717	3.758	25.93	0	0
C_2H_4	169.42	1.261	4.163	42.52	0	1.50
C_2H_6	184.55	1.355	4.443	44.3–44.7	0	0.65
C_2H_2	188.40	—	3.3	33.3–39.3	0	—
C_3H_6	225.46	1.914	4.678	62.6	0.366	—
C_3H_8	231.02	2.011	4.3–5.118	62.9–63.7	0.084	—
c-C_3H_6	240.34	1.920	4.23–4.807	56.6	0	—
i-C_4H_{10}	261.34	2.689	5.278	81.4–82.9	0.132	—
i-Butene	266.25	—	4.84	8.14–8.29	—	—
1-Butene	266.92	—	4.5	79.7–85.2	0.359–0.438	—
1,3-Butadiene	268.62	—	5.2	86.4	0	—
n-C_4H_{10}	272.66	2.704	4.687	82.0	0.05	—
trans-2-Butene	274.03	—	—	84.9	0	—
cis-2-Butene	276.87	—	4.23	—	0.253	—
neo-C_5H_{12} (2,2-dimethylpropane)	282.65	2.334 (70.922 kPa)	6.2–6.464	102.0	0	—
i-C_5H_{12}	300.99	1.120 (34.543 kPa)	5.0	—	0.13	—
n-C_5H_{12}	309.22	0.789 (24.455 kPa)	4.5	99.9	0	—
neo-C_6H_{14} (2,2-dimethylbutane)	322.87	—	6.2	—	—	—
i-C_6H_{14} (2-methylpentane)	333.40	0.343 (8.960 kPa)	5.5	—	0.1	—
3-Methylpentane	336.40	—	5.5	—	—	—
n-C_6H_{14}	341.88	0.231 (6.041 kPa)	4.3	119	0	—
C_6H_6	353.24	0.403[a] (12.695 kPa)	5.349–5.85	100–107.4	0	—
c-C_6H_{12} (cyclohexane)	353.93	0.446[a] (13.019 kPa)	6.0–6.182	108.7–110	0	—
n-C_7H_{16}	371.57	0.067 (15.250 kPa)	4.3	136.1	0	—
i-C_8H_{18} (2,2,4-trimethylpentane)	372.39	—	6.2	154.4	0	—
Toluene	383.79	0.037 (0.906 kPa)	5.25	118–123	0.375	—
Ethylbenzene	409.36	—	5.8	142	0.59	—
p-Xylene	411.53	—	5.8	137–149	0.1	—
m-Xylene	412.34	—	6.8	142	0.37	—
o-Xylene	417.59	—	6.8	141–149	0.640	—

[a] Density at 298.15 K.

for size-matching of gas molecules, which is expected to enhance kinetic separation or sieving effect and finally achieve high selectivity. If the pore aperture size of adsorbents is right between the molecular sizes of different gas components, an adsorption cut-off happens along with the inaccessibility of internal pore space to certain gas components, thus leading to molecular sieving. For some MOFs, the adjustment of pore size in MOFs can be done up to a precision level of 0.1 Å.[13] Given that most hydrocarbon gases have their molecular sizes or kinetic diameters between 3 and 5 Å, microporous MOFs with comparable pore sizes have been intensively investigated for separating hydrocarbon mixtures. Usually, MOFs with large pores can show high sorption capacity but low separation selectivity for gas, whereas the ultramicroporous ones can exhibit high selectivity but low sorption capacity (termed sorption capacity *versus* selectivity trade off). By simultaneously tuning the pore size and incorporating binding sites, the internal pore space of MOFs can integrate molecular shape matching and preferential binding toward the targeted gas molecules, which is expected to address the trade-off for exceptional separation performance. The complicated effects of MOF flexibility for separation of hydrocarbons have also been noted.[21]

By virtue of pore structural and chemical control of MOF materials, namely, tuning pore size, incorporating functional sites, or their combination, significant progress has been made for gaseous hydrocarbon separation. This review focuses on the research progress of MOF materials for separation of gaseous hydrocarbons in about recent five years. In particular, we summarize representative MOF materials with unique pores and functional sites for C_2H_2 and CO_2 separation, C_2H_2/C_2H_4 separation, C_2H_4 and C_2H_6 separation, C_3H_4/C_3H_6 separation, C_3H_6/C_3H_8 separation, and purification of butadiene, xylenes and other volatile gaseous hydrocarbons.

2. Pore structure control of MOFs for separating gaseous hydrocarbons

The separation performance of adsorbents towards target molecules can be affected by various factors, mainly dominated by the adsorbent–adsorbate and adsorbate–adsorbate interactions in the pore space. The adsorbent–adsorbate interactions for specific gases can be adjusted by controlling the pore chemistry and pore size of porous materials for optimal binding affinity, whereas adsorbate–adsorbate interactions are dependent on the physical properties of gas molecules including molecular polarity or polarizability, sizes and shapes. Therefore, rationally tuning the pore sizes of MOFs and/or functionalizing their pore surface have been demonstrated as efficient approaches to boost the separation performance for gases. Both adsorbent–adsorbate and

adsorbate–adsorbate intermolecular interactions for larger or heavier molecules with high polarizability are usually superior to those for small, light and non-polar ones, due to more supramolecular interactions (ranging from hydrogen bonding to electrostatic interactions and van der Waals forces). In this section, representative examples of MOFs for hydrocarbon separation were presented according to the sequence of the polarizability and boiling points of various gases (Table 2).

2.1. Methane purification

Natural gas is a cleanest fossil fuel and has been widely used due to its natural abundance and high energy intensity, and is usually contaminated with gas impurities such carbon dioxide (CO_2) and nitrogen (N_2). The upgrading of natural gas involves the purification of methane (CH_4). Coal-bed methane (CBM) is an excellent complement to conventional natural gas; the recovery of CH_4 from it can also reduce the emission of the greenhouse gas CH_4 from CBM as well as enhance the safety of coal mineral.[22]

Ma *et al.* used an alkyl MOF, Cu_2(ATC) (ATC-Cu, H_4ATC = 1,3,5,7-adamantane tetracarboxylic acid), as a methane nanotrap that features oppositely adjacent open metal sites (OMSs) and dense alkyl groups for capturing methane molecules.[23] At 1 bar and 298 K, this MOF exhibits the highest methane uptake capacity (2.90 mmol g^{-1}) among reported MOFs, showing a high CH_4/N_2 selectivity of 9.7 for an equimolar mixture under ambient conditions. ATC-Cu thus shows promising potential for capturing methane from CBM with low content of methane (<30%). Structural and computational modelling indicated that pairs of open Cu sites with a Cu···Cu distance of 4.43 Å between two neighboring Cu paddlewheels afford considerable dual Coulombic interactions and act as strong binding sites for methane molecules. Also, there are cavities with an aliphatic surface that can serve as the second binding sites for CH_4, with an average interaction distance of *ca.* 3.5 Å.

Yang *et al.* studied four nickel-based coordination networks with functional sites (–NH_2) or varied pore sizes for the separation of CH_4/N_2, which supports that the pore size and chemical environment of adsorbents play an important role during methane purification.[24] Among those four MOFs, Ni(ina)$_2$ showed the highest CH_4/N_2 selectivity (15.8) with an adsorption capacity of 1.82 mmol g^{-1} under ambient conditions. Ni(ina)$_2$ shows good thermal and moisture stability as well, which can be easily scaled up at a low cost.

The influence of humidity on the separation performances of MOFs for CH_4 separation has been noticed. Li *et al.* investigated a series of isostructural MOFs, [Zn_2(1,4-NDC)$_2$(DABCO)], [Zn_2(ADC)$_2$(DABCO)], [Ni_2(ADC)$_2$(DABCO)], and [Cu_2(ADC)$_2$(DABCO)] (namely, DMOF-N, DMOF-A_1, DMOF-A_2, DMOF-A_3, respectively, $H_2$1,4-NDC = 1,4-naphthalenedicarboxylic acid, H_2ADC = 9,10-anthracene dicarboxylic acid, and DABCO = 1,4-diazabicyclo[2.2.2]octane), for CH_4 purification.[25] Altering their aromatic moieties and/or metal centers results in varied pore sizes, hydrophobicity and stability. The hydrophobic pore space suppressed the water sorption and enhanced the moisture resistance of those MOFs, which show high CH_4 uptakes and CH_4/N_2 selectivity. Breakthrough experiments for the CH_4/N_2 mixture under humid conditions indicated that their CH_4/N_2 separation performance can be retained even under high humidity (40% RH).[26]

Zhang *et al.* reported two isostructural flexible metal-azolate frameworks (abbreviated as MAFs, a subclass of MOFs with azolate ligands[19]) [$Zn_3(OH)_2$(pzdc)(tz)]·DMA and [$Zn_3(OH)_2$-(pzdc)(atz)]·DMA (MAF-91·DMA and MAF-92·DMA, respectively, H_3pzdc = 3,5-pyrazoledicarboxylic acid, Htz = 1,2,4-triazole, and Hatz = 3-amino-1,2,4-triazole), which possess quasi-discrete pores with analogous sizes (MAF-91·DMA: 3.6 × 2.4 and 4.0 × 2.1 Å^2, and MAF-92·DMA: 3.7 × 1.3 and 4.0 × 2.1 Å^2).[27] Due to the stronger intra-framework hydrogen-bonding interaction in MAF-92, there is a higher gating energy than MAF-91. Thus, MAF-92 showed tremendous shrinkage of apertures (1.0 × 0.8 and 2.5 × 1.0 Å^2) after guest removal, while those in MAF-91 (3.5 × 2.2 and 4.4 × 2.0 Å^2) showed negligible changes (Fig. 1). Single-component gas adsorption revealed that MAF-92 can adsorb a large amount of CO_2 (2.1 mmol g^{-1} at 273 K and 1 bar), but completely excludes N_2 and CH_4. The molecular sieving performance was further confirmed by breakthrough experiments for CO_2/N_2 and CO_2/CH_4, giving selectivities of >1500. This work revealed that the controlled gated barrier can be expected to achieve definite and ideal molecular sieve effect. In contrast, the very commonly encountered framework flexibility of MOFs could be an important drawback to size-dependent molecular sieving for separation of similar molecules.

2.2. C_2H_4 and C_2H_6 separation

Ethylene (C_2H_4) is one of the most important chemical raw materials, which is widely used in the production of plastics, rubber, coatings, and other chemical products. It is mainly produced by cracking ethane (C_2H_6) or naphtha; thus, C_2H_6 is a major impurity in the raw mixture. However, the separation of C_2H_4 from the C_2H_4/C_2H_6 mixture is highly challenging due to their small molecular size difference (<0.5 Å) and boiling point difference (*ca.* 15 K). MOFs have been reported to exhibit significant progress in the separation of C_2H_4/C_2H_6.[28–41]

Usually, the introduction of OMSs on the pore surface of MOFs enables preferential adsorption of C_2H_4 over C_2H_6.[28–33,38,41–44] For example, HKUST-1[28] and M_2(dobdc)[29–31] (M-MOF-74; M = Mg, Mn, Fe, Co, Ni, and Zn) exhibit stronger binding enthalpies for olefins than alkanes due to the metal–π interactions. Altering the charge density of the metal centers can improve the olefin adsorption and selectivity as revealed by M_2(dobdc) isomers.[33] The appropriate aperture combined with OMSs of high density can also significantly improve the bonding affinity for olefins. In 2020, Qian *et al.* reported two microporous MOFs functionalized with different amounts of carboxylate groups, in which the carboxylate groups not only can adjust the aperture size, but also chelate with copper(I) ions *via* post-synthetic modification.[41] Therefore, Cu^I@UiO-66-$(COOH)_2$ exhibits optimal apertures and exposed Cu(I) centers to form a strong binding affinity for C_2H_4, while suppressing the adsorption of C_2H_6. Compared with other UiO-66 materials, Cu^I@UiO-66-$(COOH)_2$ showed the highest ideal adsorbed solution

Table 2 Summary of representative MOFs for adsorptive separation of important gases

Materials	Gas separation	Strategies	Uptake[a] (mmol g^{-1})	Selectivity[b]	Ref.
ATC-Cu	CH_4/N_2	Incorporating adjacent open copper sites	2.9/0.75	9.7	23
$Ni(ina)_2$		Optimizing pore sizes (5.0 × 4.8 $Å^2$)	1.82/0.53	15.8	24
DMOF-A_2		Optimizing pore sizes (5.3 Å) and incorporating parallel aromatic rings	1.65/0.39	7.2	25
MAF-92	CO_2/CH_4	Optimizing pore sizes (5.0 × 4.8 $Å^2$)	2.06/0.06	1.3×10^7	27
Cu^I@UiO-66-$(COOH)_2$	C_2H_4/C_2H_6	Optimizing pore sizes (4.1 Å) and incorporating copper(I) ions onto the pore surfaces	1.9/0.9	80.8	41
UTSA-280		Optimizing pore rigidity and pore size (3.8 Å)	2.5/0.098	>10 000	35
Co-gallate		Optimizing pore size (5.2 Å)	3.37/0.31	52	36
$ZnAtzPO_4$		Optimizing pore structure (3.8 Å) and incorporating electronegative functional groups	1.92/1.04	36.6[c]/12.4[d]	39
ZU-901		Optimizing pore size (3.4 × 4.2 $Å^2$)	1.55/0.26	—	40
MAF-49	C_2H_6/C_2H_4	Incorporating multiple hydrogen-bonding acceptors and dipole repulsion groups	1.7/1.69	2.7	59
$Cu(Qc)_2$		Optimizing pore size (3.3 Å)	1.85/0.78	3.4	60
$[Fe_2(O_2)$(dobdc)]		Incorporating Fe-peroxo sites	3.29/2.6	4.4	61
SIFSIX-2-Cu-i	C_2H_2/C_2H_4	Optimizing pore size (4.4 Å) and incorporating SiF_6^{2-} sites	4.02/2.19	44.8	70
UTSA-200a		Optimizing pore size (3.4 Å) and incorporating SiF_6^{2-} sites	3.65/0.63	6320	71
UTSA-300a		Optimizing pore size (1.3 × 2.8 $Å^2$) and incorporating SiF_6^{2-} sites	3.08/0.04	27	72
NCU-100a		Optimizing pore size (1.4 × 3.0 $Å^2$) and incorporating SiF_6^{2-} sites	4.57/0.32	7291	76
UTSA-74	C_2H_2/CO_2	Incorporating open Zn sites	4.82/3.03	9	101
Cu^I@UiO-66-$(COOH)_2$		Incorporating copper(I) ions onto the pore surfaces	2.44/0.85	185	107
JNU-4		Incorporating open Cu sites	9.82/7.1	8.2	108
CPL-1-NH_2		Incorporating amine sites	1.84/0.21	119	114
CAU-10-H		Suitable pore sizes (4.7 Å)	4.01/2.68	4	115
CAU-10-NH_2		Suitable pore sizes (3.8 Å) and incorporating amine sites	3.57/2.08	10.8	116
FJU-90		Pore space partition	8.04/4.6	4.3	122
UTSA-300a		Optimizing pore size (1.3 × 2.8 $Å^2$) and incorporating SiF_6^{2-} sites	3.08/0.18	860	72
NCU-100a		Optimizing pore size (1.4 × 3.0 $Å^2$) and incorporating SiF_6^{2-} sites	4.57/0.49	1787	125
FJI-H36		Suitable pore sizes (12.9 × 12.9 $Å^2$ and 8.4 × 10.2 $Å^2$), flexible pore structure, incorporating Ni and free N atoms sites	6.46/4.20	3.5	127
SOFOUR-TEPE-Zn		Incorporating electronegative pore surfaces	3.98/0.63	16 833	97
ZUL-330		Optimizing pore size (3.3 × 3.7 $Å^2$) and incorporating SiF_6^{2-} sites	7.33/1.1	10 086	98
Cu-F-pymo	CO_2/C_2H_2	Incorporating residual guest molecules blocking the priority site for C_2H_2	2.09/0.1	$>10^5$	143
Cd-NP		Suitable pore space (6.1 × 4.5 × 4.5 $Å^3$), window size (3.2 Å) and incorporating complementary electrostatic potentials on the pore surface	2.59/0.43	85	144
Y-bptc		Incorporating large pore cage space (pore diameter: 9.46 Å), suitable pore window (4.2 Å) and μ_3-OH^- anions sites	2.48/1.17	4.1/114[c]	136
MUF-4		Suitable pore window size (2.2 Å)	3.17/—	3363[c]	139
ALF		Incorporating electropositive surface and the hydrogen-confined pore cavities with appropriate dimensional size (4.1 × 5.3 $Å^2$)	3.85/0.15	6.5×10^5	148
MAF-23-O	C_3H_6/C_3H_8	Incorporating carbonyl oxygen atoms sites	1.34/1	8.8/71[c]	149
UTSA-400		Optimizing pore sizes (3.0 Å) and incorporating $WO_2F_4^{2-}$ sites	1.84/0.05	$>10^7$	151
Y-abtc		Optimizing pore sizes (4.7 Å)	2/0.07	—	152
HIAM-301		Optimizing pore sizes (4.6 Å)	3.16/0.27	150	153
Co-gallate		Optimizing pore sizes (4.2 × 5.1 $Å^2$)	1.79/0.14	333	154
JNU-3a		Incorporating orthogonally arrayed dynamic apertures	2.62/2.14	513	155
NTU-85		Optimizing pore sizes (4.5 Å)	0.45/0.003	1570	156
ZJU-75a		Suitable pore sizes (4.1 × 4.4 $Å^2$) and incorporating high-density open Ni sites	3.31/2.33	54.2	157
PCP-IPA	C_3H_8/C_3H_6	Suitable pore sizes (4.7 × 5.6 $Å^2$) and incorporating parallel-aligned aromatic-based units	2.23/2.25	2.48	169
FDMOF-2		Optimizing pore sizes (3.0 Å) and incorporating $-CF_3$ groups	5.04/4.15	2.18	170
ELM-12	C_3H_4/C_3H_6	Suitable pore cavities (6.1 × 4.3 × 4.3 Å3 and 6.8 × 4.0 × 4.2 $Å^3$) and incorporating dynamic dangling OTf^- groups	2.79/1.45	83	181
UTSA-200		Optimizing pore size (3.4 Å) and incorporating SiF_6^{2-} sites	3.58/1.20	>20 000	182
sql-NbOFFIVE-bpe-Cu-AB		Optimizing pore size (3.96 × 5.56 $Å^2$) and incorporating $NbOF_5^{2-}$ sites	3.04/2.10	220	189
ZU-52	C_4H_6/n-C_4H_8/i-C_4H_8	Optimizing pore size (4.31 Å) and incorporating fluoroniobate sites	2.64/2.26/0.48	—	192

Table 2 (*continued*)

Materials	Gas separation	Strategies	Uptake[a] (mmol g^{-1})	Selectivity[b]	Ref.
ZU-33		Optimizing pore size (4.20 Å) and incorporating GeF_6^{2-} sites	2.67/0.57/0.42	—	
MAF-23	i-C_4H_8/*n*-C_4H_8/C_4H_{10}/C_4H_6	Incorporating flexible quasi-discrete pores	2/2/2/2	—	193
Zn-bzc-2CH_3	*n*-C_4H_{10}/i-C_4H_{10}	Optimizing pore size (4.13 Å)	2.42/0.03	—	195
Zr-abtc	*n*HEX/3MP/23DMB	Suitable pore window size (4.5 Å)	1.28/1.02/0.58	—	197
HIAM-203	*n*HEX/3MP/22DMB	Suitable pore window size (4.8 Å)	1.7/1.43/0.07	—	198
CopzNi	*n*HEX/2MP/22DMB	Incorporating open Ni sites	2.17/1.46/0.08	—	199
Mn-dhbq	*p*X/*m*X/*o*X	Incorporating multiple open Mn sites, rich π-electrons, and structural flexibility	1.74/1.48/0.22[e]	—	206
			1.33/0.16/0.21[f]		
ZU-61		Incorporating adaptable pore structure and $NbOF_5^{2-}$ sites	3.44/3.37/3.2[g]	—	207
ZUL-C3	*p*X/*m*X/*o*X/EB	Incorporating nonaromatic low-polar pore environment	3.25/3.35/3.41/3.27	—	208
MAF-41	EB/ST/Tol/Bz	Incorporating structural flexibility	2.31/0.3	—	209

[a] Uptake amount at 1 bar and room temperature. [b] Calculated by IAST at ambient temperature and 1 bar. [c] Kinetic selectivity at ambient temperature. [d] Equilibrium-kinetic combined selectivity at ambient temperature. [e] Uptake amount at 1.05 bar and 333 K. [f] Uptake amount at 1.05 bar and 393 K. [g] Uptake amount at 7.1 mbar and 333 K.

theory (IAST) selectivity of 80.8 for an equimolar C_2H_4/C_2H_6 mixture at 298 K and 1 bar.

Molecular sieves can show the maximum C_2H_4/C_2H_6 selectivity *via* molecular size exclusion, though it is quite challenging due to their similar molecular sizes. In 2018, Chen *et al.* reported a rigid ultramicroporous MOF $[Ca(C_4O_4)(H_2O)]$ (UTSA-280, $H_2C_4O_4$ = squaric acid) with one-dimensional (1D) pore channels for molecular sieving separation of C_2H_4/C_2H_6. UTSA-280, being assembled by calcium oxide chains and squarate linkers, shows 1D pores with the minimum cross-sectional area of 14.4 $Å^2$, which falls precisely between the sizes of C_2H_4 and C_2H_6 (13.7 $Å^2$ and 15.5 $Å^2$, respectively). Therefore, UTSA-280 can adsorb C_2H_4 with an adsorption capacity of 2.5 mmol g^{-1} at 298 K and 1 bar while blocking the diffusion of the relatively large C_2H_6 molecules (Fig. 2).[35] The C_2H_4/C_2H_6 selectivity of UTSA-280 was estimated to be over 10 000. The adsorption heat (Q_{st}) of UTSA-280 for C_2H_4 ranges from 20.5 to 35.0 kJ mol^{-1}, which is lower than those of MOFs with OMSs (40–85 kJ mol^{-1}).[30,45] Breakthrough experiments confirmed that high purity (>99.2%) of C_2H_4 can be obtained from an equimolar C_2H_4/C_2H_6 mixture with a productivity of 1.86 mmol g^{-1}. It is worth noting that UTSA-280 is capable of efficiently capturing C_2H_4 from a quaternary $CH_4/C_2H_4/C_2H_6/C_3H_8$ mixture (45/25/25/5). Dispersion-corrected density functional theory (DFT-D) calculations and single-crystal X-ray diffraction experiments revealed that C_2H_4 molecules are adsorbed by UTSA-280 in a linear array with weak C–H···O hydrogen bonding, π···π stacking and van der Waals (vdW) interactions.

In 2018, Ren *et al.* reported a series of gallate-based MOFs, $[M(C_7O_5H_4)\cdot 2H_2O]$ (termed M-gallates, M = Mg, Ni, and Co), for C_2H_4/C_2H_6 separation with high sieving effect.[36] These MOFs contain 3D interconnected zigzag channels and have Brunauer–Emmett–Teller (BET) surfaces of *ca.* 424 (Ni), 559 (Mg), and 475 (Co) m^2 g^{-1}. The pore sizes (3.47–3.69 Å) of these MOFs are close to the molecular sizes of C_2H_4 (3.28 × 4.18 × 4.84 $Å^3$) and C_2H_6 (3.28 × 4.18 × 4.84 $Å^3$). Therefore, M-gallates could highly selectively adsorb C_2H_4 over C_2H_6. Among them, Co-gallate displays the highest performance for separation of C_2H_4/C_2H_6. The C_2H_4 uptake capacity of Co-gallate is much higher than that for C_2H_6 (3.37 mmol g^{-1} *vs.* 0.31 mmol g^{-1}), resulting in a high IAST selectivity of 52 at 298 K and 1 bar for an equimolar C_2H_4/C_2H_6 mixture. The IAST selectivity of Mg-gallate is about 37.3 for an equimolar C_2H_4/C_2H_6 mixture at 298 K and 1 bar. Breakthrough experiments for a 50/50 C_2H_4/C_2H_6 mixture further demonstrated the excellent C_2H_4/C_2H_6 separation performances of these low-cost M-gallates.

In 2020, Xing *et al.* reported a phosphate-pillared MOF, $[Zn_3(atz)_3(PO_4)]_n$ ($ZnAtzPO_4$, Hatz = 3-amino-1,2,4-triazole), for C_2H_4/C_2H_6 separation with high selectivity (12.4 at 298 K and 32.4 at 273 K).[39] Single-component gas adsorption and kinetic studies revealed that $ZnAtzPO_4$ has a higher C_2H_4 adsorption capacity (1.92 mmol g^{-1}) than for C_2H_6 (1.04 mmol g^{-1}) at 298 K and 1 bar, as well as a faster adsorption rate for C_2H_4 compared with C_2H_6, giving a kinetic selectivity of 36.6. DFT calculations demonstrated that electronegative groups decorated on the narrow pore apertures of $ZnAtzPO_4$ can effectively capture C_2H_4 and inhibit the diffusion of C_2H_6, resulting in an

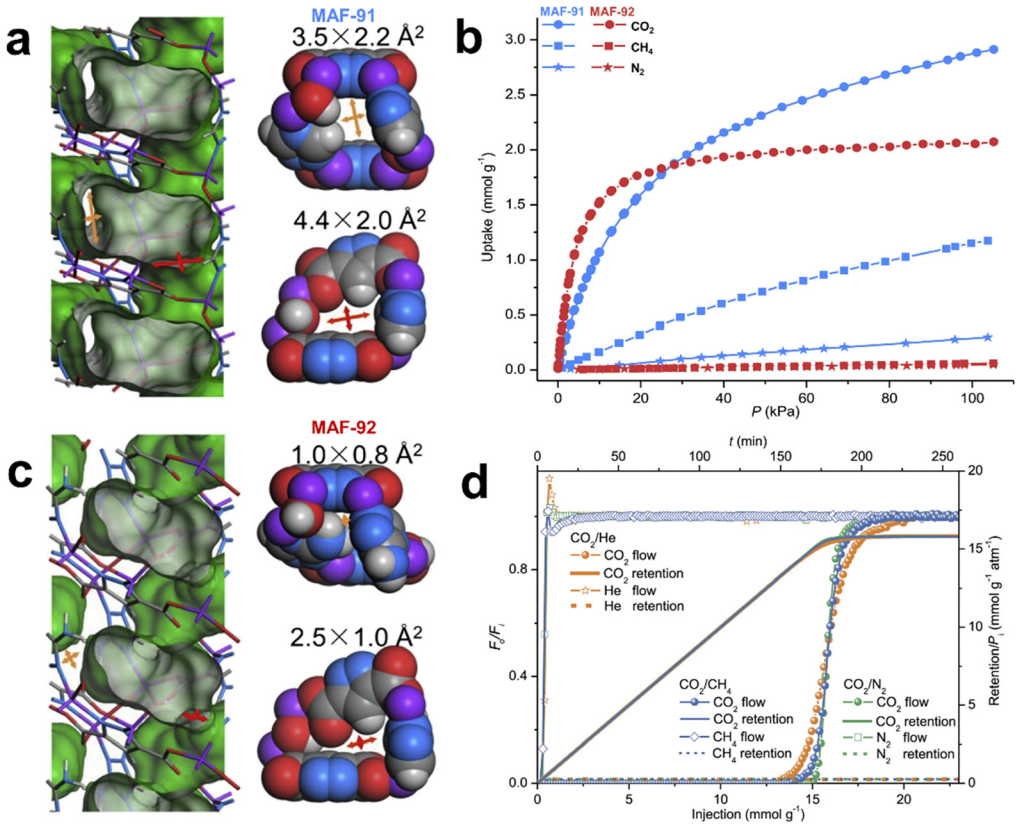

Fig. 1 (a) and (c) Crystal structures of MAF-91 and MAF-92. (b) CO_2, CH_4, and N_2 adsorption isotherms of MAF-91 and MAF-92 at 298 K. (d) Column breakthrough behaviors of MAF-92 for 10 : 90 CO_2/N_2, 10 : 90 CO_2/CH_4 and 10 : 90 CO_2/He mixtures. Reprinted with permission from ref. 27. Copyright 2021 Cell Press.

efficient equilibrium-kinetic C_2H_4/C_2H_6 separation. A flexible ultramicroporous MOF, $[Cu_2(pyz\text{-}CH_3)(pzdc)_2]$ (ZU-901, pyz-CH_3 = 2-methylpyrazine, and H_2pzdc = 2,3-pyrazinedicarboxylic acid), with a pore size of 3.4 × 4.2 Å^2 was recently reported to show a C_2H_4 adsorption–desorption curve in an *S* shape with high C_2H_4 working capacity and facile regeneration.[40] Single-component sorption experiments showed that ZU-901 can adsorb 1.55 mmol g^{-1} C_2H_4 and much less C_2H_6 (0.26 mmol g^{-1}) at 298 K and 1 bar. The adsorption selectivity of ZU-901 calculated for the pressure swing adsorption (PSA) process is 65. The Q_{st} of ZU-901 for C_2H_4 was calculated to be ~25 kJ mol^{-1}, which indicates that ZU-901 can be mildly regenerated. The simulated two-bed PSA process revealed that polymer-grade ethylene (*ca.* 99.5%) can be obtained by ZU-901 with only 1/10 of the energy consumption compared to simulating cryogenic distillation (2.03 kJ mol^{-1} *vs.* 21.84 kJ mol^{-1}).

For C_2H_4-selective MOF materials, multiple adsorption and desorption cycles are typically required to achieve high-purity ethylene. In contrast, C_2H_6-selective adsorbents can directly give pure ethylene by one single separation operation, making it simple to operate and more energy efficient. Compared to the C_2H_4 molecule, the C_2H_6 molecule has a slightly larger polarizability and two additional hydrogen atoms. MOFs with OMSs usually interact strongly with C_2H_4 molecules *via* π complexation, whereas MOFs with relatively less polar sites, usually, can preferentially adsorb C_2H_6 over C_2H_4.[46–66]

In an earlier study, Gascon *et al.* firstly reported preferential capture of C_2H_6 over C_2H_4 by utilizing the gate-opening effect of ZIF-7 (also known as MAF-3).[58] However, the separation efficiency was low due to the lack of active binding sites. In 2015, Zhang *et al.* reported a porous MAF [Zn(batz)] (MAF-49, H_2batz = bis(5-amino-1*H*-1,2,4-triazol-3-yl)methane), which shows a high C_2H_6/C_2H_4 selectivity of 9 at 316 K.[59] In MAF-49, there are quasi-discrete cages functionalized with a high density of electronegative nitrogen atoms on the surface, which are further interconnected by smaller paths into 1D channels (Fig. 3). DFT calculations and crystallographic study indicated that a C_2H_6 molecule confined in the cage can form stronger and more non-classical C–H···N hydrogen bonds or electrostatic interactions through better structural matching with the cage surface of MAF-49 as compared to the C_2H_4 molecule, which is beneficial for capture, or stronger binding of C_2H_6 compared with C_2H_4. MAF-49 showed, for the first time, an exceptional reversed selectivity compared with porous materials including MOFs, which conventionally bind more strongly with C_2H_4 *vs.* C_2H_6. Breakthrough experiments for the C_2H_4/C_2H_6 (15 : 1) mixture showed that MAF-49 can give highly pure C_2H_4 (99.95%+) within a single breakthrough operation under ambient conditions.

An appropriate combination of pore sites and pore surface can maximize the weak host–guest interactions, thus highly enhancing the performance of MOFs for C_2H_6/C_2H_4 separation.

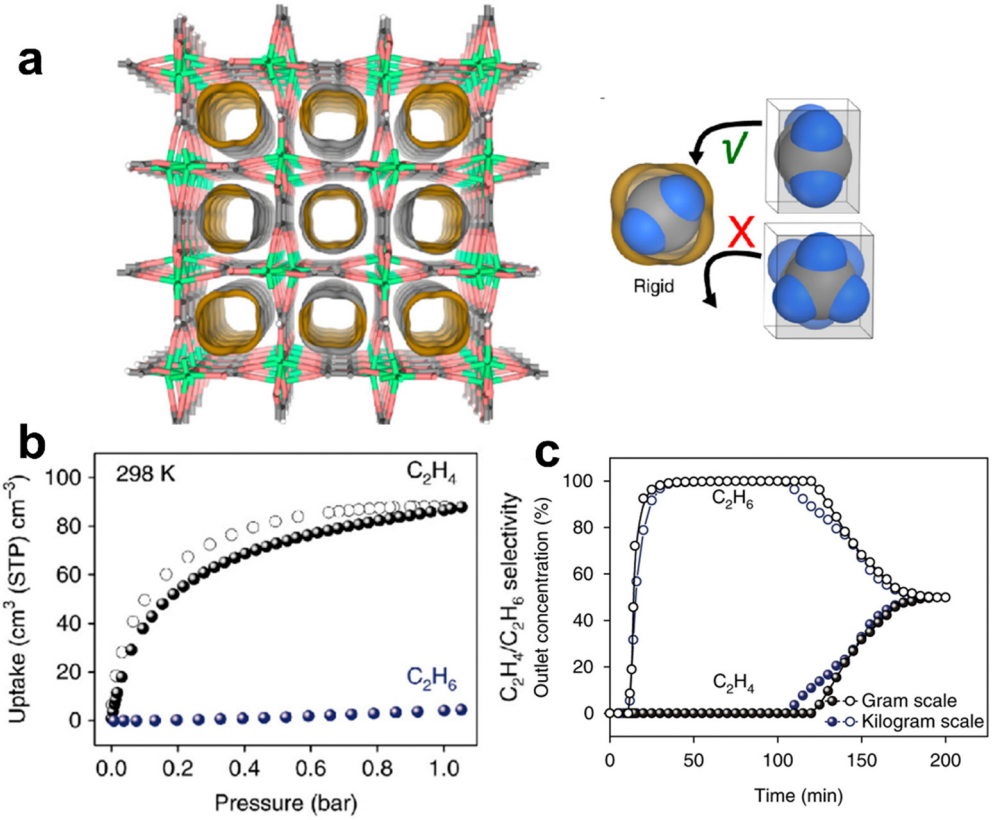

Fig. 2 (a) Structure of UTSA-280. (b) Sorption isotherms of UTSA-280 for C_2H_4 and C_2H_6 at 298 K. (c) Breakthrough curves for UTSA-280 from different scales for an equimolar mixture of C_2H_4/C_2H_6 at 298 K and 1 bar. Reprinted with permission from ref. 35. Copyright 2018 Nature Publishing Group.

In 2018, Chen *et al.* reported two isoreticular MOFs, $[Cu(Qc)_2]$ (HQc = quinoline-5-carboxylic acid) and $[Cu(ina)_2]$ (Hina = isonicotinic acid), featuring 1D channels with pore sizes of ~4.1 and ~3.3 Å, respectively, and an array of low-polarity aromatic surfaces with different contact areas on the channels (Fig. 4).[60] Single-component sorption results demonstrated that $[Cu(Qc)_2]$ shows a higher C_2H_6 uptake than C_2H_4 (60.0 cm^3 cm^{-3} *vs.* 25.3 cm^3 cm^{-3}, *i.e.*, 1.85 mmol g^{-1} *vs.* 0.78 mmol g^{-1}) at 298 K and 1 bar, thus giving a high C_2H_6/C_2H_4 selectivity of 3.4 for an equimolar C_2H_6/C_2H_4 mixture at 298 K and 1 bar. In contrast, $[Cu(ina)_2]$ shows comparable adsorption capacity for both gases (C_2H_4: 67.4 cm^3 cm^{-3}, and C_2H_6: 64.3 cm^3 cm^{-3}, *i.e.*, 1.99 mmol g^{-1} *vs.* 1.90 mmol g^{-1}) due to the smaller polar surface. Neutron powder diffraction and DFT-D calculations showed that the high C_2H_6 selectivity in $[Cu(Qc)_2]$ can be attributed to the more C–H···π interactions formed between C_2H_6 and $[Cu(Qc)_2]$. Breakthrough experiments demonstrated that high purity of C_2H_4 (> 99.9%) can be directly collected from a 50/50 C_2H_6/C_2H_4 mixture by a packed column bed of $[Cu(Qc)_2]$, with a separation productivity of 587 mmol L^{-1}.

The incorporation of the peroxo sites into MOFs can improve the affinity for C_2H_6. In 2018, Chen *et al.* reported a microporous MOF $[Fe_2(O_2)(dobdc)]$ ($dobdc^{4-}$ = 2,5-dioxido-1,4-benzenedicarboxylate) decorated with Fe–peroxo sites that exhibits a high C_2H_6 affinity with a large Q_{st} of 66.8 kJ mol^{-1} (Fig. 5).[61] Single-component sorption isotherms showed that $[Fe_2(O_2)(dobdc)]$ can adsorb a large amount of C_2H_6 (74.3 cm^3 g^{-1}, 3.32 mmol g^{-1}) at 1 bar and 298 K and the IAST selectivity for 50/50 C_2H_6/C_2H_4 was calculated to be 4.4 under the same conditions. High-resolution neutron powder diffraction showed that C_2D_6 molecules can form strong non-classical C–D···O hydrogen bonds with very short D···O distances (~2.17 to 2.22 Å). Therefore, $[Fe_2(O_2)(dobdc)]$ exhibits excellent separation performance, yielding polymer-grade C_2H_4 (≥99.99%) from 50/50 C_2H_4/C_2H_6 mixtures in a single breakthrough operation and a productivity of 0.79 mmol g^{-1}. This result further confirms the unique and important role of non-classical C–H···O hydrogen bonds in the molecular recognition and selective adsorption of ethane by MOFs.

2.3. C_2H_2/C_2H_4 separation

In the petrochemical industry, the production of C_2H_4 involves trace amounts of acetylene (C_2H_2) impurities (~1%). The removal of these impurities is crucial as even small amounts of acetylene during ethylene polymerization can cause catalyst poisoning and highly affect the production of polyethylene. Extensive research has been conducted on the adsorptive separation of MOFs for C_2H_2/C_2H_4 mixtures.[67–78] Chen *et al.* first reported a series of M'MOFs for separation of C_2H_4 from C_2H_2/C_2H_4.[67] However, these M'MOFs show modest selectivity for C_2H_2 over C_2H_4. In 2015, they further reported an amino-functionalized microporous MOF (UTSA-100) with 1D channels (4.3 Å) and small cages (4.0 Å), showing a moderately high C_2H_2 uptake of

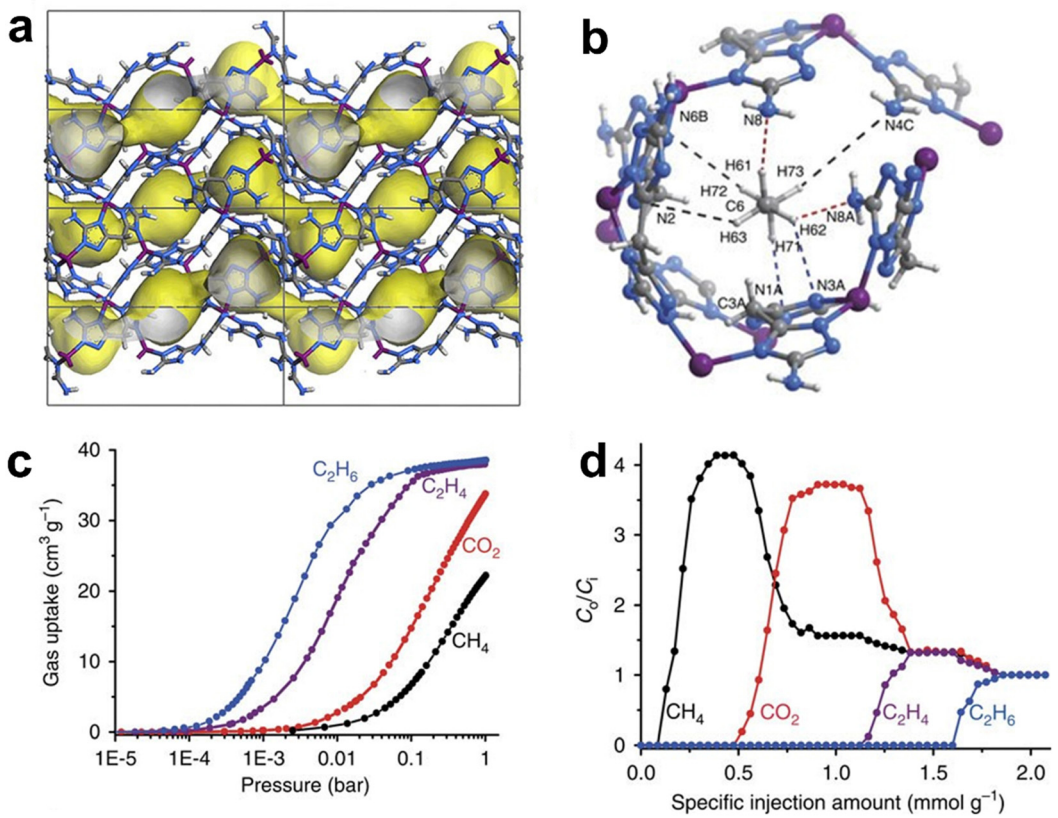

Fig. 3 (a) Crystal structure of MAF-49. (b) Preferential adsorption sites for C_2H_6 in MAF-49 revealed by DFT calculations. (c) Gas adsorption isotherms for C_2H_6, C_2H_4, CO_2 and CH_4 in MAF-49 at 316 K. (d) Breakthrough curves of the $CH_4/CO_2/C_2H_4/C_2H_6$ mixture (1 : 1 : 1 : 1 (vol)) for MAF-49 measured at 313 K and 1 bar. Reprinted with permission from ref. 59. Copyright 2018 Nature Publishing Group.

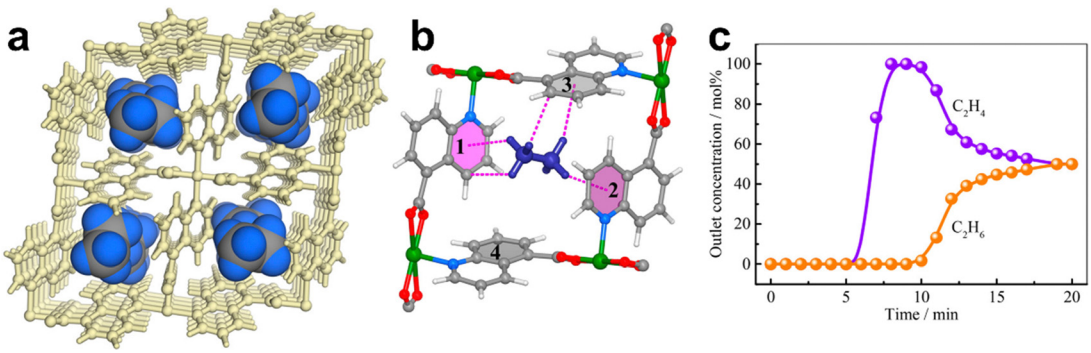

Fig. 4 (a) Neutron diffraction crystal structure of $[Cu(Qc)_2]\cdot 0.41C_2D_6$. (b) Preferential binding sites for the C_2D_6 molecule and the close vdW contacts within the rhombic cavity of aromatic rings, highlighting C–H$\cdots\pi$ interactions in pink dashed bonds. (c) Experimental column breakthrough curves for an equimolar C_2H_6/C_2H_4 mixture (298 K, 1 bar) in an adsorber bed packed with $Cu(Qc)_2$. Reprinted with permission from ref. 60. Copyright 2018 American Chemical Society.

95.6 cm^3 g^{-1} (4.27 mmol g^{-1}) at 296 K but with a much lower C_2H_4 uptake (37.2 cm^3 g^{-1}, 1.66 mmol g^{-1}). The calculated IAST selectivity of UTSA-100 for a 1/99 C_2H_2/C_2H_4 mixture is 10.7. This work well demonstrates that suitable pore sizes and binding sites can highly improve the separation performance of MOFs for removing trace C_2H_2 from C_2H_4.[68]

To obtain materials with high C_2H_2 adsorption capacity and high selectivity, in 2016, Chen *et al.* reported a series of SIFSIX MOFs, namely, SIFSIX-1-Cu, SIFSIX-2-Cu, SIFSIX-2-Cu-i, SIFSIX-3-Ni, and SIFSIX-3-Zn, which allow preferential capture of C_2H_2 from the C_2H_2/C_2H_4 mixture with high selectivity and adsorption capacity.[70] These materials possess different pore sizes, which can be systematically fine-tuned by replacing ligands, metal nodes, inorganic anions or framework interpenetration. Among them, SIFSIX-2-Cu-i with a two-fold interpenetrated framework and pore size of 5.2 × 5.2 Å^2 (BET surface area

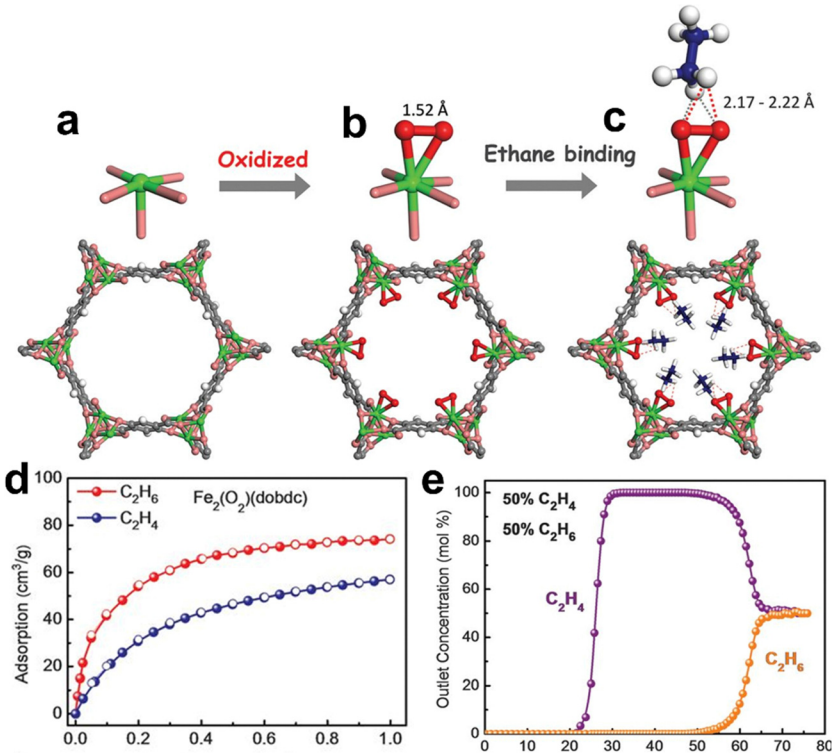

Fig. 5 Crystal structures of (a) pristine [Fe_2(dobdc)] and [$Fe_2(O_2)$(dobdc)] (b) after oxidization and (c) after final C_2D_6-loading. (d) Sorption isotherms of [$Fe_2(O_2)$(dobdc)] for C_2H_6 and C_2H_4 under ambient conditions. (e) Breakthrough curves of [$Fe_2(O_2)$(dobdc)] for an equimolar C_2H_6/C_2H_4 mixture under ambient conditions. Reprinted with permission from ref. 61. Copyright 2018 the American Association for the Advancement of Science.

503 $m^2\ g^{-1}$) exhibits a high uptake for C_2H_2 (2.1 mmol g^{-1}, *i.e.*, 47 $cm^3\ g^{-1}$) at a low pressure of 0.025 bar, indicating its strong binding affinity for C_2H_2 (Fig. 6). The IAST selectivity of SIFSIX-2-Cu-i for C_2H_2/C_2H_4 (1/99) is up to 44.54. SIFIX-2-Cu with a pore size of 8.0 × 8.0 $Å^2$ (BET surface area: 1178 $m^2\ g^{-1}$) shows the highest C_2H_2 uptake of 8.5 mmol g^{-1} and a moderate IAST selectivity for C_2H_2/C_2H_4 (1/99) of 10.6. Breakthrough experiments demonstrated that all these SIFSIX MOFs can produce polymer-grade C_2H_4 from C_2H_2/C_2H_4 (1/99 or 50/50 mixtures). DFT-D calculations and high-resolution neutron powder diffraction studies reveled that SiF_6^{2-} pillars in the framework can form strong hydrogen-bonding interactions with C_2H_2, resulting in the high selectivity and adsorption capacity for C_2H_2. This work revealed that the combination of optimal pore size and multiple active sites can greatly improve the selectivity and adsorption capacity of the MOFs.

In 2017, Chen *et al.* reported a 2-fold interpenetrated MOF SIFSIX-14-Cu-i (UTSA-200) with a smaller pore size (3.4 Å) than SIFSIX-2-Cu-i (4.4 Å) and also functional as SiF_6^{2-} sites that can enhance the binding affinity for C_2H_2 (Fig. 7).[71] The pore size of the activated structure (UTSA-200a) ideally falls between the kinetic diameter of C_2H_4 (4.2 Å) and C_2H_2 (3.3 Å), endowing UTSA-200a with a high performance of molecular sieving separation of C_2H_2/C_2H_4. Single component equilibrium adsorption isotherms showed that UTSA-200a exhibits a high low-pressure uptake (58 $cm^3\ cm^{-3}$) for C_2H_2 at 0.01 bar but a negligible uptake (~0.25 mmol g^{-1}) for C_2H_4 below 0.2 bar, which is significantly lower than the absorption of SIFSIX-2-Cu-i (2.28 mmol g^{-1}). The IAST selectivity for a 1/99 C_2H_2/C_2H_4 mixture of UTSA-200a was calculated to be 6000 at 298 K and 1 bar. High-resolution neutron powder diffraction further revealed that the strong binding affinity of UTSA-200a for the C_2D_2 molecule was achieved by short C–D···F hydrogen-bonding interactions (1.921 Å). Breakthrough experiments revealed that UTSA-200a can efficiently separate C_2H_2 from a 1/99 C_2H_2/C_2H_4 mixture to give an extremely high purity C_2H_4 (99.9999%) with a productivity of 87.5 mmol g^{-1}.

In 2017, Chen *et al.* reported an ultramicroporous SIFSIX-MOF [$Zn(dps)_2(SiF_6)$] (UTSA-300, dps = 4,4′-dipyridylsulfide) with small apertures (2.4 × 3.3 $Å^2$) for specific recognition of C_2H_2 from C_2H_4.[72] The desolvated structure UTSA-300a (aperture size: 3.3 Å) exhibits large affinity toward C_2H_2 with a Q_{st} of up to 57.6 kJ mol^{-1} and thus can be selectively gate opened by C_2H_2. It should be noted that UTSA-300 shows complete size exclusion of C_2H_4, giving IAST selectivity for the equimolar C_2H_2/C_2H_4 mixture up to $>10^4$ at 298 K. Breakthrough experiments confirmed its good separation performance for an equimolar C_2H_2/C_2H_4 mixture. Subsequently, an isostructural framework of UTSA-300 [$Cu(dps)_2(SiF_6)$] (NCU-100 or UTSA-300-Cu) was reported.[76] In contrast to UTSA-300, NCU-100 possesses elongated Cu(II)–F bonds, showing a larger cavity size (3.6 × 4.3 × 4.2 $Å^3$ *vs.* 3.5 × 3.9 × 4.1 $Å^3$) in the closed-pore phase. Single-component sorption experiments revealed that NCU-100a shows not only higher low-pressure uptake (0.73 mmol g^{-1} *vs.* 0.04 mmol g^{-1}) for C_2H_2 at 0.01 bar and 298 K but also a higher total uptake capacity (4.57 mmol g^{-1} *vs.* 3.08 mmol g^{-1}) at 298 K and 1 bar, resulting

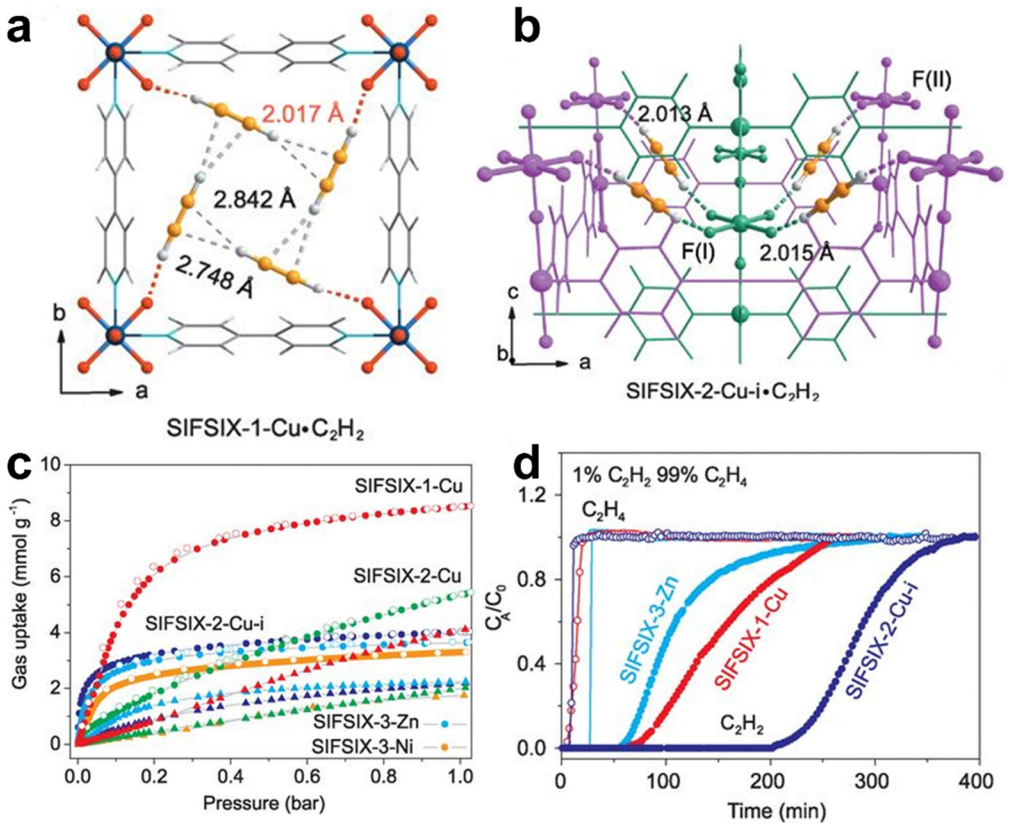

Fig. 6 (a) Crystal structure of SIFSIX-1-Cu·C_2H_2. (b) DFT-D simulated structure of C_2H_2-loaded SIFSIX-2-Cu-i. (c) Single-component sorption isotherms of SIFSIX-1-Cu, SIFSIX-2-Cu, SIFSIX-2-Cu-i, SIFSIX-3-Zn, and SIFSIX-3-Ni for C_2H_2 and C_2H_4 under ambient conditions. (d) Breakthrough curves of SIFSIX-1-Cu, SIFSIX-2-Cu, and SIFSIX-3-Zn for a 1/99 C_2H_2/C_2H_4 mixture. Reprinted with permission from ref. 70. Copyright 2016 the American Association for the Advancement of Science.

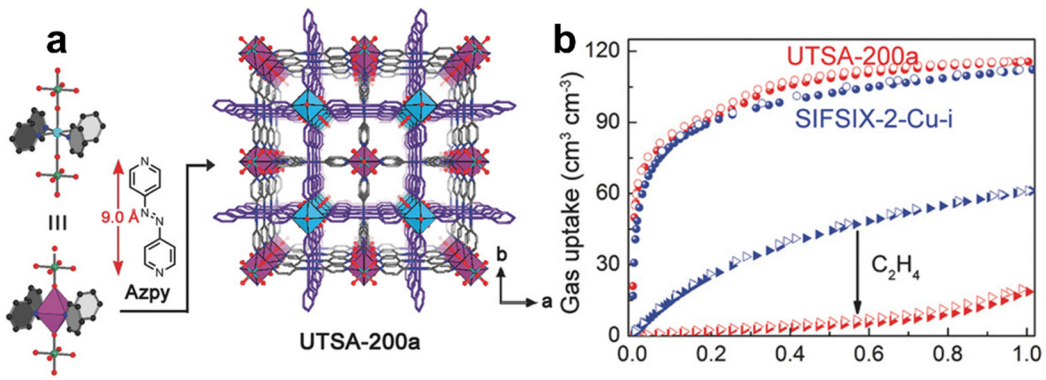

Fig. 7 (a) Crystal structure of UTSA-200. (b) C_2H_2 and C_2H_4 adsorption isotherms of UTSA-200a at 298 K. Adapted from ref. 71 with permission from Wiley-VCH, Copyright 2018.

in an IAST selectivity for 1/99 C_2H_2/C_2H_4 up to 7291 (298 K and 1 bar). This excellent performance for C_2H_2/C_2H_4 separation can also be attributed to the combination of optimal pore size and strong binding sites, as confirmed by DFT calculations and crystallographic studies. Breakthrough experiments confirmed that high purity C_2H_4 (>99.99%) can be obtained from a 1/99 C_2H_2/C_2H_4 mixture with a productivity of 14.9 mmol g^{-1}.

Recently, Zhai *et al.* synthesized a series of cluster-based MOFs, $[M_9(\mu_4\text{-TAZ})_6(\mu_3\text{-HTAZ})_x(\mu_3\text{-TAZ})_{12-x}(A)_y]$ solvent (SNNU-98-M, M = Mn, Co, Ni, and Zn), for the purification of C_2H_2, in which the tetrazolate (TAZ) ligands coordinate with metal centers in tridentate (μ_3-TAZ) and tetradentate (μ_4-TAZ) bridging modes.[78] These MOFs of **acs** topology show high framework densities and high stabilities, as well as small pore sizes of

5.2 Å (Mn), 4.8 Å (Co), 4.8 Å (Ni), and 4.2 Å (Zn), respectively, which are expected to increase the separation selectivity and volumetric storage capacity. Single-component gas adsorption revealed that SNNU-98-Mn exhibits the highest volumetric C_2H_2 uptake (222.9 cm^3 cm^{-3}) at 298 K and 1 bar, and a high uptake for C_2H_2 (175.3 cm^3 cm^{-3}) at 298 K and 0.1 bar, whereas SNNU-98-Co shows the highest C_2H_2/C_2H_4 IAST selectivity (2405.7) under room temperature and 1 bar. Column breakthrough experiments revealed that all these materials show good C_2H_2/C_2H_4 separation performance, with SNNU-98-Mn displaying a higher C_2H_4 productivity of 64.6 mmol g^{-1} from a 1/99 C_2H_2/C_2H_4 mixture and a longer breakthrough retention time (1362 min g^{-1} and 701 min g^{-1} at 273 K and 298 K, respectively, with a gas flow rate of 2 mL min^{-1}).

The separation of C_2H_4 from multicomponent mixtures in one step is significant for obtaining polymer-grade C_2H_4 due to the presence of multiple impurities in the cracking gas. Recently, more MOFs have been revealed to be capable of such multicomponent separation.[79–94] In 2018, Lu *et al.* reported the highly selective adsorption of C_2H_4 from a $C_2H_2/C_2H_4/C_2H_6$ mixture by a stable MOF, $(Me_2NH_2)[Co_3(DCPN)_2(\mu_3\text{-}OH)(H_2O)]\cdot 11H_2O$ (TJT-100, DCPN = 5-(3′,5′-dicarboxylphenyl)nicotinate).[79] TJT-100 exhibits a 1D channel (pore size: ~8.0 Å) decorated with a high density of carboxylate oxygen atoms. Single-component adsorption showed that the adsorption capacities of TJT-100 for C_2H_2, C_2H_4, and C_2H_6 were 127.7 cm^3 g^{-1}, 98.1 cm^3 g^{-1}, and 105.4 cm^3 g^{-1}, respectively. The breakthrough experimental results of TJT-100 for the $C_2H_2/C_2H_4/C_2H_6$ mixture (0.5 : 99 : 0.5) confirmed the preferential capture of C_2H_2 and C_2H_6, giving C_2H_4 with an excellent purity of 99.997%. DFT calculations revealed that C_2H_2 and C_2H_6 have multiple electrostatic interactions with the framework, which facilitates preferential adsorption of C_2H_2 and C_2H_6 by TJT-100.

In 2019, Zaworotko *et al.* reported a synergistic sorbent separation technique (SSST), which enables the one-step production of polymer-grade C_2H_4 from a ternary ($C_2H_2/C_2H_6/C_2H_4$) gas mixture, and even a quaternary ($CO_2/C_2H_2/C_2H_6/C_2H_4$) gas mixture (Fig. 8).[80] Three microporous MOFs, TIFSIX-2-Cu-I, SIFSIX-3-Ni, and Zn-atz-ipa, were placed in tandem on the sorbent bed, offering selective adsorption of C_2H_2, CO_2, and C_2H_6, respectively. Notably, Zn-atz-ipa shows a rare, higher uptake of C_2H_6 than CO_2, C_2H_2 and C_2H_4 at 0 to 0.4 bar. Breakthrough experiments showed that the packing order of the three MOFs in the sorbent bed has a significant impact on the separation performance, whereas the particle size and amount of the adsorbent have a minor effect. When the packing order is SIFSIX-3-Ni@Znatz-ipa@TIFSIX-2-Cu-i, high purity C_2H_4 can be gained from a 1/49.5/49.5 $C_2H_2/C_2H_4/C_2H_6$ or 1/33/33/33 $C_2H_2/C_2H_4/C_2H_6/CO_2$ mixture and the working capacities are 0.32 and 0.10 mmol g^{-1}, respectively. This work provides a new path for selective separation of a specific component molecule from a multicomponent gas mixture.

2.4. C_2H_2 and CO_2 separation

Acetylene (C_2H_2) is an important chemical raw material that is mainly produced by thermal cracking of hydrocarbons or the

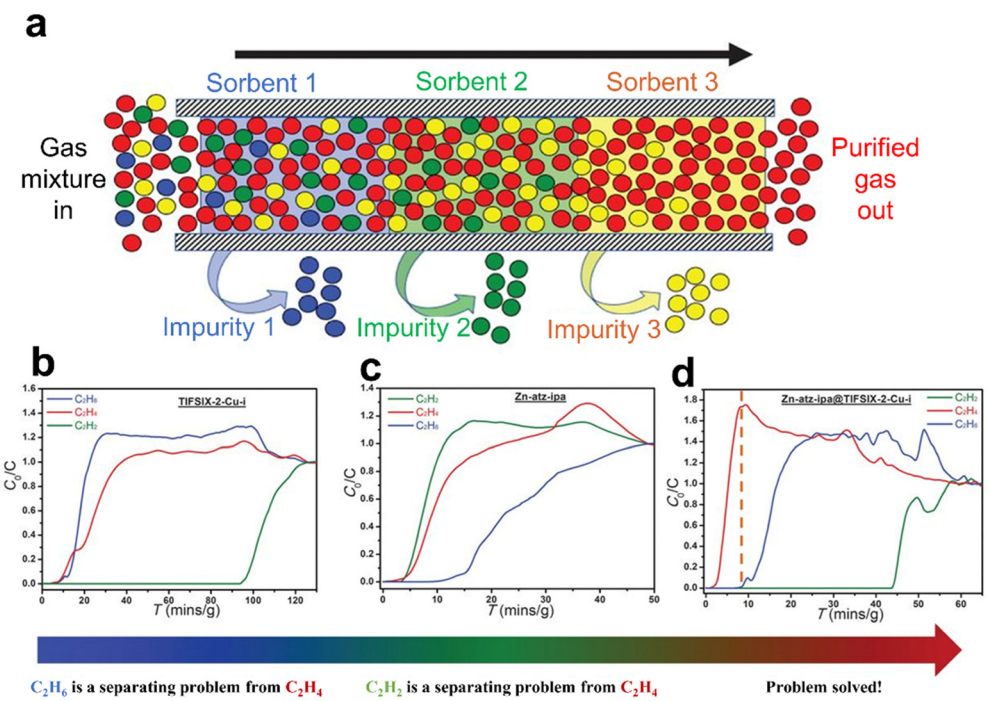

Fig. 8 (a) SSST involves an adsorption bed with three task-specific physisorbents to purify the commodity (red) with specific binding sites for each trace impurity (blue, green, and yellow). (b) and (c) Experimental column breakthrough curves for $C_2H_2/C_2H_4/C_2H_6$ separation (1 : 1 : 1 mixture) on TIFSIX-2-Cu-i and Zn-atz-ipa at 298 K and 1 bar. Breakthrough experiments were conducted in a column (inner diameter, 8 mm) at a flow rate of 2.1 ml min^{-1}. (d) Experimental column breakthrough curves for $C_2H_2/C_2H_4/C_2H_6$ separation (1 : 1 : 1 mixture) on a tandem-packed column of TIFSIX-2-Cu-i (~250 mg) and Zn-atz-ipa (~600 mg) at 298 K and 1 bar. Reprinted with permission from ref. 80. Copyright 2019 the American Association for the Advancement of Science.

partial combustion of methane. The resulting gas stream contains various impurities, with carbon dioxide (CO_2) being the major one. Thus, the separation of C_2H_2 from CO_2/C_2H_2 mixtures is important in industry. Although CO_2 and C_2H_2 have similar sizes (CO_2: 3.18 × 3.33 × 5.36 Å^3, and C_2H_2: 3.32 × 3.34 × 5.7 Å^3) and physical properties (boiling point of CO_2 = 194.7 K and of C_2H_2 = 189.3 K), the opposite quadrupole moments and slightly discrepant polarizabilities between C_2H_2 and CO_2, as well as the stronger π-bonding ability with metal sites and hydrogen-bonding donor ability of C_2H_2, allow the realization of their separation by means of rational design of pore surfaces and flexible framework amplification.[72,95–98]

In the early studies, Kitagawa *et al.* reported that a microporous MOF material, $Cu_2(pzdc)_2(pyz)$, with non-coordinated oxygen atoms on the pore surface forms strong hydrogen-bonding interactions with C_2H_2, showing high C_2H_2/CO_2 separation potential.[99] This study firstly demonstrates the effective role of Lewis base sites in enhancing the affinity of a MOF for C_2H_2. In addition, MOFs with high density of OMSs can facilitate the recognition of acetylene.[100–108] In 2016, Chen *et al.* reported a MOF-74 isomer, namely, UTSA-74, which has two different (octahedral and tetrahedral) metal coordination geometries along the 1D channel.[101] Each octahedrally coordinated metal ion provides two OMSs upon removal of the coordinated water molecules, leading to enhanced C_2H_2/CO_2 separation. The single-component adsorption isotherms showed that UTSA-74 has a comparable C_2H_2 uptake capacity (145 cm^3 cm^{-3}) to Zn-MOF-74 but a smaller CO_2 uptake capacity (90 cm^3 cm^{-3} *vs.* 146 cm^3 cm^{-3}), resulting in UTSA-74 with a good C_2H_2/CO_2 separation performance. This result can be attributed to that each open Zn site can bind with two C_2H_2 molecules, whereas two oxygen atoms of a CO_2 molecule occupy two adjacent OMSs, as demonstrated by the single-crystal X-ray structures and molecular modeling studies. Breakthrough experiments for a 50/50 C_2H_2/CO_2 mixture further demonstrate its good practical separation performance. This is also the first example of using breakthrough experiments to demonstrate the separation performance of MOFs for the C_2H_2/CO_2 mixture.

Based on copper(I)-alkynyl chemistry, anchoring Cu(I) on the surface of a MOF can significantly improve its specific recognition for C_2H_2. Qian *et al.* reported a Cu(I)-modified porous MOF, Cu(I)@UiO-66-$(COOH)_2$, which exhibits significantly enhanced C_2H_2/CO_2 separation performance with a high C_2H_2/CO_2 IAST selectivity of 185, compared to the prototype UiO-66-$(COOH)_2$.[107] The strong π-complexation between the π electrons on C_2H_2 and Cu ions enables Cu(I)@UiO-66-$(COOH)_2$ to adsorb a large amount of C_2H_2 (0.9 mmol g^{-1}) at low pressure (0.01 bar) and exhibit a high Q_{st} of 74.5 kJ mol^{-1}. Breakthrough experiments demonstrated its highly efficient separation performance for C_2H_2/CO_2. In addition, optimal distribution of OMSs on the pore surface of MOFs can achieve the maximum utilization of these sites. Recently, Li *et al.* reported a microporous MOF (JNU-4) with high-density OMSs.[108] These sites consist of square-planar copper centers separated by organic ligands, allowing each metal center to effectively bind with C_2H_2; thus, JNU-4 achieves a high C_2H_2 adsorption capacity (222 cm^3 g^{-1}, 9.91 mmol g^{-1}) and a moderate IAST selectivity of 8.2 for an equimolar C_2H_2/CO_2 mixture. Notably, this material absorbs C_2H_2 up to 200 cm^3 g^{-1} (8.93 mmol g^{-1}) at 298 K and 0.5 bar, but demonstrates a low Q_{st} of 26.8 kJ mol^{-1}. Grand Canonical Monte Carlo (GCMC) simulations demonstrated that C_2H_2 molecules can bind on both sides of OMSs, while CO_2 molecules can only bind on one side. Breakthrough experiments revealed that it has a high C_2H_2 absorption capacity (160 cm^3 g^{-1}, 7.14 mmol g^{-1}) from an equimolar C_2H_2/CO_2 mixture and can provide fuel-grade C_2H_2 gas.

Although a high density of OMSs can improve the selectivity for C_2H_2, electrostatic interactions between CO_2 and metal also exist simultaneously.[109–111] This requires a rational distribution of metal sites or the combination of multiple functions such as the pore size and shape to achieve a better C_2H_2 selectivity.[100,105,112] However, OMSs of high density may result in a high Q_{st}, thus leading to an increase of the energy consumption for adsorbent regeneration. In addition to OMSs, the introduction of functional groups (–NH_2, –F, –Cl, –Br, –CF_3, *etc.*) on organic ligands is also an effective strategy to promote selective adsorption of C_2H_2.[113–116] In 2021, Zhao *et al.* reported that an amine-functionalized flexible MOF (CPL-1-NH_2) with a 1D channel (3.8 × 4.4 Å^2) exhibits a high IAST selectivity of 119 for a 50/50 C_2H_2/CO_2 mixture at 298 K and 1 bar.[114] Theoretical calculations showed that the high selectivity of CPL-1-NH_2 for C_2H_2 can be attributed to the NH_2 functionalization that enhances C_2H_2 interaction with the framework, but blocks the stronger interaction between the non-coordinated oxygen atoms and CO_2 molecules by occupying the adsorption site of CO_2. In the same year, Qian *et al.* reported an Al-MOF (CAU-10-H) with a pore size of 4.7 Å, exhibiting a high C_2H_2 storage density (392 g L^{-1}) and a separation factor (3.4).[115] GCMC simulations showed that the suitable pore size not only enhances the interaction of C_2H_2 with high density oxygen atoms and aromatic rings on the pore surface, but also enables synergistic interaction between adjacent C_2H_2 molecules. Subsequently, CAU-10-H was functionalized with amine to furnish a new MOF (CAU-10-NH_2).[116] The later study showed that the amine groups can improve the uptake capacity of C_2H_2 at low pressure, and significantly enhance the stacking density (0.46 cm^3 g^{-1}) and C_2H_2/CO_2 selectivity (10.8) compared with the prototype MOF. In addition, these materials have the advantages of high stability, low Q_{st}, easy scale-up, and low cost.

It is well known that pore size and shape play an important role in the separation process, as an appropriate pore size can enhance the strength of interactions between the pore surface and adsorbate, as well as among adsorbates themselves.[97,100,112,117–123] MOFs can be designed and modified to alter the pore sizes, even at the sub-nanometer scale, through substitutions of metal ions, organic ligands, or inorganic anions. Strategies such as building self-interpenetrated networks and pore space partition (PSP) can also be used for the pore size or space modulation.[13,124] In 2019, Chen *et al.* reported a PSP approach for highly efficient C_2H_2/CO_2 separation. The new porous MOF (FJU-90) was synthesized by inserting a triangular ligand (2,4,6-tris(4-pyridyl)pyridine) into the cylindrical channel of prototype FJU-88.[122] The 1D channel of FJU-88 was separated into a number of aperture cavities with the aperture size decreasing from 12.0 × 9.4 to 5.4 × 5.1 Å^2.

Thus, the combination of optimized pore space and oxygen atom sites endows FJU-90a with a high C_2H_2 adsorption capacity (180 $cm^3\ g^{-1}$, 8.04 mmol g^{-1}). The separation performance of the activated MOF (FJU-90a) for a 50/50 C_2H_2/CO_2 mixture was further confirmed by breakthrough experiments with a productivity of 1.87 mol kg^{-1}.

In 2017, Chen *et al.* reported a SIFSIX-MOF UTSA-300 that exhibits not only efficient separation of C_2H_2/C_2H_4 but also a high selective uptake for C_2H_2 from the C_2H_2/CO_2 mixture.[72] Single-component adsorption isotherms revealed that the activated MOF (UTSA-300a) shows a high capacity for C_2H_2 adsorption (68.9 $cm^3\ g^{-1}$, 3.08 mmol g^{-1}) but adsorbs negligible CO_2 (3.25 $cm^3\ g^{-1}$, 0.14 mmol g^{-1}) at 298 K and 1 bar, resulting in a high IAST C_2H_2/CO_2 selectivity of 743 (298 K and 1 bar) (Fig. 9). Due to the strong C–H···F interactions formed between C_2H_2 molecules and SiF_6^{2-}, C_2H_2 can easily diffuse into UTSA-300a, while CO_2 is restricted because of electrostatic repulsion, as confirmed by DFT calculations and neutron powder diffraction studies. The separation performance of UTSA-300a for a 50/50 C_2H_2/CO_2 mixture was further demonstrated by breakthrough experiment in a packed column bed of UTSA-300a. Subsequently, systematic fine-tuning of the pore size of UTSA-300 was performed by replacing the fluoride anionic linkers and metal ions.[125] Three new SIFSIX-type MOFs, namely SIFSIX-dps-Cu (NCU-100), GeFSIX-dps-Cu, and NbOFFIVE-dps-Cu, were reported to exhibit different pore sizes (1.4 × 3.0 $Å^2$, 1.5 × 3.0 $Å^2$, and 2.2 × 2.7 $Å^2$, respectively) and interlayer distances (4.10 Å, 4.06 Å, and 3.69 Å, respectively). Single-component adsorption isotherms indicated that SIFSIX-dps-Cu shows the highest C_2H_2 uptake (4.57 mmol g^{-1}) with a high IAST C_2H_2/CO_2 selectivity up to 1787 at 298 K and 1 bar. In addition, the gate-opening pressure of SIFSIX-dps-Cu for C_2H_2 is 0.035 bar, which is lower than those of GeFSIX-dps-Cu (0.05 bar), NbOFFIVE-dps-Cu (0.3 bar), and UTSA-300 (0.06 bar), probably because of its larger interlayer distance. DFT and grand canonical Monte Carlo simulations further revealed that C_2H_2 molecules have multiple host–guest interactions (H···F hydrogen-bonding interactions) in both inter- and intra-layer cavities. Breakthrough experiments confirmed that high purity C_2H_2 (≥99.9%) can be obtained from C_2H_2/CO_2 (50/50) with a high productivity of 2.48 mmol g^{-1}.

A suitable pore size combined with active sites and a flexible structure can greatly improve the adsorption capacity of a material for C_2H_2.[95,106,114,125–127] Recently, Hong *et al.* reported that a flexible MOF, namely, $[Ni(DTBDA)(MeOH)_2(DMA)(H_2O)_2]$ (FJI-H36, DTBDA = 3′,5′-di(1*H*-1,2,4-triazol-1-yl)-[1,1′-biphenyl]-3,5-dicarboxylic acid), with adaptive channels shows efficient adsorption of C_2H_2.[127] FJI-H36 contains two types of cavities with the size of 12.9 × 12.9 $Å^2$ and 8.4 × 10.2 $Å^2$, respectively, as well as high-density active sites of open Ni^{II} (4.52 mol L^{-1}) and

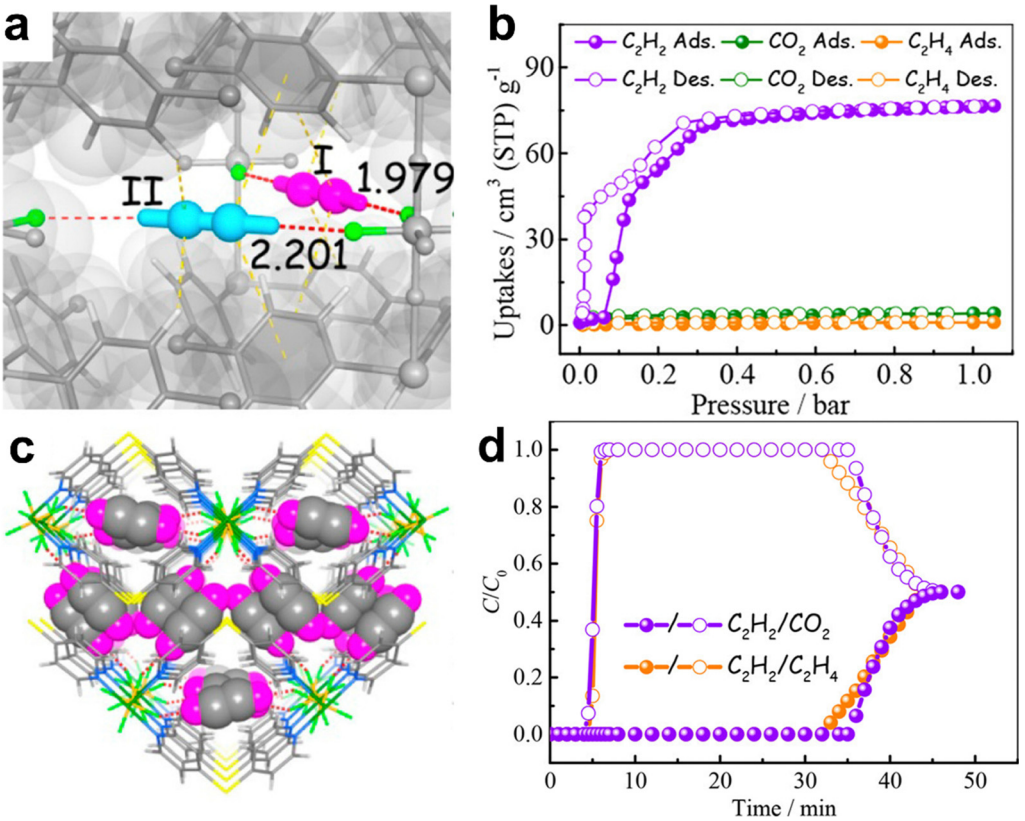

Fig. 9 (a) and (c) Neutron diffraction crystal structure of UTSA-300⊃C_2D_2 and (b) C_2H_2, CO_2, and C_2H_4 sorption isotherms for UTSA-300a at 273 K. (d) Experimental column breakthrough curves for equimolar C_2H_2/CO_2 (purple) and C_2H_2/C_2H_4 (orange) mixtures (298 K, 1 bar) in a fixed-bed packed with UTSA-300a. Reprinted with permission from ref. 72. Copyright 2017 American Chemical Society.

free N atoms (9.04 mol L^{-1}). Single-component sorption experiments confirmed that FJI-H36 shows a high C_2H_2 uptake of 159.9 $cm^3\,cm^{-3}$ at 298 K and 1 bar, and an ultra-high C_2H_2 storage density of 561 g L^{-1}. Breakthrough experiments for a 50/50 C_2H_2/CO_2 mixture further demonstrated its high adsorption capacity for C_2H_2 (3.82 mmol g^{-1}). The structure of FJI-H36 adaptively changes with the adsorption of C_2H_2, leading to a dense packing of C_2H_2 in it, as demonstrated by the X-ray crystal structure of C_2H_2@FJI-H36.

Recently, Wang *et al.* reported a sulfate-pillared MOF [Zn(tepb)(SO_4)] (SOFOUR-TEPE-Zn, TEPB = tetra(4-pyridyl)-benzene), which possesses dense electronegative pore surfaces to highly promote the separation of C_2H_2/CO_2 (Fig. 10).[97] SOFOUR-TEPE-Zn is an isostructural framework with SOFOUR-1-Zn,[128] but with more electron-rich pore surfaces due to the higher electronegative ethylene groups in the TEPE ligand in contrast to the phenyl ring in the TEPB ligand. Single-component sorption results of SOFOUR-TEPE-Zn reveled a higher C_2H_2 uptake (89.1 $cm^3\,g^{-1}$, 3.98 mmol g^{-1}) than SOFOUR-1-Zn (69.4 $cm^3\,g^{-1}$, 3.10 mmol g^{-1}) at 1 bar and 298 K, but a much lower CO_2 uptake (14.1 $cm^3\,g^{-1}$, 0.63 mmol g^{-1}), resulting in a very high IAST selectivity of 16833 for 50/50 C_2H_2/CO_2. Breakthrough experiments for 50/50 C_2H_2/CO_2 of SOFOUR-TEPE-Zn give a productivity of 60.1 $cm^3\,g^{-1}$ (2.68 mmol g^{-1}) of 99.5% purity or 33.2 $cm^3\,g^{-1}$ (1.48 mmol g^{-1}) of 99.99% purity in its desorption process by stepped helium purging and mild heating. Moreover, SOFOUR-TEPE-Zn also maintains a high C_2H_2 productivity of 75.5 $cm^3\,g^{-1}$ (3.37 mmol g^{-1}) of 99.5% purity with 99.82% C_2H_2 recovery in the simulated pressure swing adsorption processes. DFT-D and GCMC simulation studies revealed that the preferential binding of C_2H_2 in SOFOUR-TEPE-Zn can be mainly attributed to electron-rich pore surfaces, providing multiple optimal adsorption sites for C_2H_2.

CO_2-selective adsorbents can yield high purity C_2H_2 in one step rather than multiple adsorption–desorption steps, making the operation simple and more energy efficient. Currently, only a limited number of CO_2-selective MOF materials have been reported, manifesting the challenge in the design of CO_2-selective materials.[129–148] Fortunately, several strategies have been reported to promote the selective adsorption of CO_2 in MOFs. For example, Chen *et al.* introduced hydroxyl functional groups into MOF frameworks, enabling selective capture of CO_2 from C_2H_2, with a high IAST selectivity of 118.7 for CO_2/C_2H_2 (1 : 2, v : v) at 0.1 bar and ambient temperature.[137] In 2021, Chen *et al.* reported an ultramicroporous MOF [$Cu(F\text{-}pymo)_2$]·1.25H_2O (Cu-F-pymo, F-pymo = 5-fluoropyrimidin-2-olate) with zeolitic gismondine (GIS) topology exhibiting a high selective adsorption of CO_2 over C_2H_2, which depends on activation temperature (Fig. 11).[143] Cu-F-pymo contains two distinct pore environments, namely, spherical cavities and 1D helical channels, both of which are occupied by removable water molecules. Single-component adsorption isotherms revealed that partially dehydrated Cu-F-pymo can adsorb 1.19 mmol g^{-1} C_3H_6

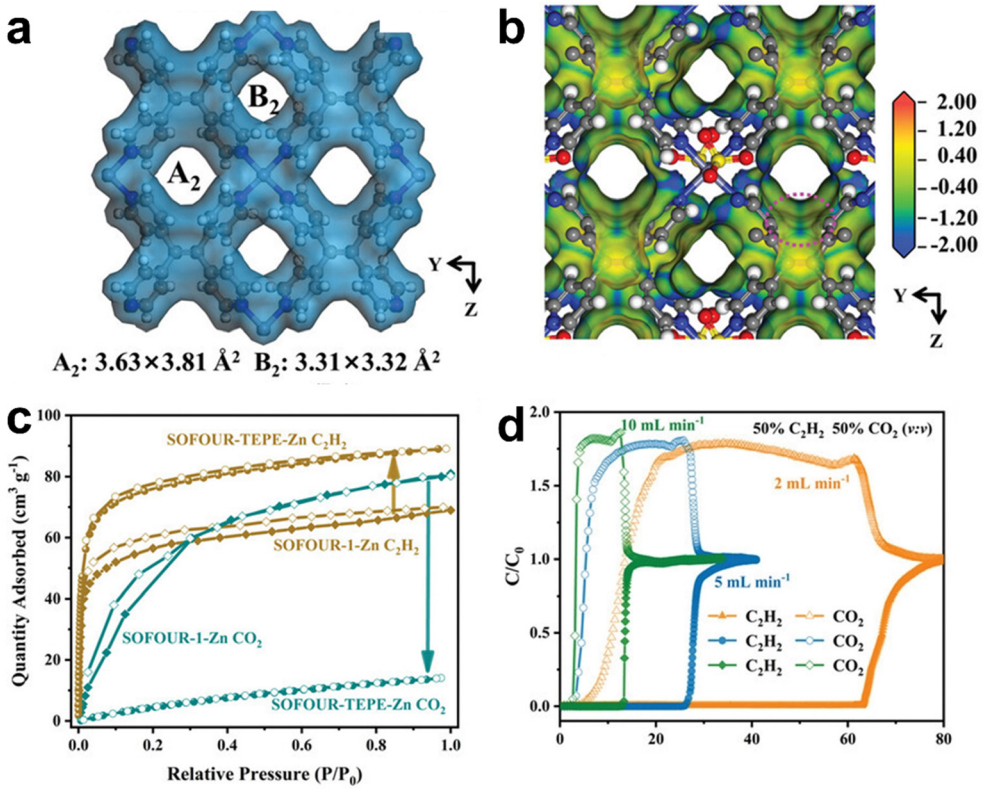

Fig. 10 (a) and (b) The building blocks of SOFOUR-TEPE-Zn and electrostatic surface potential. (c) C_2H_2 and CO_2 adsorption isotherms for SOFOUR-1-Zn and SOFOUR-TEPE-Zn at 298 K. (d) Breakthrough curves of SOFOUR-TEPE-Zn for C_2H_2/CO_2 (50/50, v/v) at different flow rates at 298 K. Reprinted with permission from ref. 97. Copyright 2023 Wiley-VCH.

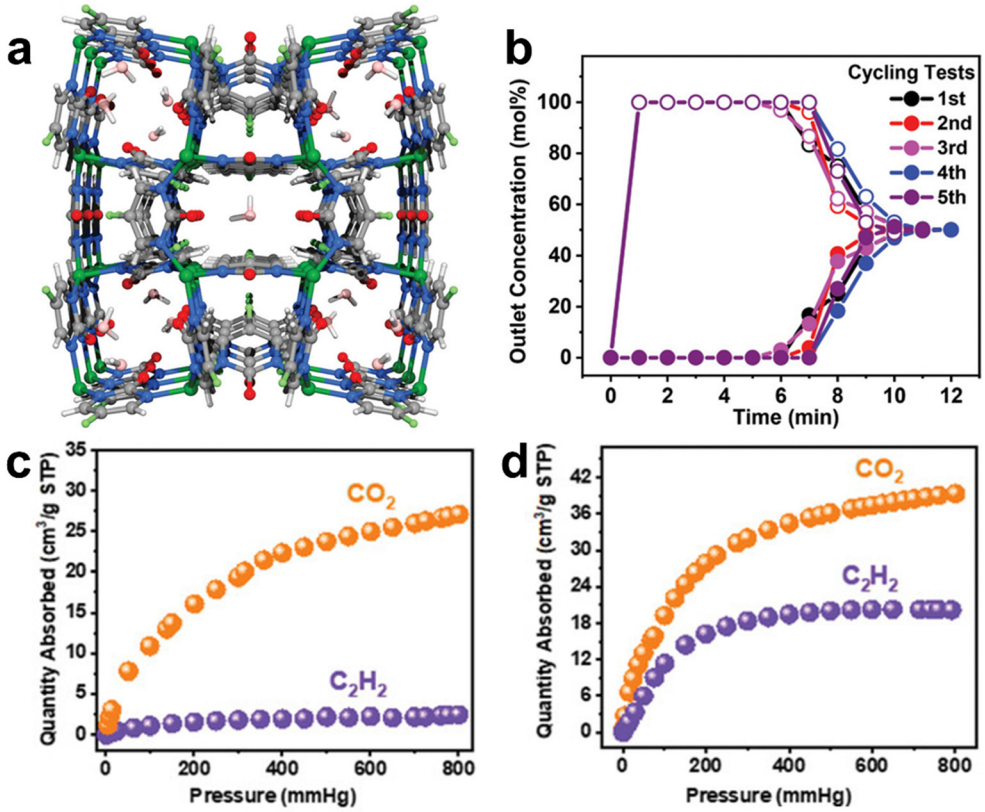

Fig. 11 (a) Schematic structure of Cu-F-pymo MOF with residual water molecules. (b) Breakthrough cycling tests of the equimolar CO_2/C_2H_2 mixture. (c) and (d) Separation performance toward CO_2 and C_2H_2 in Cu-F-pymo under different activation conditions. Reprinted with permission from ref. 143 Copyright 2021 Wiley-VCH.

and show negligible C_2H_2 uptake (0.1 mmol g^{-1}) at 298 K and 1 bar. Breakthrough experiments revealed that highly pure acetylene (>99.9%) can be obtained directly from a 50/50 CO_2/C_2H_2 mixture by a single separation operation. Modeling studies demonstrated that CO_2 can be preferentially adsorbed in the 1D channels, while C_2H_2 primarily occupies the spherical cavities. Therefore, the remaining water molecules in the spherical cavities blocked the preferential site, leading to the molecular sieving effect of Cu-F-pymo for CO_2/C_2H_2.

Besides size-matching between gas molecules and the pore structure, reasonable charge distribution would also facilitate the selective recognition of CO_2 over C_2H_2. Chen *et al.* reported an ultramicroporous porous material $Cd[Fe(CN)_5NO]$ (Cd-NP) that exhibits stronger affinity for CO_2 in contrast to C_2H_2. Cd-NP contains quasi-discrete ellipsoidal cavities (6.1 × 4.5 × 4.5 $Å^3$) connected by small apertures (3.2 Å), and its BET surface area is 305 m^2 g^{-1} (Fig. 12).[144] Thanks to suitable pore sizes and electrostatic distribution on pore surfaces, Cd-NP shows a high CO_2 uptake of 58.0 cm^3 g^{-1} (2.59 mmol g^{-1}) but a lower C_2H_2 uptake of 9.7 cm^3 g^{-1} (0.43 mmol g^{-1}) at 1 bar and 298 K, thus showing a high IAST selectivity (85) for an equimolar CO_2/C_2H_2 mixture. The Q_{st} of CO_2 was calculated to be 27.7 kJ mol^{-1}, which would facilitate regeneration of the material under mild conditions. The breakthrough process showed that Cd-NP was capable of producing a high purity C_2H_2 (99.9%) directly from 50/50 CO_2/C_2H_2 with a productivity of 2.34 mol L^{-1}. GCMC simulations and neutron powder diffraction experiments showed that the preferential adsorption of CO_2 in Cd-NP can be attributed to the confinement effect of the pore cavity and electrostatically complementary pore surface.

CO_2/C_2H_2 inverse separation can also be achieved using synergistic effects of thermodynamics and kinetics. Li *et al.* reported an ultramicroporous MOF, Y-bptc, to achieve one-step C_2H_2 purification from a CO_2/C_2H_2 mixture. Y-bptc processes small windows (4.2 Å) interconnected with large cubic cages with **ftw** topology. Equilibrium and kinetic adsorption studies reveled that Y-bptc absorbs 55 cm^3 g^{-1} (2.45 mmol g^{-1}) CO_2 and a lower C_2H_2 uptake at 298 K and 1 bar with an IAST selectivity of 4.1 for 50/50 CO_2/C_2H_2.[136] Moreover, CO_2 diffuses faster than C_2H_2 in Y-bptc, and the calculated kinetic separation coefficient reaches 114 at 298 K. Breakthrough experiments confirmed that CO_2 in a 1 : 1 CO_2/C_2H_2 mixture can be readily removed by Y-bptc, giving C_2H_2 with a purity of >99% and productivity of 1.52 mmol g^{-1} in a one-step separation process. GCMC simulations further revealed the high affinity of Y-bptc for CO_2 resulting from the formation of hydrogen-bonding interactions between μ_3-OH^- groups of the framework and CO_2 molecules.

In 2023, Wade *et al.* reported two isostructural MOFs $[Zn_5Cl_4(bbta)_3]$ (MUF-4, $bbta^{2-}$ = benzo-1,2,4,5-bistriazolate) and MUF-4-F, which exhibited completely opposite adsorption

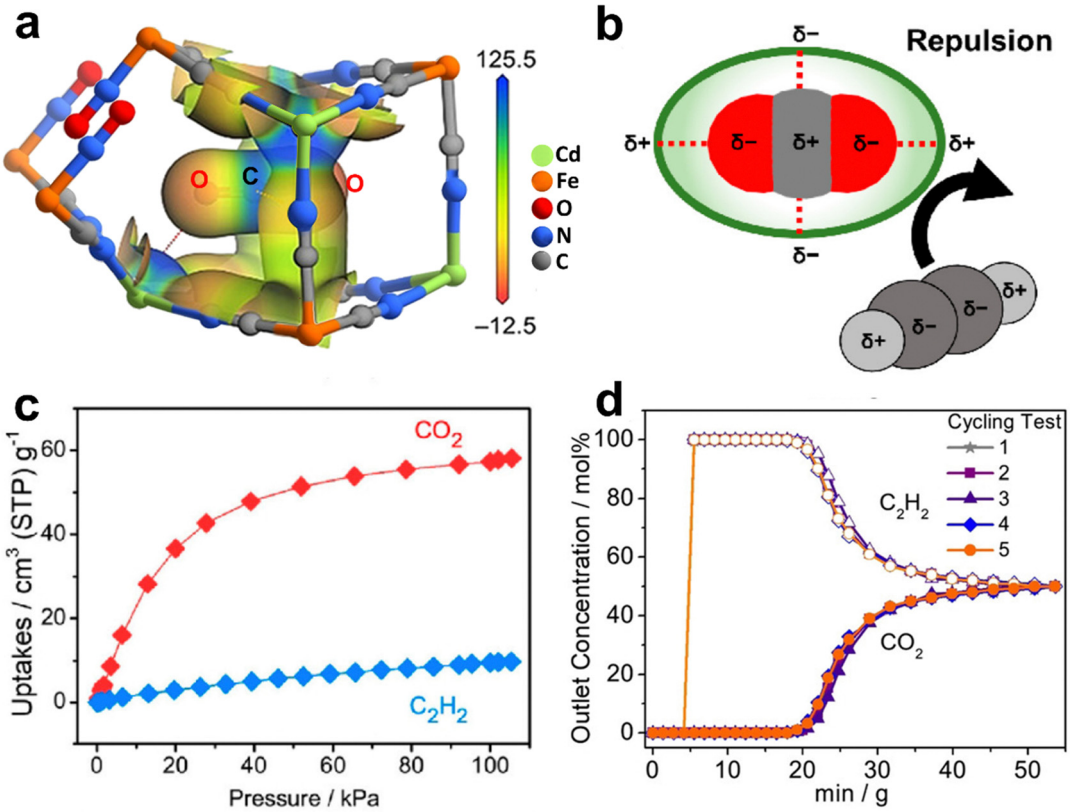

Fig. 12 (a) Electrostatic potential (ESP) of Cd-NP⊃CO_2 mapped onto the 0.15 $e^- Å^{-3}$ electron density isosurface. (b) Electrostatically driven adsorption mechanism towards CO_2 and C_2H_2 molecules. (c) CO_2 and C_2H_2 sorption isotherms for Cd-NP at 298 K. (d) Cycling tests of the equimolar CO_2/C_2H_2 mixture in a column packed with Cd-NP at 298 K and 1 bar. Reproduced with permission from ref. 144. Copyright 2021 Wiley-VCH.

selectivity for CO_2/C_2H_2. MUF-4-F can be derived by F^- to Cl^- ligand exchange of MUF-4.[139] Both MUF-4-F and MFU-4 possess alternating large pore and small pore cavities but have different connecting windows (~3.7 Å and ~2.2 Å, respectively). C_2H_2 molecules can easily enter MFU-4-F. Equilibrium and kinetic adsorption studies revealed that MFU-4-F exhibits a higher C_2H_2 (6.66 mmol g^{-1}) uptake than CO_2 (3.24 mmol g^{-1}) at 300 K and 1 bar and shows a fast adsorption rate for both gases. In contrast, MFU-4 exhibits high kinetic selectivity for uptake of CO_2 over C_2H_2 up to 3360 at 300 K. Computational studies revealed that C_2H_2 was blocked by the smaller windows created by the Zn–Cl groups in MUF-4. Breakthrough experiments demonstrated that high purity (>98%) C_2H_2 can be obtained directly from a 50/50 CO_2/C_2H_2 mixture in MUF-4.

2.5. C_3H_6 and C_3H_8 separation

Propylene (C_3H_6) is also an essential industrial feedstock with large demand that is only lower than that of ethylene. The industrial production of C_3H_6 inevitably contains a certain amount of propane (C_3H_8) impurity. However, they have very similar molecular sizes (C_3H_6: 3.8 × 4.0 × 6.5 $Å^3$, and C_3H_8: 3.8 × 4.2 × 6.8 $Å^3$), kinetic diameters (C_3H_6: 4.0 Å, and C_3H_8: 4.2 Å) and physical properties (boiling points of 189.3 and 194.7 K, respectively). Therefore, it is more challenging to tune the pore size for sieving separation of C_3H_6/C_3H_8, because they have highly similar molecular sizes and kinetic diameters, whereas possible changes of the size and shapes of MOF apertures may occur in the adsorption process, as many MOFs are actually flexible. Fortunately, significant research progress about highly efficient separation of C_3H_6/C_3H_8 has been recently realized by MOFs through rational structural design and modification of the pore size and pore surface.[149–168]

The incorporation of active sites in MOFs' pore surface improves not only kinetic selectivity but also thermodynamic selectivity for gas separation. In 2019, Zhang *et al.* reported a MAF, MAF-23-O, which can be easily synthesized by heating the flexible prototype [Zn_2(btm)$_2$] (MAF-23, H_2btm = bis(5-methy-1*H*-1,2,4-triazol-3-yl)methane) under oxygen gas flow (Fig. 13).[149] Single-crystal structure analyses showed that MAF-23-O is isostructural to MAF-23 and contains half the amount of the oxidized btm^{2-} ligands, namely, btk^{2-} (H_2btk = bis(5-methyl-1,2,4-triazol-3-yl)methanone). This *in situ* ligand oxidative modification makes the framework more rigid and more hydrophilic. The IAST selectivity for C_3H_6/C_3H_8 in MAF-23-O was calculated to be 8-9, which was higher than that of MAF-23 (3-4). Moreover, C_3H_6 and C_3H_8 exhibit similar diffusion rates in MAF-23, but show very different diffusion rates in MAF-23-O with a high kinetic selectivity of 71. Theoretical calculations demonstrated that the exposed oxygen atoms in the framework of MAF-23-O can form strong C–H···O/N interaction with C_3H_6, improving the thermodynamic selectivity of

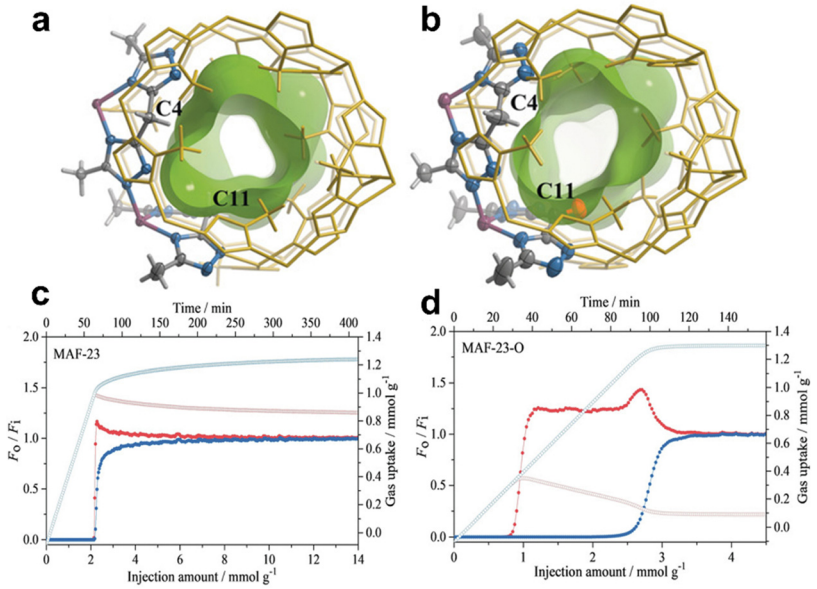

Fig. 13 Crystal and pore structures of (a) MAF-23 and (b) MAF-23-O. Breakthrough curves (filled symbols) and adsorption kinetic curves (open symbols) for (c) MAF-23 and (d) MAF-23-O using an equimolar C_3H_6/C_3H_8 (blue/red) mixture at 298 K and 1 bar. Reprinted with permission from ref. 149. Copyright 2019 Wiley-VCH.

MAF-23-O for C_3H_6. Additionally, the decreased flexibility of the framework slows down the diffusion of C_3H_6, thus improving the kinetic selectivity. Breakthrough experiments revealed that MAF-23-O exhibits efficient separation for an equimolar C_3H_6/C_3H_8 mixture at 298 K and 1 bar with an adsorption selectivity of 15, which is 10 times that of MAF-23.

In 2016, Eddaoudi *et al.* reported a oxyfluoride-based MOF $[Ni(pyr)_2(NbOF_5)]\cdot 2H_2O$ (NbOFFIVE-1-Ni, or KAUST-7, pyr = pyrazine) for selective adsorption of C_3H_6 from C_3H_8.[150] KAUST-7 is isostructural to SIFSIX-3 and composed of Ni(II)-pyrazine square-grid layers and $(NbOF_5)^{2-}$ pillars with **pcu** topology, exhibiting 1D channels with an aperture size of 3.0 Å and a periodic array of fluoride anions on the pore surface. Single-component sorption experiments revealed that KAUST-7 can adsorb ~60 mg g^{-1} (1.43 mmol g^{-1}) C_3H_6 but negligible C_3H_8 uptake at 298 K and 1 bar. Breakthrough experiments demonstrated that C_3H_8 of 97% purity can be obtained from C_3H_6/C_3H_8 50/50 mixed-gas by a packed column bed of KAUST-7, with a separation productivity of 0.6 mol g^{-1}. KAUST-7 also can adsorb C_3H_8 by pore-opening sorption behavior at 273 K.

In 2023, Chen *et al.* reported another SIFSIX MOF $[Ni(WO_2F_4)(pyz)_2]$ (UTSA-400) featuring 1D channels that can exclude C_3H_8 molecules and adsorb C_3H_6 molecules with a high binding affinity (Fig. 14).[151] UTSA-400 shows an isostructural framework with SIFSIX-3 and NbOFFIVE-1-Ni, but with highly tilted pyrazine linkers owing to larger $WO_2F_4^{2-}$ in contrast to SiF_6^{2-} and $NbOF_5^{2-}$. The pore cavities in UTSA-400 are 6.7 × 5.5 × 3.7 $Å^3$ with exposed oxide/fluoride pairs on the pore surface (BET surface area: 226 m^2 g^{-1}) that can serve as the binding sites for propylene molecules. Single-component sorption results of UTSA-400 indicated a much higher C_3H_6 capacity (92.1 cm^3 cm^{-3}, 2.62 mmol g^{-1}) than NbOFFIVE-1-Ni (54.3 cm^3 cm^{-3}, 1.34 mmol g^{-1}) by 63%, at 1 bar and 298 K, which is also higher than those of Y-abtc (64.6 cm^3 cm^{-3}, 1.98 mmol g^{-1}) and Co-gallate (66.6 cm^3 cm^{-3}, 1.79 mmol g^{-1}). Under the same conditions, UTSA-400 showed negligible C_3H_8 uptake because of inaccessible inward diffusion of propane molecules. The Q_{st} of UTSA-400 for C_3H_6 is 60.5 kJ mol^{-1}, being comparable to those of MOFs with OMSs (44–57 kJ mol^{-1}).[30,45] Breakthrough separation experiment demonstrated that polymer-grade (99.7%) propylene can be obtained from an equimolar C_3H_6/C_3H_8 mixture with a productivity of 56.7 L L^{-1}. Besides size exclusion, the separation performance of UTSA-400 can also be attributed to strong C–H···O/F interactions, as confirmed by *in situ* infrared spectroscopy and DFT-D calculations.

In 2018, Li *et al.* studied four microporous MOFs, namely, Zr-bptc, Zr-abtc, Y-bptc, and Y-abtc, which were obtained by the combination of two analogous metal clusters (Zr_6 and Y_6 clusters) and two different ligands (abtc = 3,3′,5,5′-azobenzenetetracarboxylates, and bptc = 3,3′,5,5′-biphenyltetracarboxylates).[152] Among these materials, Y-abtc has cage-like pores connected through small windows, exhibiting **ftw** topology and optimal pore size (4.72 Å) that enables it to adsorb small C_3H_6 molecules (4.48 Å) with fast kinetics but completely exclude larger C_3H_8 molecules (5.1 Å). Single-component sorption experiments revealed that Zr-bptc exhibits similar adsorption capacities for C_3H_6 and C_3H_8, whereas its isostructural Y-bptc excludes both gases, attributable to the presence of equilibrium cations (dimethylammonium) in the Y-bptc affecting its pore size. In contrast, Y-abtc with the optimal pore size shows a high adsorption capacity for C_3H_6 (~2 mmol g^{-1}) and a negligible C_3H_8 uptake at 298 K. Column breakthrough experiments indicated that polymer-grade C_3H_6 (99.5%) can be obtained from 5/95 C_3H_6/C_3H_8 mixtures by Y-abtc. Recently, the same group reported a new Y-based MOF, $Y_6(OH)_8(eddi)_3(DMA)_2$ (HIAM-301, H_4eddi = 5,5′-(ethene-1,2-diyl)diisophthalic acid, and DMA = dimethylammonium), also

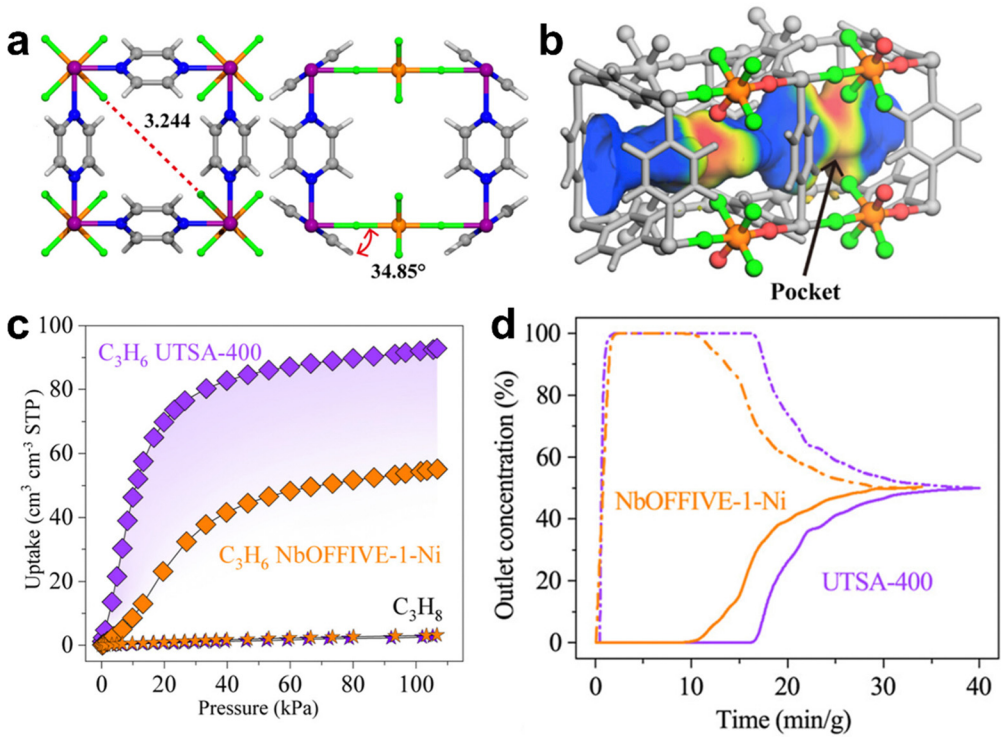

Fig. 14 (a) Crystal structure of UTSA-400. (b) Connolly surface of UTSA-400 mapped with electrostatic potential with a probe of 1.2 Å. (c) Single-component adsorption isotherms of C_3H_6 and C_3H_8 for UTSA-400 and NbOFFIVE-1-Ni at 298 K. (d) Breakthrough curves for NbOFFIVE-1-Ni and UTSA-400 for an equimolar binary mixture of C_3H_6 (solid line)/C_3H_8 (dashed line) at 298 K and 1 bar. Reprinted with permission from ref. 151. Copyright 2023 American Chemical Society.

exhibiting the molecular sieving separation of C_3H_6/C_3H_8 mixtures. HIAM-301 is composed of 12-connected $Y_6(OH)_8(COO)_{12}$ clusters bridged by 4-connected eddi^{4-} linkers to form a 3D framework with **ftw** topology and a pore size of 4.6 Å.[153] It is isostructural to Y-abtc and possesses distorted cubic cages (size: 10×10 Å^2), which provides better control over guest accessibility. Single-component adsorption isotherms revealed that HIAM-301 can adsorb 3.16 mmol g^{-1} C_3H_6 and exhibit minor C_3H_8 adsorption (<0.3 mmol g^{-1}) at 298 K and 1 bar, resulting in a high IAST selectivity (>150) for equimolar C_3H_6/C_3H_8 under the same condition. The practical performance for separation of 5/95 C_3H_6/C_3H_8 was confirmed by dynamic breakthrough experiments with a high productivity of 46.4 cm^3 g^{-1} (>99.5% purity).

In 2020, Chen *et al.* reported an ultramicroporous Co-gallate MOF [$Co(C_7O_5H_4)$] (Co-gallate) with 3D channels, which exhibits efficient C_3H_6/C_3H_8 separation by molecular sieving effect.[154] Co-gallate shows elliptical windows (size: 4.2 × 5.1 Å^2), which are precisely between the sizes of C_3H_8 and C_3H_6 (Fig. 15). Single-component adsorption isotherms showed that Co-gallate has a high adsorption capacity of C_3H_6 (66.6 cm^3 cm^{-3}, 1.79 mmol g^{-1}), whereas the adsorption of C_3H_8 (5.2 cm^3 cm^{-3}, 0.14 mmol g^{-1}) is minor at 298 K. The IAST selectivity of Co-gallate for a 50/50 C_3H_6/C_3H_8 mixture was calculated up to 330 at 1 bar and 298 K. Fixed-bed breakthrough experiments further confirmed its molecular sieving separation performance for 50/50 C_3H_6/C_3H_8, with a C_3H_6 productivity of 36.4 cm^3 cm^{-3}, 0.98 mmol g^{-1} (97.7%+ purity).

In 2021, Li *et al.* reported a MOF (JNU-3a) featuring 1D channels (size ~4.5 × 5.3 Å^2) attached with small pockets arranged on both sides for C_3H_6/C_3H_8 separation, where 1D channels could facilitate fast adsorption–desorption kinetics (Fig. 16).[155] In addition, the small pockets were connected with the 1D channel through small apertures (~3.7 Å) that can undergo gate-opening for C_3H_6 and C_3H_8 at different partial pressures. JNU-3a exhibits a stepwise adsorption isotherm and shows temperature-dependent gate-opening for C_3H_6 and C_3H_8, where C_3H_8 exhibits a higher gate-opening pressure than C_3H_6. Therefore, the high selectivity of JNU-3a for C_3H_6/C_3H_8 can be obtained at optimal temperature (303 K). JNU-3a can adsorb 58.6 cm^3 g^{-1} (2.62 mmol g^{-1}) C_3H_6 at 303 K, and the C_3H_6 packing density inside JNU-3a was calculated to be 404 g L^{-1}. The dynamic feature of pore aperture was further revealed by single-crystal X-ray diffraction and theoretical calculation studies. Breakthrough experiment revealed that high-purity C_3H_6 (≥99.5%) can be obtained from a 50/50 C_3H_6/C_3H_8 mixture by JNU-3a. After applying helium purge to those adsorbed gases, C_3H_6 was collected with a maximum productivity of 53.5 L kg^{-1}. The unique pore structure reported in this work would inspire future design of novel MOFs for application in adsorptive separation.

In 2023, Bai *et al.* reported a supertetrahedral-cluster ($Cu_{10}O_{13}$)-based MOF (NTU-85) which possesses square-shaped 1D channels that host lattice water molecules.[156] The partial lattice water molecules can be precisely removed to form a

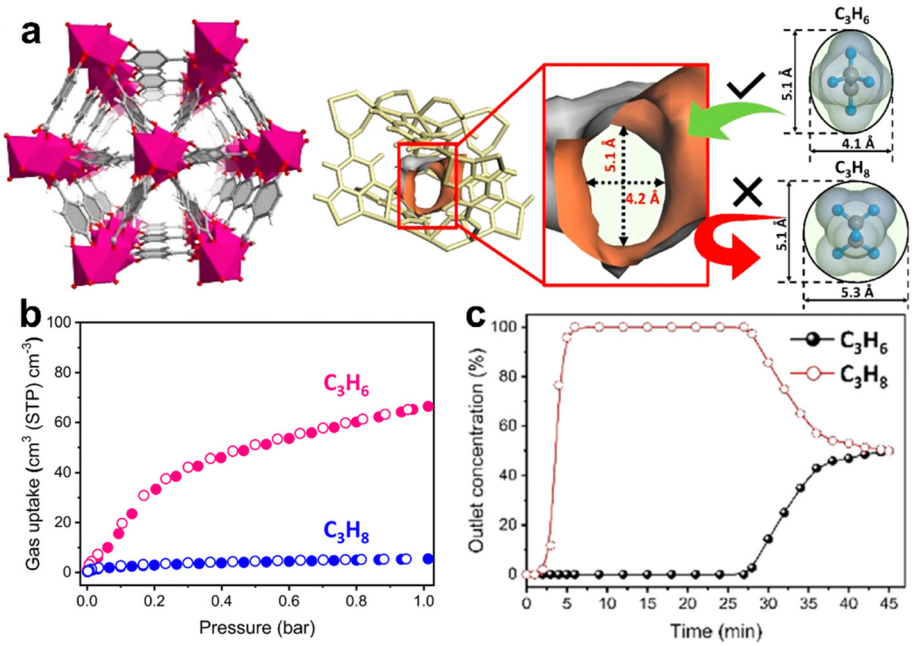

Fig. 15 (a) Structure of the Co-gallate MOF and rationale for C_3H_6/C_3H_8 separation. (b) Gas sorption isotherms of propylene and propane at 298 K for Co-gallate. (c) The breakthrough experiments were carried out in a packed column. Reprinted with permission from ref. 154. Copyright 2020 American Chemical Society.

MOF (NTU-85-WNT) of pore surface decorated with water nanotubes (~4.5 Å). Single-component sorption results of NTU-85-WNT indicated a rapid C_3H_6 uptake (20.9 mL mL^{-1}, 0.45 mmol g^{-1}), while the adsorption of C_3H_8 (0.13 mL mL^{-1}, 0.003 mmol g^{-1}) at 298 K can be neglected. The IAST selectivity of NTU-85-WNT for an equimolar C_3H_6/C_3H_8 mixture reaches up to 1570. Fixed-bed breakthrough experiments further confirmed its molecular sieving performance for an equimolar C_3H_6/C_3H_8 mixture, with a C_3H_6 productivity of 1.6 mL mL^{-1} (98.8%+ purity). It is worth noting that high purity C_3H_8 (>99.5%) can be obtained in one adsorption–desorption cycle due to the efficient sieving performance.

An optimal pore size combined with high-density binding sites can efficiently separate C_3H_6/C_3H_8, allowing for high-density stacking of C_3H_8 and maximizing its adsorption capacity. Recently, Chen *et al.* reported a robust Hofmann-type MOF, $[Co(pyz\text{-}NH_2)Ni(CN)_4]$ (ZJU-75a, pyz-NH_2 = 2-aminopyrazine), with high-density binding sites, showing excellent separation performance for C_3H_6/C_3H_8.[157] ZJU-75a exhibits an isostructural framework with $[Co(pyz)Ni(CN)_4]$ (ZJU-74a, pyz = pyrazine), decorated with amino groups. ZJU-75a exhibits an appropriate pore size (4.1 × 4.4 $Å^2$) and OMSs of high density (8.89 mmol cm^{-3}). Single-component sorption isotherms showed that ZJU-75a and ZJU-74a exhibit comparable C_3H_6 uptakes of 104.3 cm^{-3} cm^3 (3.31 mmol g^{-1}) and 111.4 cm^{-3} cm^3 (3.68 mmol g^{-1}) at 1 bar and 296 K, respectively, whereas the C_3H_8 adsorption capacity of ZJU-75a (73.5 cm^{-3} cm^3, 2.33 mmol g^{-1}) is obviously smaller than that of ZJU-74a (103.6 cm^{-3} cm^3, 3.42 mmol g^{-1}). Thus, the IAST selectivity of ZJU-75a for C_3H_6/C_3H_8 was calculated to be 54.2 at 296 K and 1 bar, much higher than that of ZJU-74a (4.3). The breakthrough studies indicate that ZJU-75a can yield C_3H_6 of high-purity (99.5%+) with a productivity of 18.7 L kg^{-1} and separation factor of 14.7. Structural and computational studies indicated that high-density OMSs and nitrogen atoms (from $[Ni(CN)_4]_2$ units and -NH_2 groups) in ZJU-75a contribute jointly to the strong adsorption of C_3H_6, thus resulting in a high C_3H_6 storage density (0.818 g mL^{-1}).

C_3H_8-selective adsorptive separation would be a relatively simple and energy-efficient way to get pure propylene. However, the differences of the molecular size (~0.5 Å) and polarizability (C_3H_6: 62.6 × 10^{-25}, and C_3H_8: 62.9–63.7 × 10^{-25} cm^3) between C_3H_6 and C_3H_8 are smaller than those between C_2H_4 and C_2H_6. So far, only a few C_3H_8-selective MOFs have been reported.[169–180]

In 2022, Xing *et al.* reported an ultramicroporous pillared layered MOF $[Co(IPA)(DPG)]_n$ (PCP-IPA, IPA = isophthalic acid, and DPG = *meso*-α,β-di(4-pyridyl)glycol) featuring 1D pores (size ~4.7 × 5.6 $Å^2$) and periodic parallel-aligned isophthalic acid units on the pore surface, exhibiting an excellent selectivity for C_2H_6 and C_3H_8.[169] Although C_2H_6 and C_3H_8 have different molecular sizes, the suitable pore size of PCP-IPA facilitates their directional adsorption and maximizes the interaction between PCP-IPA and C_3H_8/C_2H_6. Therefore, PCP-IPA exhibits not only a C_3H_8/C_3H_6 (50/50) IAST selectivity of 2.48 but also a relatively high adsorption selectivity (2.80) for C_2H_6/C_2H_4 (50/50) at 1.0 bar and 298 K. Both C_3H_8 and C_2H_4 can be directly obtained with high purity (99.99%) through a fixed-bed column from C_3H_8/C_3H_6 (50/50) and C_2H_4/C_2H_6 (50/50) mixtures, respectively, affording a high C_3H_6 productivity (15.23 L kg^{-1}) and excellent C_2H_4 productivity (26.2 L kg^{-1}). Modeling simulation studies revealed that tighter and more multiple vdW interactions (C–H···O/C) can be formed between paraffins and PCP-IPA compared to olefins.

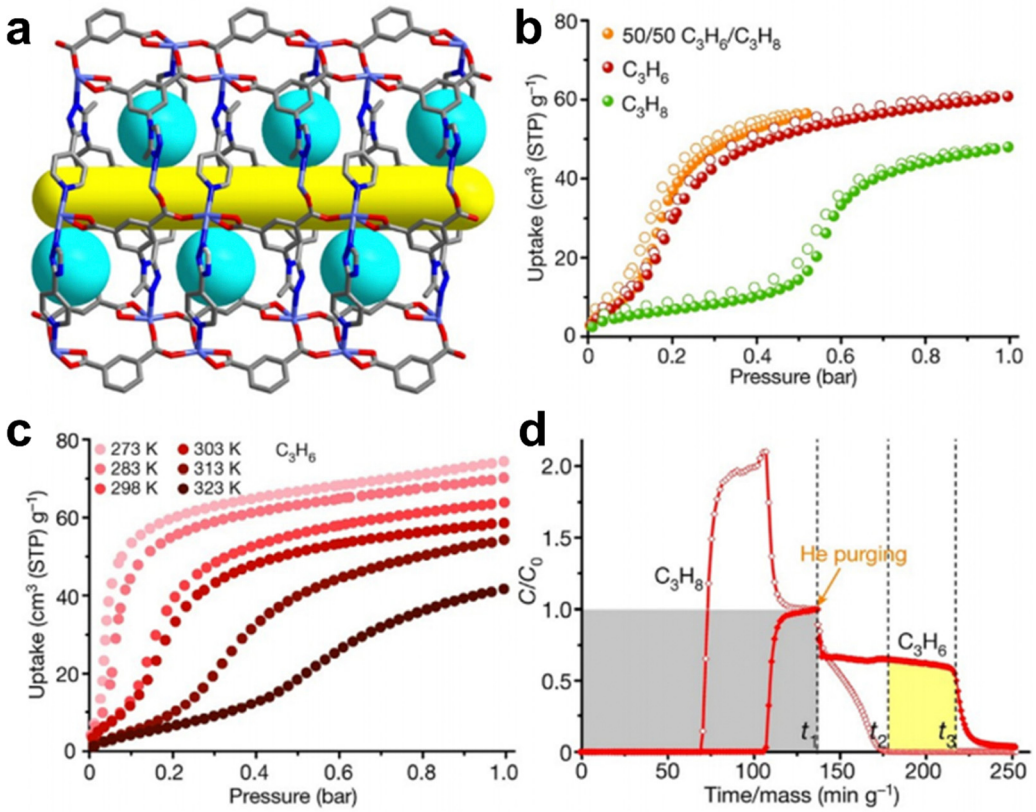

Fig. 16 (a) Pore structure of JNU-3 viewed along the *b* axis showing the molecular pockets (turquoise) and 1D channels (yellow); (b) pure C_3H_8 (green), pure C_3H_6 (red), and an equimolar C_3H_6/C_3H_8 mixture (orange) adsorption/desorption isotherms of JNU-3a at 303 K; (c) C_3H_6 adsorption isotherms of JNU-3a at different temperatures; (d) breakthrough curves (starting at $t = 0$) of an equimolar C_3H_6/C_3H_8 mixture (1.0 mL min^{-1}) on JNU-3a, followed by desorption curves (starting at $t = t_1$) under helium gas (10.0 mL min^{-1}) sweeping at 303 K. C_3H_8, open diamonds; C_3H_6, solid diamonds. *C* and C_0 are the concentrations of each gas at the outlet and inlet, respectively. Grey area, mixed gas input; yellow area, C_3H_6 gas output; t_1, the beginning of desorption; t_2, starting point of collecting C_3H_6; t_3, the end point of collecting C_3H_6. Reprinted with permission from ref. 155. Copyright 2021 Nature Publishing Group.

Very recently, Li *et al.* reported two isostructural MOFs (FDMOF-1 and FDMOF-2) functionalized with different amounts of fluorinated functional groups ($-CF_3$), showing strong affinity for C_3H_8 over C_3H_6 (Fig. 17).[170] Compared with the protype MOF $Zn_2(BDC)_2(DABCO)$ (Zn-DMOF, BDC = 1,4-benzenedicarboxylate), the introduction of different amounts of $-CF_3$ groups into a MOF not only increases its stability but also adjusts the pore size/shape. Therefore, FDMOF-2 with the maximal amount of $-CF_3$ groups shows the smallest aperture (5.1 Å) and exhibits the optimal C_3H_8 affinity. Single-component sorption isotherms showed that FDMOF-2 displays a higher C_3H_8 uptake of 140 cm^3 cm^{-3} (5.04 mmol g^{-1}) but a lower C_3H_6 uptake of 115 cm^3 cm^{-3} (4.14 mmol g^{-1}), resulting in the IAST selectivity for 50/50 C_3H_8/C_3H_6 up to 2.18 at 298 K and 1 bar. Breakthrough experiments revealed that high purity (>99.99%) C_3H_6 can be directly produced from 50/50 C_3H_8/C_3H_6 mixtures, affording 0.501 mol L^{-1} production of C_3H_6. It is worth pointing out that the excellent separation performance of FDMOF-2 for C_3H_8/C_3H_6 can be maintained under 70% relative humidity conditions. Single-crystal X-ray diffraction and theoretical calculation studies confirmed that the strong affinity of UTSA-400 for C_3H_8 can be attributed to strong non-classical C–H···π/F hydrogen-bonding interactions, resulting in a stronger binding affinity for C_3H_8 *vs.* C_3H_6 with an initial Q_{st} value difference of −3.7 kJ mol^{-1}.

2.6. C_3H_4/C_3H_6 separation

The removal of traces of propyne (C_3H_4 of ~1%) from propylene is essential to obtain high purity propylene (C_3H_6). However, it is very difficult to separate trace amounts of C_3H_4 from C_3H_6, because their chemical/physical properties and molecular sizes (C_3H_4: 6.2 × 3.8 × 3.8 $Å^3$; C_3H_6: 6.5 × 4.0 × 4.2 $Å^3$) are highly similar. Nevertheless, some MOFs have been reported to show great potential for the separation of C_3H_4/C_3H_6.[181–189]

In 2017, Chen *et al.* reported a flexible-robust MOF $[Cu(bpy)_2(OTf)_2]$ (ELM-12, bpy = 4,4′-bipyridine, and OTf^- = trifluoromethanesulfonate) which exhibits excellent performance for removing trace C_3H_4 from a 1/99 C_3H_4/C_3H_6 mixture. ELM-12 composed of 2D square-grid sheets with dynamic dangling OTf^- groups exhibit two kinds of cavities of different shapes and sizes (6.1 × 4.3 × 4.3 $Å^3$ and 6.8 × 4.0 × 4.2 $Å^3$), which were comparable with the size and shape of C_3H_4 (6.2 × 3.8 × 3.8 $Å^3$) (Fig. 18).[181] Single-component adsorption isotherms revealed that ELM-12 shows a sharp increasing adsorption for C_3H_6 with an uptake of 1.83 mmol g^{-1} at 298 K and 1 bar, as well as a large Q_{st}

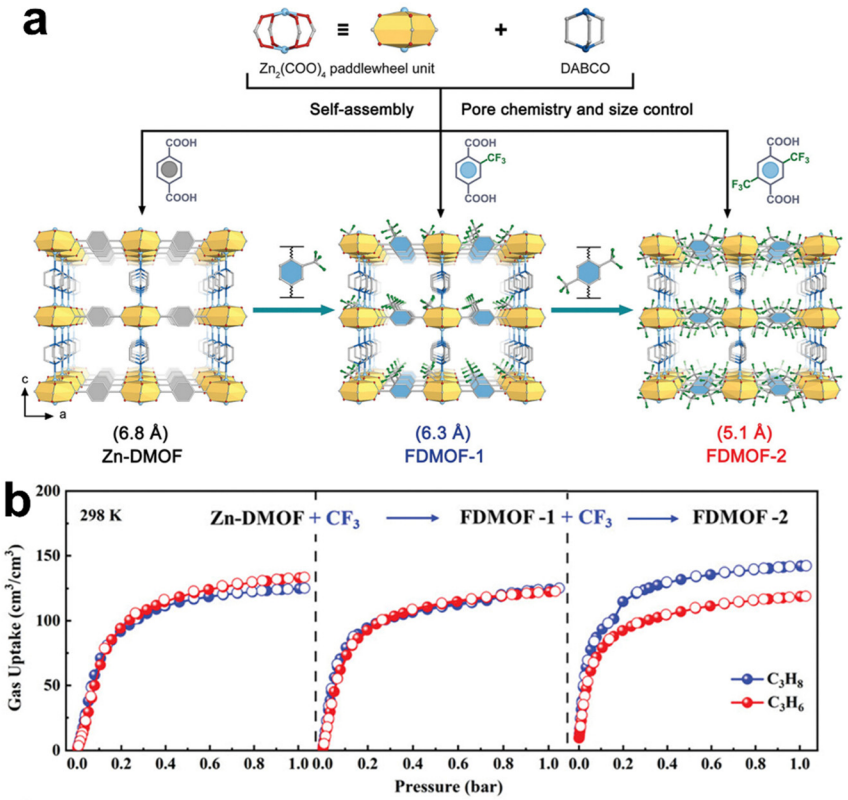

Fig. 17 (a) Crystal structures of Zn-DMOF, FDMOF-1, and FDMOF-2. (b) Single-component gas adsorption isotherms of the samples at 298 K. Reprinted with permission from ref. 170. Copyright 2023 Wiley-VCH.

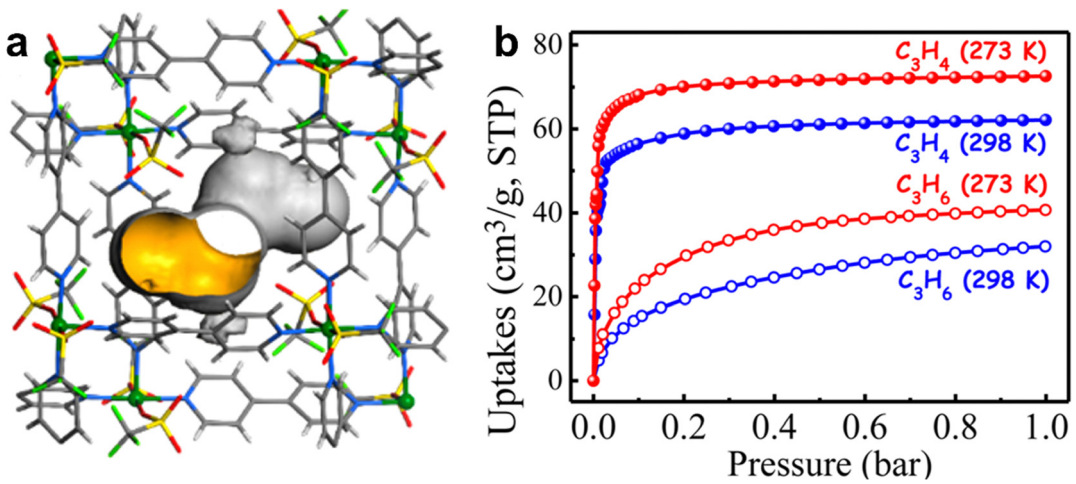

Fig. 18 (a) Crystal structure of ELM-12. (b) C_3H_4 and C_3H_6 adsorption isotherms of ELM-12. Reprinted with permission from ref. 181. Copyright 2017 American Chemical Society.

of 60.6 kJ mol^{-1} for C_3H_6, indicating its strong interaction with the C_3H_6 molecule. In contrast, both the uptake capacity (0.67 mmol g^{-1} at 0.1 bar and 298 K) and Q_{st} (15.8 kJ mol^{-1}) of ELM-12 for C_3H_8 are significantly lower. The multiple interactions, such as weak or non-classical C–D$\cdots$O hydrogen bonds, between ELM-12 and C_3D_4 molecules were further confirmed by high-resolution neutron powder diffraction studies. Breakthrough experiments demonstrated that high purity (99.9998%) of C_3H_6 can be obtained from a 1/99 C_3H_4/C_3H_6 mixture.

In 2018, Chen *et al.* studied a series of MOFs with different types of structures, functionalities, and pore sizes (Fig. 19).[182] Besides for highly selective C_2H_2/C_2H_4 separation,[70,71] SIFSIX-type MOFs such as SIFX-1-Cu, SIFSIX-2-Cu-i, SIFSIX-3-Ni, and UTSA-200 also exhibit strong binding affinities for C_3H_4 compared to C_3H_6 and show high C_3H_4 adsorption capacities at very

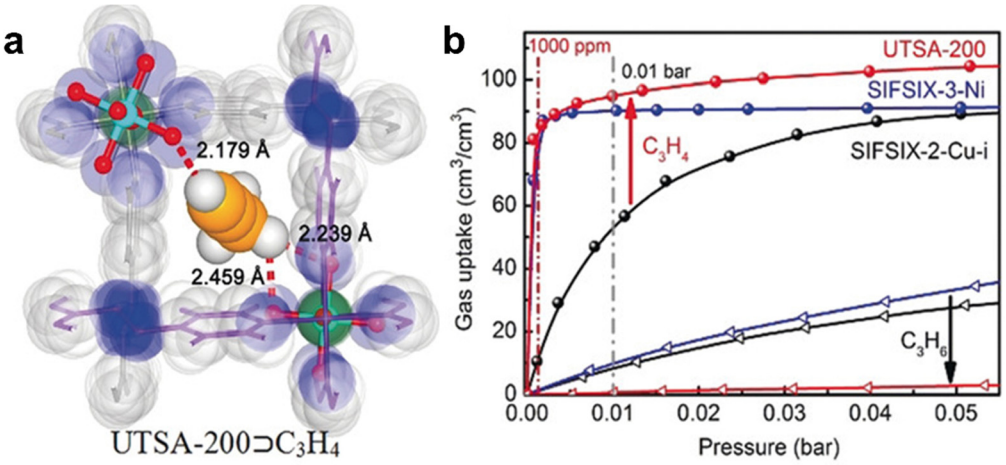

Fig. 19 (a) DFT-D optimized structure and binding sites of UTSA-200 ⊃ C_3H_4. (b) C_3H_4 and C_3H_6 adsorption isotherms of UTSA-200 at 298 K. Reprinted with permission from ref. 182. Copyright 2018 Wiley-VCH.

low pressure. The former three SIFSIX-MOFs show slightly larger pore sizes than both C_3H_4 and C_3H_6, which lead to moderate C_3H_4/C_3H_6 selectivity. The activated UTSA-200 with the optimal pore size (3.4 Å) and strong binding sites has the best separation performance for C_3H_4/C_3H_6. Single-component adsorption isotherms revealed that UTSA-200 exhibits the highest C_3H_4 uptake capacity of 95 cm^3 cm^{-3} (2.99 mmol g^{-1}) at 0.01 bar and 298 K, while adsorbs negligible C_3H_6 (0.33 mmol g^{-1}, at 298 K and 0.4 bar), resulting in an extremely high IAST selectivity of 20 000 for 1/99 C_3H_4/C_3H_6 at 298 K and 1 bar. Breakthrough experiments demonstrated that high purity (99.9999%) C_3H_6 can be yielded from 1 : 99 and 0.1 : 99.9 C_3H_4/C_3H_6 mixtures with a productivity of 62.9 mmol g^{-1} and 143.8 mmol g^{-1}, respectively. Neutron powder diffraction studies and DFT-D calculations revealed that C_3H_4 molecules can open the pores of UTSA-200 and form strong C–H···F interactions with the framework.

In 2022, Xing *et al.* reported a flexible MOF GeFSIX-14-Cu-i (ZU-33, GeFSIX = hexafluorogermanate, and 14 = 4,4′- azopyridine), which exhibits guest/temperature-dependent structural dynamics and shows strong binding affinity towards acetylene and propadiene.[188] ZU-33 featuring a 2-fold interpenetrated structure is composed of Cu(II)-4,4′-azobipyridne 2D layers and GeF_6^{2-} pillars, and its pore size (3.08–5.04 Å) was dynamically adjustable by the rotational motion of GeF_6^{2-} pillars and the organic ligands. Single-component gas adsorption experiments revealed that ZU-33 shows a steep uptake for alkynes (acetylene and propyne) and propadiene at low pressure (0.01 bar) and 303 K, while there is a threshold pressure for olefin adsorption and a size exclusion effect for alkanes. In addition, for C_2H_4 that is smaller than propyne and propadiene regarding the kinetic diameters, ZU-33 nearly inhibits C_2H_4 molecules to diffuse into its pores, suggesting the inverse size sieving below 0.5 bar at 303 K. Molecular simulations and single-crystal X-ray diffraction revealed that the interactions between the alkyne molecules (propyne and propadiene) and ZU-33 are more intense, thus requiring less input energy to overcome the energy barrier for the structural deformation. Breakthrough tests on a ZU-33 packed column verified that acetylene and propadiene can be directly removed from simulated cracking gases.

2.7. C_4 hydrocarbon separation

C_4 olefins including 1,3-butadiene (1,3-C_4H_6), 1-butene (*n*-C_4H_8) and isobutene (i-C_4H_8) are important raw materials for the production of synthetic rubbers and chemicals. However, C_4 olefin separation represents one of the great challenges in hydrocarbon purification owing to the similar structures and physical properties.[190,191]

Xing *et al.* reported several interpenetrated anion-pillared ultra-microporous MOFs, such as GeFSIX-2-Cu-i (ZU-32), NbFSIX-2-Cu-i (ZU-52) and GeFSIX-14-Cu-i (ZU-33), and realized highly efficient separation of C_4 olefins through molecular recognition.[192] This series of materials show ultrafine-tuning of the pore size/shape (4.20–4.83 Å) by replacing pillared inorganic anions with different bulks and different lengths of organic ligands. Among them, NbFSIX-2-Cu-i with a pore aperture size of 4.31 Å (F···F distance) exhibits high C_4H_6 (2.64 mmol g^{-1}) and *n*-C_4H_8 (2.26 mmol g^{-1}) uptake but negligible i-C_4H_8 uptake (0.48 mmol g^{-1}), showing uptake selectivities of about 5.00 and 5.74 for *n*-C_4H_8/i-C_4H_8 and C_4H_6/i-C_4H_8, respectively. In contrast, GeFSIX-14-Cu-i shows a smaller pore size of 4.20 Å (F···F distance), resulting in negligible adsorption of *n*-C_4H_8 (0.57 mmol g^{-1}) and i-C_4H_8 (0.42 mmol g^{-1}), but still retaining large uptake for C_4H_6 (2.67 mmol g^{-1}), accompanying a gate-opening adsorption behavior for C_4H_6. Breakthrough experiments demonstrated that these materials can efficiently separate C_4H_6 from C_4H_6/*n*-C_4H_8/i-C_4H_8/He (50/15/30/5) mixtures, as well as efficiently separate C_4H_6/*n*-C_4H_8 (50/50) and *n*-C_4H_8/i-C_4H_8 (50/50) mixtures.

Because of its high degree of unsaturation and strong coordination ability, 1,3-C_4H_6 is commonly adsorbed preferentially over other C_4 hydrocarbons by MOFs with functional sites. It is thus energy-intensive and might induce undesired polymerization as the purification involves capture of 1,3-C_4H_6 and

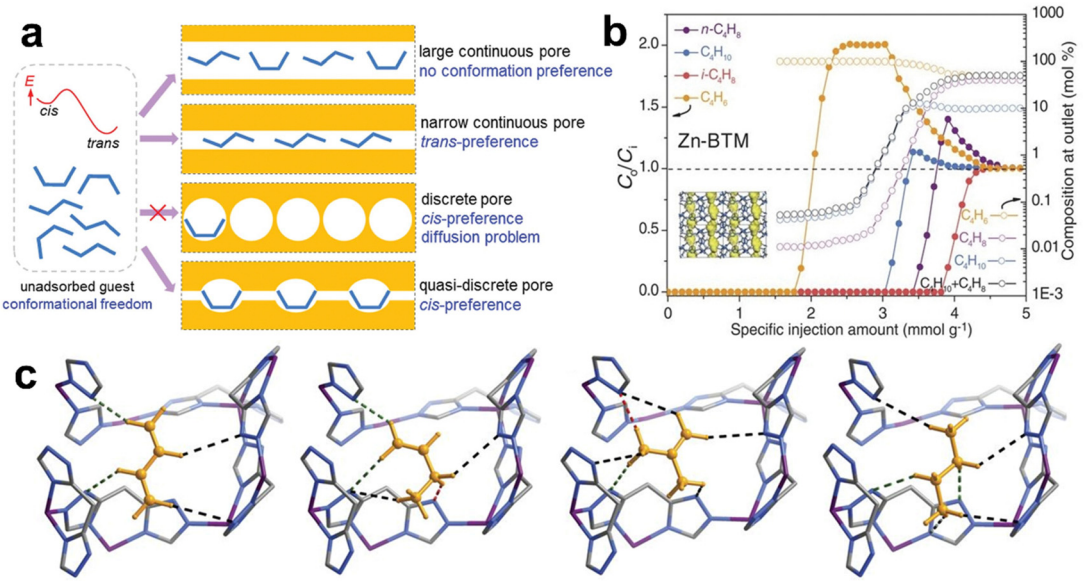

Fig. 20 (a) Schematic diagrams of controlling the guest conformation through the quasi-discrete pore in MAF-23. (b) Breakthrough curves of MAF-23 for a 5 : 2 : 2 : 1 C_4H_6/*n*-C_4H_8/i-C_4H_8/C_4H_{10} mixture. (c) Crystal structures of host–guest complexes of C_4H_6, *n*-C_4H_8, i-C_4H_8, and C_4H_{10}. Reprinted with permission from ref. 193. Copyright 2017 the American Association for the Advancement of Science.

its subsequent release through heating in general. Zhang *et al.* noticed that the collaborative interactions between the host framework and guest flexibility can significantly change the conformation of certain C_4 hydrocarbons and thus exhibit abnormal adsorption and reversed selectivity (Fig. 20).[193] In particular, a hydrophilic pore of a MAF with free N atoms, namely, $[Zn_2(btm)]_2$ (MAF-23), with 1D quasi-discrete pores (aperture size 3.6 Å, and cage size *ca.* 6 Å) was employed for separation of four hydrocarbons, *n*-C_4H_8, i-C_4H_8, C_4H_{10} and 1,3-C_4H_6. As revealed by experimental and DFT calculations, *n*-C_4H_8, the most similar one to 1,3-C_4H_6 among these gas molecules, adopts a metastable *cis* conformation to form stronger non-classical C–H···N interactions, and hence has a significantly stronger binding affinity, whereas 1,3-C_4H_6 adopts the stable *trans* conformation and has the weakest binding affinity because of the unfitting configuration for forming stronger non-classical hydrogen-bonding interactions. In other words, MAF-23 with a unique pore structure and surface serves as a guest conformation-controlling adsorbent to achieve preferential adsorption of *n*-C_4H_8, i-C_4H_8 and C_4H_{10} over 1,3-C_4H_6. Therefore, 1,3-C_4H_6 can be first eluted during the breakthrough operation under ambient conditions, and directly purified for the desired purity ($\geq$99.5%) to meet the industrial requirement in one single separation operation.

The separation of C_4 geometric isomers is also a challenging separation process, among which the separation of *trans*/*cis*-2-butene is of prime importance to increase the value of C_4 olefins. Ren *et al.* reported that M-gallate (M = Ni, Mg, and Co), featuring oval-shaped pores, are ideally suitable for shape-selective separation of *trans*/*cis*-2-butene through their difference in the minimum molecular cross-section sizes, in addition to a highly efficient separation of 1,3-butadiene, 1-butene, and i-butene.[194] Mg-gallate displays a narrow pore window size of 3.6 × 4.6 Å^2, capturing the smaller *trans*-2-butene (3.5 × 4.6 Å^2) while excluding the slightly larger *cis*-2-butene (3.6 × 4.9 Å^2), affording a high *trans*/*cis*-2-butene uptake selectivity of 3.19 at 298 K and 1.0 bar in single-component adsorption isotherms. DFT-D study showed that Mg-gallate interacts with *trans*-2-butene and 1,3-butadiene through short distances of intermolecular C···H–O interactions (C···H distances 2.57–2.83 and 2.45–2.79 Å, respectively).

The separation of isomeric C_4 paraffins is also an important task in the petrochemical industry. Zhong *et al.* regulated the pore aperture of the cage-like Zn-bzc by stepwise installation of methyl groups on its narrow aperture to achieve both molecular-sieving separation and a high *n*-C_4H_{10} uptake.[195] The resulting Zn-bzc-2CH_3 is not only a new benchmark adsorbent featuring molecular sieving for *n*-C_4H_{10}/*iso*-C_4H_{10} separation and a high *n*-C_4H_{10} adsorption capacity (2.42 mmol g^{-1}), but also hydrophobic to eliminate the negative effect of water vapor on gas separation under humid conditions. Breakthrough tests proved that high-purity i-C_4H_{10} (99.99%) can be collected. The minimum energy path of *n*-C_4H_{10} and i-C_4H_{10} from cage to cage passing through the narrow aperture was determined for Zn-bzc-*n*CH_3 (*n* = 0, 1, 2), and the results suggested easy transports of both *n*-C_4H_{10} and i-C_4H_{10} for the larger apertures of the parent Zn-bzc MOF and Zn-bzc-CH_3 due to the low energy barrier together with a small barrier difference, while kinetic forbiddance with a dramatical increase of the diffusion energy barrier from 23.8 to 131.6 kJ mol^{-1} for *n*-C_4H_{10} to migrate through Zn-bzc-2CH_3.

2.8. Linear/branched alkane separation

The branched C_5–C_6 paraffins are major components in high-octane gasoline, which have relatively higher Research Octane Number (RON) values than their normal counterparts. To boost octane ratings in gasoline, the separation of linear alkanes

from their branched isomers is very important in the petroleum industry, which is traditionally done by energy-intensive distillation processes.

Eddaoudi *et al.* reported two new 12-connected rare-earth metal (Y^{3+} and Tb^{3+}) fumarate based fcu-MOFs with both octahedral and tetrahedral cages that were solely interconnected with triangular windows of aperture size *ca.* 4.7 Å, and discovered that both of them can act as a adsorbate-size cut-off for the total sieving of C_4 and C_5 branched paraffins.[196]

In addition, Li *et al.* prepared two Zr-MOF compounds, Zr-bptc and Zr-abtc, which are highly stable with optimal pore structures for the separation of C_6 alkane isomers (Fig. 21).[197] For instance, Zr-abtc featuring an scu-type structure with 1D channels (d = 7 Å) accommodates all C_6 alkane isomers (*n*-hexane, 3-methylpentane and 2,3-dimethylbutane), but favors *n*-hexane because of its stronger interactions with the pore surface, resulting in a mono/dibranched separation factor (~1.3) in the breakthrough test.

In 2020, Li *et al.* reported a new flexible MOF, calcium chloranilate (HIAM-203), which specially possesses chloro-decorated 1D channels.[198] HIAM-203 exhibits structural flexibility upon adsorption of C_6 alkanes with different branching, as well as similar temperature-dependent adsorption behavior toward alkane isomers. It can take up a plentiful amount of *n*-hexane and 3-methylpentane at 30 °C, but completely excludes 2,2-dimethylbutane, while at 150 °C 3-methylpentane is also excluded. This phenomenon may be rationalized by the significant difference in binding affinity near the pore aperture of HIAM-203. As the pore size of HIAM-203 (5.6 Å) is between the kinetic diameters of 3-methylpentane (5.5 Å) and 2,2-dimethylbutane (6.2 Å), it thus inhibits the diffusion of 2,2-dimethylbutane.

In 2023, Bao *et al.* employed the Hofmann-type MOFs, $[M(pz)Ni(CN)_4]$ (M = Co and Ni) to demonstrate similar temperature-swing molecular exclusion for separation of hexane isomers.[199] CopzNi displays excellent separation efficiency for linear/mono-branched and mono-branched/di-branched alkanes with the highest adsorption capacity to date. CopzNi exhibits lower-energy regeneration, scalability, recyclability and high stability, representing a promising candidate for relevant separation processes.

There are also needs for purification of valuable C_5-C_7 olefins. Isoprene, which accounts for 15–25% of C_5 fractions including important olefins like 1-pentene and *trans*-2-pentene, is widely used in the production of synthetic rubber, pharmaceutical and pesticide intermediates.[200] The regeneration and desorption efficiency should also be taken into account for separation.[201] Cui *et al.* found that anion-pillared hybrid porous materials, namely, ZU-62 (also termed NbOFFIVE-2-Cu-i) and TIFSIX-2-Cu-i, exhibit a good separation performance for C_5 olefin mixtures (*trans*-2-pentene, 1-pentene and isoprene).[202] Owing to a contraction of pore aperture originating from the rotation of 4,4′-dipyridylacetylene ligand, ZU-62 excludes the relatively large molecule of isoprene in the low pressure range (0–6 kPa), while

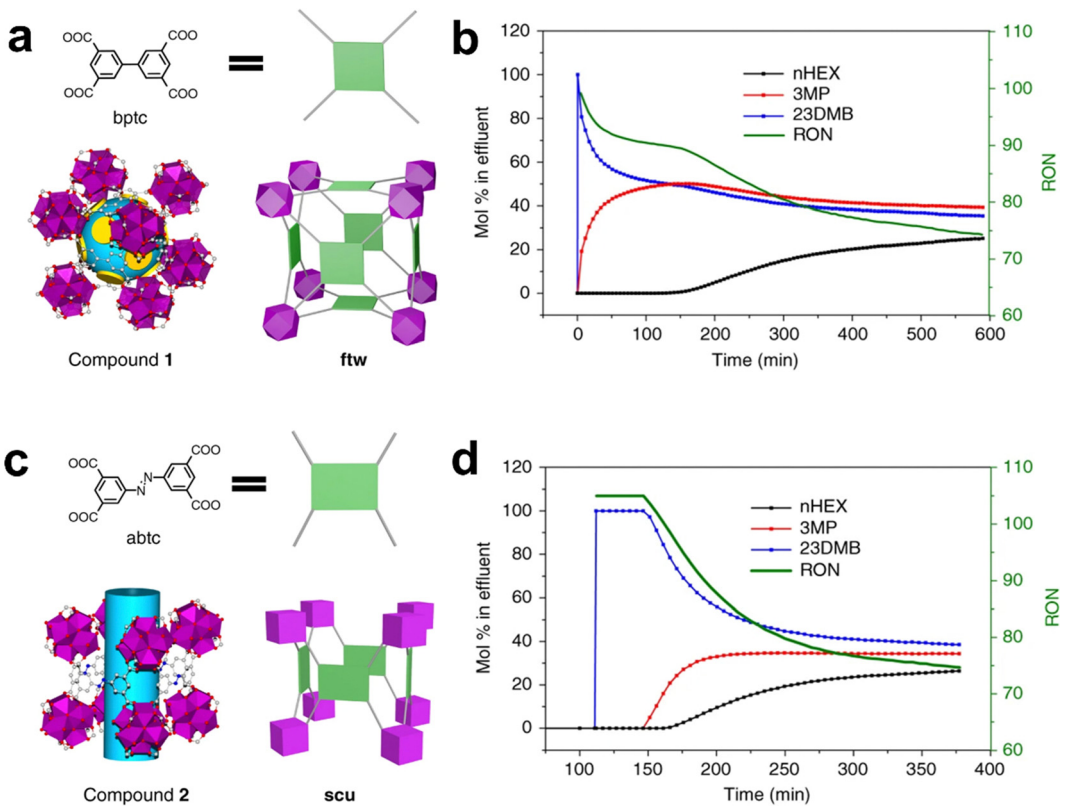

Fig. 21 (a) and (c) Organic ligands, crystal structures, and topologies of Zr-bptc and Zr-abtc. (b) and (d) Breakthrough curves of an equimolar ternary mixture of C_6 alkane isomers at 150 °C for Zr-bptc (top) and Zr-abtc (bottom). The green curve represents the real-time RON of the eluted products. Reprinted with permission from ref. 197. Copyright 2018 Nature Publishing Group.

TIFSIX-2-Cu-i is able to distinguish the three C_5 olefins with a high uptake of *trans*-2-pentene (3.1 mmol·g^{-1}), superior to that of zeolite 5A (2.0 mmol·g^{-1}). DFT-D calculations confirmed that the selective adsorption was achieved by a favorable electrostatic environment as well as suitable pore confinement. Also, the regeneration tests showed that C_5 olefins can be easily desorbed from ZU-62 and TIFSIX-2-Cu-i at 298 K.

2.9. Aromatic isomer separation

The separation of C_8 aromatic compounds (xylene isomers, ethylbenzene and styrene) is also one of the important separations.[1] Tremendous efforts have been devoted to developing MOF adsorbents for relevant separations. Most of these adsorbents contain aromatic organic ligands, in which the phenyl or heterocycle rings allow strong π–π stacking interactions with C_8 aromatic molecules to facilitate the adsorption.[203,204]

MOFs featuring structural flexibility like breathing or gate-opening have been applied for separation of aromatic isomers.[18,37,205] Li *et al.* reported that a stacked 1D manganese-based MOF [Mn(dhbq)(H_2O)$_2$] (Mn-dhbq, H_2dhbq = 2,5-dihydroxy-1,4-benzoquinone) exhibits temperature-dependent discriminative adsorption of xylene isomers owing to reversible framework swelling.[206] At 363 K, *p*X can be fully intercepted from the *p*X/*m*X/*o*X ternary mixture by a column of Mn-dhbq, whereas the effluent of the *m*X/*o*X mixture can be further separated by another column of Mn-dhbq at a lower temperature (303 K) where mainly *o*X finally flows out. The purity of *p*X is over 97% collected during the desorption cycle when using 1,4-diethylbenzene as an eluent at 433 K for 1 hour after liquid-phase adsorption of a quaternary mixture (*p*X/*m*X/*o*X/EB, 22/22/50/6) at 393 K. DFT calculations indicated that the temperature-dependent flexibility between 1D coordination chains (different degrees of swelling at different temperatures) endows such selective adsorption of xylene isomers through π–π stacking interactions with the aromatic ligand.

Xing *et al.* reported a flexible anion pillared MOF [Ni(bpy)$_2$($NbOF_5$)] (ZU-61) with **pcu** topology and a pore size of 7.8 Å exhibiting efficient separation performance for xylene isomer.[207] Single-component adsorption revealed that ZU-61 shows a higher low-pressure uptake for *m*X and *o*X than *pX* at 0.01 bar and 333 K, as well as a high capacity for *m*X (3.4 mmol g^{-1}) and *o*X (3.2 mmol g^{-1}). Breakthrough experiments for a 1 : 1 : 1 *p*X/*m*X/*o*X mixture confirmed that high purity (>99.9%) *p*X can elute from the column first, and then followed by mX and oX. The excellent performance for xylene isomer separation can be attributed to the rotational $NbOF_5^{2-}$ anions, which allows adaptive host–guest interaction (C–H···F interactions) depending on the shape of the xylene isomer, as confirmed by DFT calculations and crystallographic studies. These results showed that ZU-61 exhibits great potential for the purification of *p*X.

Given that all xylene isomers contain phenyl rings for π–π stacking interactions, another approach to enhance the separation selectivity would be utilizing the difference of their alkyl groups while inhibiting the interactions with phenyl rings. Yang *et al.* constructed a pillar-layered MOF Cu(bpdc)(ted)$_{0.5}$ (ZUL-C3) by using poly-cycloalkane-type ligands to show a non-aromatic pore environment for xylene separation.[208] The pore space of the MOF magnifies the difference of host–guest interactions with xylene isomers and ethylbenzene owing to their different distribution of methyl (ethyl) groups. Liquid-phase batch experiment indicated that this MOF can separate xylene isomers and ethylbenzene from each other, showing separation potential for *o*X/*p*X and *o*X/*m*X separation.

A flexible MOF, [Cu_2(fbdim)]·*p*-xylene (MAF-41·*p*X), showing a 3D hinged-fence-like framework and 1D channels (4.2 × 9.8 × 10.1 Å^3 cavities and 3.9 × 6.7 Å^2 apertures), was demonstrated by Zhang *et al.* to exhibit unprecedented inversed molecular sieving (so called intermediate-sized molecular sieving) for the purification of styrene (Fig. 22).[209] The framework structure can transform to a nonporous one upon removal of template molecules. The activated MAF-41 can adsorb styrene (ST) to restore the as-synthesized structure while totally excluding ethylbenzene (EB), toluene (Tol), and benzene (Bz). Styrene with a purity of 99.9%+ can be obtained from the multicomponent mixture after one single adsorption–desorption cycle because the pores are individually opened and simultaneously occupied by the target guest. The aperiodic pore opening is believed to avoid co-adsorption of guest molecules smaller than the opened pores. Kinetic sorption studies revealed that the EB/Tol/Bz

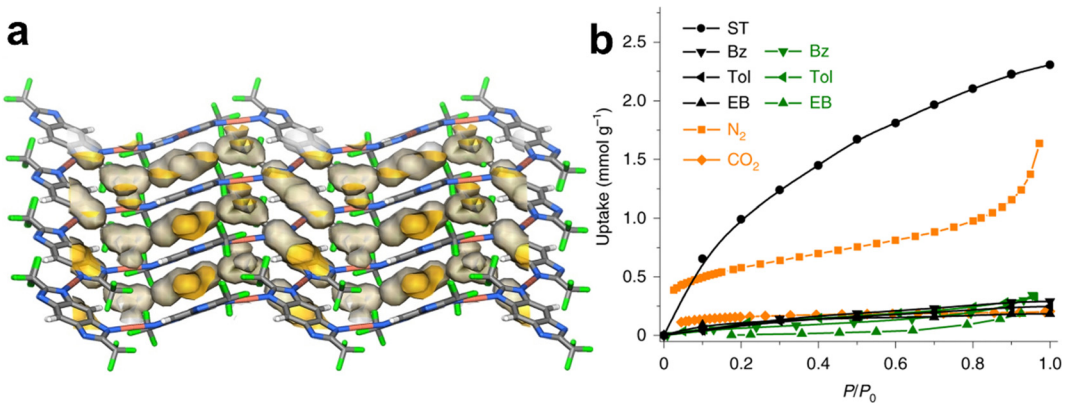

Fig. 22 (a) Crystal structure of guest-free MAF-41. (b) Adsorption isotherms of activated MAF-41 for ST (styrene, 298 K), EB (ethylbenzene, 298 K), Tol (toluene, 298 K), Bz (benzene, 298 K), N_2 (77 K), and CO_2 (195 K). Reprinted with permission from ref. 209. Copyright 2019 Nature Publishing Group.

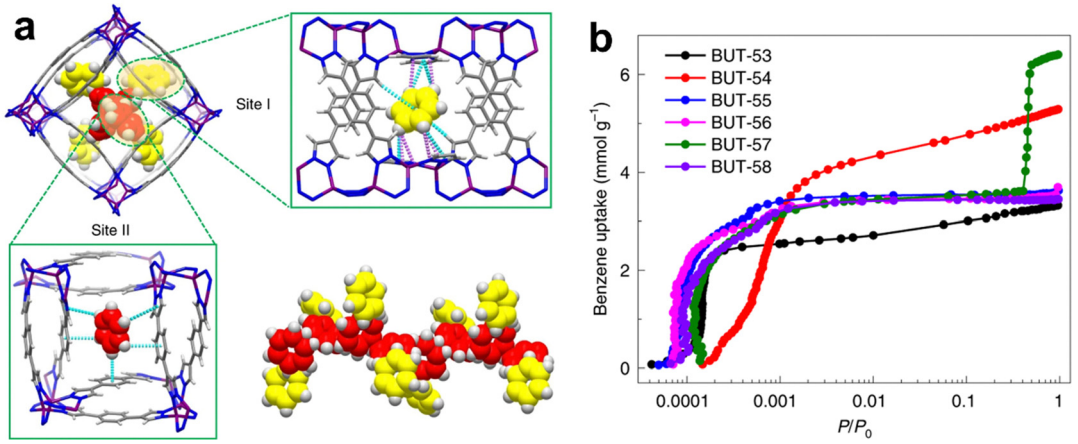

Fig. 23 (a) Structures of C_6H_6@BUT-55 and benzene–benzene interactions. (b) Logarithmic-scale plots of P/P_0 to view the benzene adsorption of BUT-53 to BUT-58 at low partial pressure. Reprinted with permission from ref. 210. Copyright 2022 Nature Publishing Group.

adsorptions stayed quite low all the time, while the ST uptake of MAF-41 significantly increased for both the single-component and mixtures, which confirms no EB/Tol/Bz co-adsorption or replacement of ST in MAF-41. Although Cu(I) complexes and Cu(I)-based MOFs may have poor stability in air and/or water, guest-free MAF-41 did not collapse not only at temperatures up to 500 °C, but also in boiling water for at least one week, and even remained stable in a solution of pH 3–14 at room temperature for at least 3 days.

In 2022, Li *et al.* reported a family of double-walled metal-dipyrazolate frameworks (BUT-53 to -58) composed of divalent metal ions and dipyrazolate ligands with different symmetries, lengths, and functionalities for trace benzene removal (Fig. 23).[210] In this study, multiple merits, *e.g.*, high stability, tunable pore, high adsorption capacity and selectivity, were integrated into these hydrophobic MOFs, which all exhibited high benzene uptakes (2.47–3.28 mmol g^{-1}) at room temperature and ultra-low pressures (<10 Pa). BUT-55 is the best-performing adsorbent for the capture of trace benzene among them. It shows an extremely long breakthrough time of ~8000 h g^{-1} for a benzene-containing (10 ppm, 10 mL min^{-1}) gas mixture under both dry and humid (relative humidity = 50%) conditions. When the relative humidity was 80%, the breakthrough time decreased to ~6000 h g^{-1}, which is still much higher than that of other previously reported materials. After adsorption of benzene, BUT-55 can be regenerated under mild heating. As revealed by both the single-crystal structure of benzene-loaded BUT-55 and DFT calculations, multiple non-classical hydrogen-bonding C–H···X (X = N, O, π) interactions are the key to its strong affinity and high sensitivity toward benzene. The high benzene binding energy of BUT-55 contributes to its high adsorption selectivity of benzene over water or other volatile organic compounds (VOCs), such as cyclohexane and ethanol. It should also be pointed out that the BUT-55 sample is able to work continuously around one year under the breakthrough experiment conditions. In other words, a certain amount of BUT-55 can be used to capture trace airborne benzene for a long time due to its high benzene adsorption capacity under ultra-low pressures and high adsorption selectivity. The performance of these MOFs demonstrates high potential in the removal of benzene from ambient air.

Very recently, Mo *et al.* reported a flexible MOF, [Sr_2(BINDI)(H_2O)$_2$)] (WYU-62, H_4BINDI = N,N′-bis(5-isophthalic acid)-naphthalenediimide) with electron-deficient NDI cores, which shows fast adsorption of trace benzene vapor at low pressure,

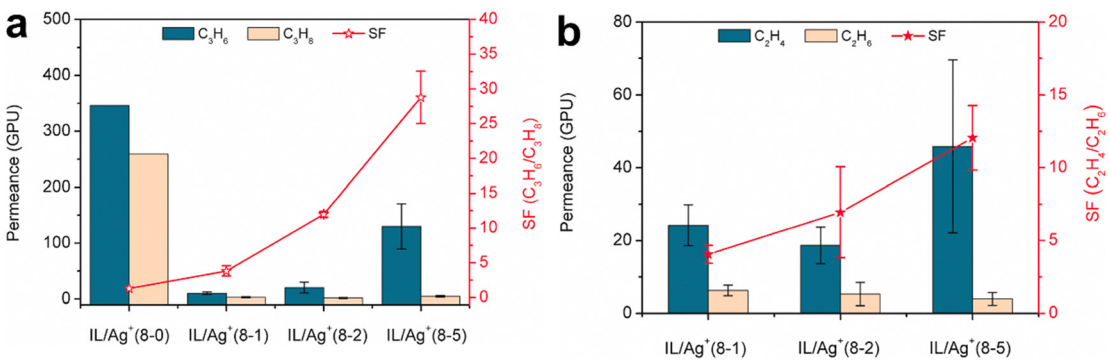

Fig. 24 (a) C_3H_6/C_3H_8 separation performance of $Zn_2(bim)_4$ membranes modified by diversified composites, IL/Ag$^+$(8-0), IL/Ag$^+$(8-1), IL/Ag$^+$(8-2) and IL/Ag$^+$(8-5). (b) C_2H_4/C_2H_6 separation performance of $Zn_2(bim)_4$ membranes modified by diversified composites, IL/Ag$^+$(8-1), IL/Ag$^+$(8-2) and IL/Ag$^+$(8-5). Reprinted with permission from ref. 217. Copyright 2021 Elsevier.

accompanying a fluorescence-enhanced sensing (limit of detection = 0.133 mg L^{-1}).[211] WYU-62 could be easily obtained by immersing the as-synthesized MOF [Sr_2(BINDI)(DMF)(H_2O)] (MYU-61) in water, during which discrete 0D pores of MYU-61 have transformed to 1D channels (aperture size = 5.1 × 9.1 $Å^2$). Aromatic hydrocarbon vapor adsorption isotherms revealed that WYU-62a can show high benzene uptake at very low pressure ($P/P_0 < 0.01$). DFT calculations and crystallographic studies indicated that electron-rich benzene was tightly wrapped between the two electron-deficient NDI moieties with strong π–π and C−H···π interactions. Therefore, it has excellent benzene adsorption capacity, whereas the accompanying host–guest charge transfer enables visual detection of trace benzene vapor.

3. MOF-based membranes for separating gaseous hydrocarbons

Though a variety of MOFs have been extensively studied for light-hydrocarbon purification in recent two decades, only a few have been fabricated into MOF-based mixed matrix membranes (MMMs), which may integrate the advantages of the separation performance of MOFs and processability of polymers for olefin/paraffin separation.[212] For example, MAF-4 (or ZIF-8) and Zr-fum-fcu-MOF (or MOF-801) have been incorporated with membranes for C_3H_6/C_3H_8 separation.[213,214]

Modification of MOF membranes with the composite ionic liquid/Ag^+ (IL/Ag^+) can efficiently improve their olefin/paraffin separation properties. Yang *et al.* synthesized layered $Zn_2(bim)_4$ membranes[215] using the *in situ* interfacial assembly (ISIA)[216] method and further modified them with varied IL/Ag^+ composites.[217] Adsorption isotherms for $Zn_2(bim)_4$ powder and its IL/Ag^+ modified sample showed that the adsorption capacity for olefin can significantly improve after modification with IL/Ag^+ but the adsorption for paraffin shows negligible changes, which is attributed to the strong π-complexation of olefins with Ag^+. Further study revealed that the pristine $Zn_2(bim)_4$ membrane showed a C_3H_6/C_3H_8 separation factor of 1.14 with a C_3H_6 permeance of 106 GPU ($SF_{C_2H_4/C_2H_6}$: 1.42, and $P_{C_2H_4}$: 311) (Fig. 24). In contrast, the modified membranes exhibited a significant improvement in olefin/paraffin separation with the optimized C_3H_6/C_3H_8 separation factor of 28.8 ± 3.8 with the C_3H_6 permeance of 129.8 ± 40.4 GPU ($SF_{C_2H_4/C_2H_6}$: 12.0 ± 2.2, and $P_{C_2H_4}$: 45.6 ± 23.7 GPU). The preferential binding affinity of Ag^+ in IL for olefins facilitates the delivery of olefins in the modified $Zn_2(bim)_4$ membranes. On the other hand, Ag^+ filling in the space of laminated modified $Zn_2(bim)_4$ membranes further blocks paraffin penetration and thus improves the olefin/paraffin selectivity. In addition to the composite modification membrane strategy, intrinsic structural regulation of MOF membranes is also crucial. Recently, a series of $Zn_2(bim)_4$ membranes functionalized with different amounts of amino groups, namely, N*x*-$Zn_2(bim)_4$(*x* represents the molar ratio of raw 5-aminobenzimidazole, bim) were also investigated for separation.[218] Among them, the N10-$Zn_2(bim)_4$ membrane exhibits the highest H_2/CO_2 separation performance with a separation factor of 1158 and a H_2 permeance of 1417 GPU. Moreover, its ideal selectivities for H_2/CO_2, H_2/CH_4 and H_2/C_3H_8 were 829, 99, and 33, respectively, showing a distinct size exclusion effect for relatively large molecules.

Long *et al.* fabricated a series of membranes with M_2(dobdc) (M = Co, Ni, Mg, and Mn) as fillers and 6FDA-DAM as the primary polymer by reducing the filler size to the sub-100 nm level to specially improve the filler-polymer compatibility and dispersion.[219] Among them, Ni_2(dobdc) showed the best C_2H_4/C_2H_6 separation performance without reduction in selectivity even under high-pressure owing to the presence of strong and multiple nanocrystal-polymer interactions, which suppresses plasticization by reducing polymer chain mobility.

Polycrystalline MOF membranes are less explored but also important. Liu *et al.*[220] have recently prepared a polycrystalline Co-gallate membrane with a reported freezing contra-diffusion protocol[221] that can enable more accurate control over the reaction kinetics between metal ions and ligands to effectively tune the MOF nucleation and growth in the bulk solution. Maintaining the frozen state of the metal precursor inside the macroporous α-Al_2O_3 substrate resulted in the formation of the preferred *c*-oriented and well-intergrown Co-gallate membrane with not only abundant open metal sites (at the increased missing-linker defects), but also reduced the thickness of the membrane. The multiscale structure endows the Co-gallate membrane with an outstanding C_2H_4/C_2H_6 separation performance superior to those of state-of-the-art membranes including polycrystalline MOF membranes, MOF-based MMMs, and polymeric membranes. The optimized C_2H_4/C_2H_6 selectivity is 8.3 with a C_2H_6 permeance of 72.6 GPU. The resultant membrane also shows a negative correlation with the operation temperature and high long-term stability.

4. Conclusion and outlook

MOF materials have made significant progress in the separation of gaseous hydrocarbons in the past few years, which was achieved by rational control over their pore chemistry/size, affording an alternative separation technology for relevant applications. The high crystallinity of MOFs facilitates systematic and deep investigation on the exact adsorbent–adsorbate interactions in the type of porous materials for high separation performance, as demonstrated by their crystallographic studies on the host–guest interactions. Controlling of the pore structure of MOF materials at high-accuracy level is applicable due to the high modularity and diverse functionality of MOFs, which facilitates highly efficient separation of methane, olefin/paraffin, alkyne/olefin, alkane isomers and aromatics. As outlined in this review, the collaborative control of the pore size and pore surface has been explored for the potential of MOFs for hydrocarbon separation. MOFs with high separation selectivities and large gas uptakes have been documented. The development of this realm has gradually turned to evaluate the potential of MOFs in practical separation processes, which required continuous research endeavors.

There are many important issues remaining unaddressed before further industrial and commercial usage of MOFs. Shaping/pelleting of MOFs would be the first step in actual processes given engineering considerations, but that would lead to loss of adsorption capacity; thus, further study on mechanical stabilities of MOFs might be necessary. Simultaneously, the diffusion kinetics of MOF pellets should be comprehensively investigated. There are also concerns on current research for evaluations of their separation performances through swing adsorption or membrane separation processes, as these evaluations mainly focus on evaluating candidate materials under simulated conditions rather than the actual applications. In relevant simulated evaluations, the presence of contaminants such as water has gradually got involved. In contrast, the actual gas streams would be more complicated, while the separation condition can be even harsher (under elevated pressures/temperatures), which require the adsorbents to show good stability and durability, including good water resistance and impurity tolerance. The long-term durability and regeneration of MOFs during separation processes have been rarely involved in current research. Moreover, systematic evaluation of materials production, including capital and operating costs, should be performed prior to large-scale deployments of MOF-based adsorptive separation technology. Solvent-free and continuous synthesis methods have been demonstrated to be applicable for MOFs, which show great potential for large-scale production of MOF materials. In addition, new technical issues such as thermal management during the adsorption process would come out when sorption is scaled up. For membrane-based separation, there are also several challenges although it is capable of direct production of pure gas and can be simply operated under mild conditions. Several mixed-matrix MOF-based membranes have been developed, which show large permeance differences for hydrocarbon separation. However, the processability, defect, compatibility, and scaling up in membrane fabrication as well as the permeability-selectivity trade-off are still quite challenging. In terms of membrane separation, molecular sieving of hydrocarbons is still highly desirable. As the structure numbers of MOFs keep growing, there are also emerging technologies like machine learning under artificial intelligence for the computational design and discovery of novel MOF materials, while automated chemistry for high-throughput screening is also possible by combination with robotics.

As promising adsorbent materials for hydrocarbon separation, MOFs with high separation performance can be synthesized by combination of rational control of their pore size and pore surface. Continuous collaborative efforts among scientists, engineers and industrial partners will promote the application of MOF adsorbents to scientifically and technologically important industrial hydrocarbon separation, which would reap great benefits for society.

Conflicts of interest

There are no conflicts to declare.

Acknowledgements

The authors acknowledge supports from the National Natural Science Foundation of China (22090061, 22101307), the Hundred Talents Program of Sun Yat-Sen University and the Fundamental Research Funds for the Central Universities (Sun Yat-Sen University, 22qntd2301).

Notes and references

1 D. S. Sholl and R. P. Lively, Seven chemical separations to change the world, *Nature*, 2016, **532**, 435–437.
2 S. Chu, Y. Cui and N. Liu, The path towards sustainable energy, *Nat. Mater.*, 2017, **16**, 16–22.
3 H. Furukawa, K. E. Cordova, M. O'Keeffe and O. M. Yaghi, The Chemistry and Applications of Metal-Organic Frameworks, *Science*, 2013, **341**, 1230444.
4 S. Kitagawa, R. Kitaura and S. I. Noro, Functional Porous Coordination Polymers, *Angew. Chem., Int. Ed.*, 2004, **43**, 2334–2375.
5 B. Chen, S. Xiang and G. Qian, Metal-Organic Frameworks with Functional Pores for Recognition of Small Molecules, *Acc. Chem. Res.*, 2010, **43**, 1115–1124.
6 Y. Cui, B. Li, H. He, W. Zhou, B. Chen and G. Qian, Metal-Organic Frameworks as Platforms for Functional Materials, *Acc. Chem. Res.*, 2016, **49**, 483–493.
7 I. M. Hönicke, I. Senkovska, V. Bon, I. A. Baburin, N. Bönisch, S. Raschke, J. D. Evans and S. Kaskel, Balancing Mechanical Stability and Ultrahigh Porosity in Crystalline Framework Materials, *Angew. Chem., Int. Ed.*, 2018, **57**, 13780–13783.
8 Z.-S. Wang, M. Li, Y.-L. Peng, Z. Zhang, W. Chen and X.-C. Huang, An Ultrastable Metal Azolate Framework with Binding Pockets for Optimal Carbon Dioxide Capture, *Angew. Chem., Int. Ed.*, 2019, **58**, 16071–16076.
9 R.-B. Lin, S. Xiang, B. Li, Y. Cui, G. Qian, W. Zhou and B. Chen, Our journey of developing multifunctional metal-organic frameworks, *Coord. Chem. Rev.*, 2019, **384**, 21–36.
10 R.-B. Lin, S. Xiang, H. Xing, W. Zhou and B. Chen, Exploration of porous metal-organic frameworks for gas separation and purification, *Coord. Chem. Rev.*, 2019, **378**, 87–103.
11 K. Adil, Y. Belmabkhout, R. S. Pillai, A. Cadiau, P. M. Bhatt, A. H. Assen, G. Maurin, M. Eddaoudi and K. Adil, Gas/vapour separation using ultra-microporous metal-organic frameworks: insights into the structure/separation relationship, *Chem. Soc. Rev.*, 2017, **46**, 3402–3430.
12 J.-R. Li, R. J. Kuppler, H.-C. Zhou and J.-R. Li, Selective gas adsorption and separation in metal-organic frameworks, *Chem. Soc. Rev.*, 2009, **38**, 1477–1504.
13 R.-B. Lin, S. Xiang, W. Zhou and B. Chen, Microporous Metal-Organic Framework Materials for Gas Separation, *Chem*, 2020, **6**, 337–363.
14 R.-B. Lin, Z. Zhang and B. Chen, Achieving High Performance Metal-Organic Framework Materials through Pore Engineering, *Acc. Chem. Res.*, 2021, **54**, 3362–3376.

15 H. Wang and J. Li, Microporous Metal-Organic Frameworks for Adsorptive Separation of C_5–C_6 Alkane Isomers, *Acc. Chem. Res.*, 2019, **52**, 1968–1978.
16 H. Wang, Y. Liu and J. Li, Designer Metal-Organic Frameworks for Size-Exclusion-Based Hydrocarbon Separations: Progress and Challenges, *Adv. Mater.*, 2020, **32**, 2002603.
17 F. Xie, L. Yu, H. Wang and J. Li, Metal-Organic Frameworks for C_6 Alkane Separation, *Angew. Chem., Int. Ed.*, 2023, **62**, e202300722.
18 D.-D. Zhou and J.-P. Zhang, On the Role of Flexibility for Adsorptive Separation, *Acc. Chem. Res.*, 2022, **55**, 2966–2977.
19 J.-P. Zhang, Y.-B. Zhang, J.-B. Lin and X.-M. Chen, Metal Azolate Frameworks: From Crystal Engineering to Functional Materials, *Chem. Rev.*, 2011, **112**, 1001–1033.
20 Y. Wang and D. Zhao, Beyond Equilibrium: Metal-Organic Frameworks for Molecular Sieving and Kinetic Gas Separation, *Cryst. Growth Des.*, 2017, **17**, 2291–2308.
21 J.-P. Zhang, H.-L. Zhou, D.-D. Zhou, P.-Q. Liao and X.-M. Chen, Controlling flexibility of metal-organic frameworks, *Natl. Sci. Rev.*, 2018, **5**, 907–919.
22 I. Karakurt, G. Aydin and K. Aydiner, Mine ventilation air methane as a sustainable energy source, *Renewable Sustainable Energy Rev.*, 2011, **15**, 1042–1049.
23 Z. Niu, X. Cui, T. Pham, P. C. Lan, H. Xing, K. A. Forrest, L. Wojtas, B. Space and S. Ma, A Metal-Organic Framework Based Methane Nano-trap for the Capture of Coal-Mine Methane, *Angew. Chem., Int. Ed.*, 2019, **58**, 10138–10141.
24 S.-M. Wang, M. Shivanna and Q.-Y. Yang, Nickel-Based Metal-Organic Frameworks for Coal-Bed Methane Purification with Record CH_4/N_2 Selectivity, *Angew. Chem., Int. Ed.*, 2022, **61**, e202201017.
25 T. Li, X. Jia, H. Chen, Z. Chang, L. Li, Y. Wang and J. Li, Tuning the Pore Environment of MOFs toward Efficient CH_4/N_2 Separation under Humid Conditions, *ACS Appl. Mater. Interfaces*, 2022, **14**, 15830–15839.
26 M. Chang, Y. Zhao, D. Liu, J. Yang, J. Li and C. Zhong, Methane-trapping metal-organic frameworks with an aliphatic ligand for efficient CH_4/N_2 separation, *Sustainable Energy Fuels*, 2019, **4**, 138–142.
27 X.-W. Zhang, D.-D. Zhou and J.-P. Zhang, Tuning the gating energy barrier of metal-organic framework for molecular sieving, *Chem*, 2021, **7**, 1006–1019.
28 Q. Min Wang, D. Shen, M. Bülow, M. Ling Lau, S. Deng, F. R. Fitch, N. O. Lemcoff and J. Semanscin, Metallo-organic molecular sieve for gas separation and purification, *Microporous Mesoporous Mater.*, 2002, **55**, 217–230.
29 Z. Bao, S. Alnemrat, L. Yu, I. Vasiliev, Q. Ren, X. Lu and S. Deng, Adsorption of Ethane, Ethylene, Propane, and Propylene on a Magnesium-Based Metal-Organic Framework, *Langmuir*, 2011, **27**, 13554–13562.
30 E. D. Bloch, W. L. Queen, R. Krishna, J. M. Zadrozny, C. M. Brown and J. R. Long, Hydrocarbon Separations in a Metal-Organic Framework with Open Iron(II) Coordination Sites, *Science*, 2012, **335**, 1606–1610.
31 S. J. Geier, J. A. Mason, E. D. Bloch, W. L. Queen, M. R. Hudson, C. M. Brown and J. R. Long, Selective adsorption of ethylene over ethane and propylene over propane in the metal-organic frameworks M2(dobdc) (M = Mg, Mn, Fe, Co, Ni, Zn), *Chem. Sci.*, 2013, **4**, 2054.
32 G. Chang, M. Huang, Y. Su, H. Xing, B. Su, Z. Zhang, Q. Yang, Y. Yang, Q. Ren, Z. Bao and B. Chen, Immobilization of Ag(I) into a metal-organic framework with $-SO_3H$ sites for highly selective olefin–paraffin separation at room temperature, *Chem. Commun.*, 2015, **51**, 2859–2862.
33 J. E. Bachman, M. T. Kapelewski, D. A. Reed, M. I. Gonzalez and J. R. Long, M_2(m-dobdc) (M = Mn, Fe, Co, Ni) Metal-Organic Frameworks as Highly Selective, High-Capacity Adsorbents for Olefin/Paraffin Separations, *J. Am. Chem. Soc.*, 2017, **139**, 15363–15370.
34 S. Sen, N. Hosono, J.-J. Zheng, S. Kusaka, R. Matsuda, S. Sakaki and S. Kitagawa, Cooperative Bond Scission in a Soft Porous Crystal Enables Discriminatory Gate Opening for Ethylene over Ethane, *J. Am. Chem. Soc.*, 2017, **139**, 18313–18321.
35 R.-B. Lin, L. Li, H.-L. Zhou, H. Wu, C. He, S. Li, R. Krishna, J. Li, W. Zhou and B. Chen, Molecular sieving of ethylene from ethane using a rigid metal-organic framework, *Nat. Mater.*, 2018, **17**, 1128–1133.
36 Z. Bao, J. Wang, Z. Zhang, H. Xing, Q. Yang, Y. Yang, H. Wu, R. Krishna, W. Zhou, B. Chen and Q. Ren, Molecular Sieving of Ethane from Ethylene through the Molecular Cross-Section Size Differentiation in Gallate-based Metal-Organic Frameworks, *Angew. Chem., Int. Ed.*, 2018, **57**, 16020–16025.
37 C. Gu, N. Hosono, J.-J. Zheng, Y. Sato, S. Kusaka, S. Sakaki and S. Kitagawa, Design and control of gas diffusion process in a nanoporous soft crystal, *Science*, 2019, **363**, 387–391.
38 M. H. Mohamed, Y. Yang, L. Li, S. Zhang, J. P. Ruffley, A. G. Jarvi, S. Saxena, G. Veser, J. K. Johnson and N. L. Rosi, Designing Open Metal Sites in Metal-Organic Frameworks for Paraffin/Olefin Separations, *J. Am. Chem. Soc.*, 2019, **141**, 13003–13007.
39 Q. Ding, Z. Zhang, C. Yu, P. Zhang, J. Wang, X. Cui, C.-H. He, S. Deng and H. Xing, Exploiting equilibrium-kinetic synergetic effect for separation of ethylene and ethane in a microporous metal-organic framework, *Sci. Adv.*, 2020, **6**, eaaz4322.
40 C. Yu, Z. Guo, L. Yang, J. Cui, S. Chen, Y. Bo, X. Suo, Q. Gong, S. Zhang, X. Cui, S. He and H. Xing, A Robust Metal-Organic Framework with Scalable Synthesis and Optimal Adsorption and Desorption for Energy-Efficient Ethylene Purification, *Angew. Chem., Int. Ed.*, 2023, **62**, e202218027.
41 L. Zhang, L. Li, E. Hu, L. Yang, K. Shao, L. Yao, K. Jiang, Y. Cui, Y. Yang, B. Li, B. Chen and G. Qian, Boosting Ethylene/Ethane Separation within Copper(I)-Chelated Metal-Organic Frameworks through Tailor-Made Aperture and Specific π-Complexation, *Adv. Sci.*, 2020, **7**, 1901918.
42 P. J. Bereciartua, Á. Cantín, A. Corma, J. L. Jordá, M. Palomino, F. Rey, S. Valencia, E. W. Corcoran, P. Kortunov, P. I. Ravikovitch, A. Burton, C. Yoon,

Y. Wang, C. Paur, J. Guzman, A. R. Bishop and G. L. Casty, Control of zeolite framework flexibility and pore topology for separation of ethane and ethylene, *Science*, 2017, **358**, 1068–1071.

43 B. Li, Y. Zhang, R. Krishna, K. Yao, Y. Han, Z. Wu, D. Ma, Z. Shi, T. Pham, B. Space, J. Liu, P. K. Thallapally, J. Liu, M. Chrzanowski and S. Ma, Introduction of π-Complexation into Porous Aromatic Framework for Highly Selective Adsorption of Ethylene over Ethane, *J. Am. Chem. Soc.*, 2014, **136**, 8654–8660.

44 Y. Yang, L. Li, R.-B. Lin, Y. Ye, Z. Yao, L. Yang, F. Xiang, S. Chen, Z. Zhang, S. Xiang and B. Chen, Ethylene/ethane separation in a stable hydrogen-bonded organic framework through a gating mechanism, *Nat. Chem.*, 2021, **13**, 933–939.

45 J. W. Yoon, Y.-K. Seo, Y. K. Hwang, J.-S. Chang, H. Leclerc, S. Wuttke, P. Bazin, A. Vimont, M. Daturi, E. Bloch, P. L. Llewellyn, C. Serre, P. Horcajada, J.-M. Grenèche, A. E. Rodrigues and G. Férey, Controlled Reducibility of a Metal-Organic Framework with Coordinatively Unsaturated Sites for Preferential Gas Sorption, *Angew. Chem., Int. Ed.*, 2010, **49**, 5949–5952.

46 C.-X. Chen, Z.-W. Wei, T. Pham, P. C. Lan, L. Zhang, K. A. Forrest, S. Chen, A. M. Al-Enizi, A. Nafady, C.-Y. Su and S. Ma, Nanospace Engineering of Metal-Organic Frameworks through Dynamic Spacer Installation of Multifunctionalities for Efficient Separation of Ethane from Ethane/Ethylene Mixtures, *Angew. Chem., Int. Ed.*, 2021, **60**, 9680–9685.

47 J. Pires, M. L. Pinto and V. K. Saini, Ethane Selective IRMOF-8 and Its Significance in Ethane–Ethylene Separation by Adsorption, *ACS Appl. Mater. Interfaces*, 2014, **6**, 12093–12099.

48 H. Yang, Y. Wang, R. Krishna, X. Jia, Y. Wang, A. N. Hong, C. Dang, H. E. Castillo, X. Bu and P. Feng, Pore-Space-Partition-Enabled Exceptional Ethane Uptake and Ethane-Selective Ethane–Ethylene Separation, *J. Am. Chem. Soc.*, 2020, **142**, 2222–2227.

49 Z. Y. Di, C. P. Liu, J. D. Pang, S. X. Zou, Z. Y. Ji, F. L. Hu, C. Chen, D. Q. Yuan, M. C. Hong and M. Y. Wu, A Metal-Organic Framework with Nonpolar Pore Surfaces for the One-Step Acquisition of C_2H_4 from a C_2H_4 and C_2H_6 Mixture, *Angew. Chem., Int. Ed.*, 2022, **61**, e202210343.

50 S. Geng, E. Lin, X. Li, W. Liu, T. Wang, Z. Wang, D. Sensharma, S. Darwish, Y. H. Andaloussi, T. Pham, P. Cheng, M. J. Zaworotko, Y. Chen and Z. Zhang, Scalable Room-Temperature Synthesis of Highly Robust Ethane-Selective Metal-Organic Frameworks for Efficient Ethylene Purification, *J. Am. Chem. Soc.*, 2021, **143**, 8654–8660.

51 M. Kang, S. Yoon, S. Ga, D. W. Kang, S. Han, J. H. Choe, H. Kim, D. W. Kim, Y. G. Chung and C. S. Hong, High-Throughput Discovery of $Ni(IN)_2$ for Ethane/Ethylene Separation, *Adv. Sci.*, 2021, **8**, 2004940.

52 Y.-P. Li, Y.-N. Zhao, S.-N. Li, D.-Q. Yuan, Y.-C. Jiang, X. Bu, M.-C. Hu and Q.-G. Zhai, Ultrahigh-Uptake Capacity-Enabled Gas Separation and Fruit Preservation by a New Single-Walled Nickel-Organic Framework, *Adv. Sci.*, 2021, **8**, 2003141.

53 W. Liu, S. Geng, N. Li, S. Wang, S. Jia, F. Jin, T. Wang, K. A. Forrest, T. Pham, P. Cheng, Y. Chen, J.-G. Ma and Z. Zhang, Highly Robust Microporous Metal-Organic Frameworks for Efficient Ethylene Purification under Dry and Humid Conditions, *Angew. Chem., Int. Ed.*, 2023, **62**, e202217662.

54 A. A. Lysova, D. G. Samsonenko, K. A. Kovalenko, A. S. Nizovtsev, D. N. Dybtsev and V. P. Fedin, A Series of Mesoporous Metal-Organic Frameworks with Tunable Windows Sizes and Exceptionally High Ethane over Ethylene Adsorption Selectivity, *Angew. Chem., Int. Ed.*, 2020, **59**, 20561–20567.

55 J. Pei, J.-X. Wang, K. Shao, Y. Yang, Y. Cui, H. Wu, W. Zhou, B. Li and G. Qian, Engineering microporous ethane-trapping metal-organic frameworks for boosting ethane/ethylene separation, *J. Mater. Chem. A*, 2020, **8**, 3613–3620.

56 O. T. Qazvini, R. Babarao, Z.-L. Shi, Y.-B. Zhang and S. G. Telfer, A Robust Ethane-Trapping Metal-Organic Framework with a High Capacity for Ethylene Purification, *J. Am. Chem. Soc.*, 2019, **141**, 5014–5020.

57 Y. Ye, Y. Xie, Y. Shi, L. Gong, J. Phipps, A. M. Al-Enizi, A. Nafady, B. Chen and S. Ma, A Microporous Metal-Organic Framework with Unique Aromatic Pore Surfaces for High Performance C_2H_6/C_2H_4 Separation, *Angew. Chem., Int. Ed.*, 2023, **62**, e202302564.

58 C. Gücüyener, J. van den Bergh, J. Gascon and F. Kapteijn, Ethane/Ethene Separation Turned on Its Head: Selective Ethane Adsorption on the Metal-Organic Framework ZIF-7 through a Gate-Opening Mechanism, *J. Am. Chem. Soc.*, 2010, **132**, 17704–17706.

59 P.-Q. Liao, W.-X. Zhang, J.-P. Zhang and X.-M. Chen, Efficient purification of ethene by an ethane-trapping metal-organic framework, *Nat. Commun.*, 2015, **6**, 8697.

60 R.-B. Lin, H. Wu, L. Li, X.-L. Tang, Z. Li, J. Gao, H. Cui, W. Zhou and B. Chen, Boosting Ethane/Ethylene Separation within Isoreticular Ultramicroporous Metal-Organic Frameworks, *J. Am. Chem. Soc.*, 2018, **140**, 12940–12946.

61 L. Li, R.-B. Lin, R. Krishna, H. Li, S. Xiang, H. Wu, J. Li, W. Zhou and B. Chen, Ethane/ethylene separation in a metal-organic framework with iron-peroxo sites, *Science*, 2018, **362**, 443–446.

62 S. Jiang, J. Li, M. Feng, R. Chen, L. Guo, Q. Xu, L. Chen, F. Shen, Z. Zhang, Y. Yang, Q. Ren, Q. Yang and Z. Bao, Hydrophobic paraffin-selective pillared-layer MOFs for olefin purification, *J. Mater. Chem. A*, 2022, **10**, 24127–24136.

63 G. D. Wang, R. Krishna, Y. Z. Li, W. J. Shi, L. Hou, Y. Y. Wang and Z. H. Zhu, Boosting Ethane/Ethylene Separation by MOFs through the Amino-Functionalization of Pores, *Angew. Chem., Int. Ed.*, 2022, **61**, e202213015.

64 L. Yang, L. Yan, W. Niu, Y. Feng, Q. Fu, S. Zhang, Y. Zhang, L. Li, X. Gu, P. Dai, D. Liu, Q. Zheng and X. Zhao, Adsorption in Reversed Order of C_2 Hydrocarbons on an Ultramicroporous Fluorinated Metal-Organic Framework, *Angew. Chem., Int. Ed.*, 2022, **61**, e202204046.

65 M. H. Yu, H. Fang, H. L. Huang, M. Zhao, Z. Y. Su, H. X. Nie, Z. Chang and T. L. Hu, Tuning the Trade-Off

between Ethane/Ethylene Selectivity and Adsorption Capacity within Isoreticular Microporous Metal-Organic Frameworks by Linker Fine-Fluorination, *Small*, 2023, **19**, 2300821.

66 H. Zeng, X.-J. Xie, M. Xie, Y.-L. Huang, D. Luo, T. Wang, Y. Zhao, W. Lu and D. Li, Cage-Interconnected Metal-Organic Framework with Tailored Apertures for Efficient C_2H_6/C_2H_4 Separation under Humid Conditions, *J. Am. Chem. Soc.*, 2019, **141**, 20390–20396.

67 S.-C. Xiang, Z. Zhang, C.-G. Zhao, K. Hong, X. Zhao, D.-R. Ding, M.-H. Xie, C.-D. Wu, M. C. Das, R. Gill, K. M. Thomas and B. Chen, Rationally tuned micropores within enantiopure metal-organic frameworks for highly selective separation of acetylene and ethylene, *Nat. Commun.*, 2011, **2**, 204.

68 T.-L. Hu, H. Wang, B. Li, R. Krishna, H. Wu, W. Zhou, Y. Zhao, Y. Han, X. Wang, W. Zhu, Z. Yao, S. Xiang and B. Chen, Microporous metal-organic framework with dual functionalities for highly efficient removal of acetylene from ethylene/acetylene mixtures, *Nat. Commun.*, 2015, **6**, 7328.

69 S. Yang, A. J. Ramirez-Cuesta, R. Newby, V. Garcia-Sakai, P. Manuel, S. K. Callear, S. I. Campbell, C. C. Tang and M. Schröder, Supramolecular binding and separation of hydrocarbons within a functionalized porous metal-organic framework, *Nat. Chem.*, 2015, **7**, 121–129.

70 X. Cui, K. Chen, H. Xing, Q. Yang, R. Krishna, Z. Bao, H. Wu, W. Zhou, X. Dong, Y. Han, B. Li, Q. Ren, M. J. Zaworotko and B. Chen, Pore chemistry and size control in hybrid porous materials for acetylene capture from ethylene, *Science*, 2016, **353**, 141–144.

71 B. Li, X. Cui, D. O'Nolan, H.-M. Wen, M. Jiang, R. Krishna, H. Wu, R.-B. Lin, Y.-S. Chen, D. Yuan, H. Xing, W. Zhou, Q. Ren, G. Qian, M. J. Zaworotko and B. Chen, An Ideal Molecular Sieve for Acetylene Removal from Ethylene with Record Selectivity and Productivity, *Adv. Mater.*, 2017, **29**, 1704210.

72 R.-B. Lin, L. Li, H. Wu, H. Arman, B. Li, R.-G. Lin, W. Zhou and B. Chen, Optimized Separation of Acetylene from Carbon Dioxide and Ethylene in a Microporous Material, *J. Am. Chem. Soc.*, 2017, **139**, 8022–8028.

73 T. Ke, Q. Wang, J. Shen, J. Zhou, Z. Bao, Q. Yang and Q. Ren, Molecular Sieving of C_2-C_3 Alkene from Alkyne with Tuned Threshold Pressure in Robust Layered Metal-Organic Frameworks, *Angew. Chem., Int. Ed.*, 2020, **59**, 12725–12730.

74 S. Mukherjee, S. Chen, A. A. Bezrukov, M. Mostrom, V. V. Terskikh, D. Franz, S.-Q. Wang, A. Kumar, M. Chen, B. Space, Y. Huang and M. J. Zaworotko, Ultramicropore Engineering by Dehydration to Enable Molecular Sieving of H2 by Calcium Trimesate, *Angew. Chem., Int. Ed.*, 2020, **59**, 16188–16194.

75 J. Shen, X. He, T. Ke, R. Krishna, J. M. van Baten, R. Chen, Z. Bao, H. Xing, M. Dincă, Z. Zhang, Q. Yang and Q. Ren, Simultaneous interlayer and intralayer space control in two-dimensional metal-organic frameworks for acetylene/ethylene separation, *Nat. Commun.*, 2020, **11**, 6259.

76 J. Wang, Y. Zhang, P. Zhang, J. Hu, R.-B. Lin, Q. Deng, Z. Zeng, H. Xing, S. Deng and B. Chen, Optimizing Pore Space for Flexible-Robust Metal-Organic Framework to Boost Trace Acetylene Removal, *J. Am. Chem. Soc.*, 2020, **142**, 9744–9751.

77 Z. Zhang, S. B. Peh, Y. Wang, C. Kang, W. Fan and D. Zhao, Efficient Trapping of Trace Acetylene from Ethylene in an Ultramicroporous Metal-Organic Framework: Synergistic Effect of High-Density Open Metal and Electronegative Sites, *Angew. Chem., Int. Ed.*, 2020, **59**, 18927–18932.

78 J.-W. Wang, S.-C. Fan, H.-P. Li, X. Bu, Y.-Y. Xue and Q.-G. Zhai, De-Linker-Enabled Exceptional Volumetric Acetylene Storage Capacity and Benchmark C_2H_2/C_2H_4 and C_2H_2/CO_2 Separations in Metal-Organic Frameworks, *Angew. Chem., Int. Ed.*, 2023, **62**, e202217839.

79 H.-G. Hao, Y.-F. Zhao, D.-M. Chen, J.-M. Yu, K. Tan, S. Ma, Y. Chabal, Z.-M. Zhang, J.-M. Dou, Z.-H. Xiao, G. Day, H.-C. Zhou and T.-B. Lu, Simultaneous Trapping of C_2H_2 and C_2H_6 from a Ternary Mixture of $C_2H_2/C_2H_4/C_2H_6$ in a Robust Metal-Organic Framework for the Purification of C_2H_4, *Angew. Chem., Int. Ed.*, 2018, **57**, 16067–16071.

80 K.-J. Chen, D. G. Madden, S. Mukherjee, T. Pham, K. A. Forrest, A. Kumar, B. Space, J. Kong, Q.-Y. Zhang and M. J. Zaworotko, Synergistic sorbent separation for one-step ethylene purification from a four-component mixture, *Science*, 2019, **366**, 241–246.

81 Q. Dong, X. Zhang, S. Liu, R.-B. Lin, Y. Guo, Y. Ma, A. Yonezu, R. Krishna, G. Liu, J. Duan, R. Matsuda, W. Jin and B. Chen, Tuning Gate-Opening of a Flexible Metal-Organic Framework for Ternary Gas Sieving Separation, *Angew. Chem., Int. Ed.*, 2020, **59**, 22756–22762.

82 Z. Xu, X. Xiong, J. Xiong, R. Krishna, L. Li, Y. Fan, F. Luo and B. Chen, A robust Th-azole framework for highly efficient purification of C2H4 from a C2H4/C2H2/C2H6 mixture, *Nat. Commun.*, 2020, **11**, 3163.

83 J.-W. Cao, S. Mukherjee, T. Pham, Y. Wang, T. Wang, T. Zhang, X. Jiang, H.-J. Tang, K. A. Forrest, B. Space, M. J. Zaworotko and K.-J. Chen, One-step ethylene production from a four-component gas mixture by a single physisorbent, *Nat. Commun.*, 2021, **12**, 6507.

84 S. Mukherjee, N. Kumar, A. A. Bezrukov, K. Tan, T. Pham, K. A. Forrest, K. A. Oyekan, O. T. Qazvini, D. G. Madden, B. Space and M. J. Zaworotko, Amino-Functionalised Hybrid Ultramicroporous Materials that Enable Single-Step Ethylene Purification from a Ternary Mixture, *Angew. Chem., Int. Ed.*, 2021, **60**, 10902–10909.

85 Y. Wang, C. Hao, W. Fan, M. Fu, X. Wang, Z. Wang, L. Zhu, Y. Li, X. Lu, F. Dai, Z. Kang, R. Wang, W. Guo, S. Hu and D. Sun, One-step Ethylene Purification from an Acetylene/Ethylene/Ethane Ternary Mixture by Cyclopentadiene Cobalt-Functionalized Metal-Organic Frameworks, *Angew. Chem., Int. Ed.*, 2021, **60**, 11350–11358.

86 B. Zhu, J. W. Cao, S. Mukherjee, T. Pham, T. Zhang, T. Wang, X. Jiang, K. A. Forrest, M. J. Zaworotko and K. J. Chen, Pore Engineering for One-Step Ethylene Purification from a Three-Component Hydrocarbon Mixture, *J. Am. Chem. Soc.*, 2021, **143**, 1485–1492.

87 Q. Ding, Z. Zhang, Y. Liu, K. Chai, R. Krishna and S. Zhang, One-Step Ethylene Purification from Ternary Mixtures in a Metal-Organic Framework with Customized Pore Chemistry and Shape, *Angew. Chem., Int. Ed.*, 2022, **61**, e202208134.

88 X. W. Gu, J. X. Wang, E. Wu, H. Wu, W. Zhou, G. Qian, B. Chen and B. Li, Immobilization of Lewis Basic Sites into a Stable Ethane-Selective MOF Enabling One-Step Separation of Ethylene from a Ternary Mixture, *J. Am. Chem. Soc.*, 2022, **144**, 2614–2623.

89 G. D. Wang, Y. Z. Li, W. J. Shi, L. Hou, Y. Y. Wang and Z. Zhu, One-Step C_2H_4 Purification from Ternary C_2H_6/C_2H_4/C_2H_2 Mixtures by a Robust Metal-Organic Framework with Customized Pore Environment, *Angew. Chem., Int. Ed.*, 2022, **61**, e202205427.

90 Y. Wang, M. Fu, S. Zhou, H. Liu, X. Wang, W. Fan, Z. Liu, Z. Wang, D. Li, H. Hao, X. Lu, S. Hu and D. Sun, Guest-molecule-induced self-adaptive pore engineering facilitates purification of ethylene from ternary mixture, *Chem*, 2022, **8**, 3263–3274.

91 P. Zhang, Y. Zhong, Y. Zhang, Z. Zhu, Y. Liu, Y. Su, J. Chen, S. Chen, Z. Zeng, H. Xing, S. Deng and J. Wang, Synergistic binding sites in a hybrid ultramicroporous material for one-step ethylene purification from ternary C2 hydrocarbon mixtures, *Sci. Adv.*, 2022, **8**, eabn9231.

92 Y. Jiang, Y. Hu, B. Luan, L. Wang, R. Krishna, H. Ni, X. Hu and Y. Zhang, Benchmark single-step ethylene purification from ternary mixtures by a customized fluorinated anion-embedded MOF, *Nat. Commun.*, 2023, **14**, 401.

93 H. Sun, F. Chen, R. Chen, J. Li, L. Guo, Y. Liu, F. Shen, Q. Yang, Z. Zhang, Q. Ren and Z. Bao, Customizing Metal-Organic Frameworks by Lego-Brick Strategy for One-Step Purification of Ethylene from a Quaternary Gas Mixture, *Small*, 2023, **19**, e2208182.

94 L. Wang, H. Huang, X. Zhang, H. Zhao, F. Li and Y. Gu, Designed metal-organic frameworks with potential for multi-component hydrocarbon separation, *Coord. Chem. Rev.*, 2023, **484**, 215111.

95 J.-P. Zhang and X.-M. Chen, Optimized Acetylene/Carbon Dioxide Sorption in a Dynamic Porous Crystal, *J. Am. Chem. Soc.*, 2009, **131**, 5516–5521.

96 C.-T. He, Z.-M. Ye, Y.-T. Xu, D.-D. Zhou, H.-L. Zhou, D. Chen, J.-P. Zhang and X.-M. Chen, Hyperfine adjustment of flexible pore-surface pockets enables smart recognition of gas size and quadrupole moment, *Chem. Sci.*, 2017, **8**, 7560–7565.

97 X. Liu, P. Zhang, H. Xiong, Y. Zhang, K. Wu, J. Liu, R. Krishna, J. Chen, S. Chen, Z. Zeng, S. Deng and J. Wang, Engineering Pore Environments of Sulfate-pillared Metal-Organic Framework for Efficient C_2H_2/CO_2 Separation with Record Selectivity, *Adv. Mater.*, 2023, **35**, 2210415.

98 X. Zhu, T. Ke, J. Zhou, Y. Song, Q. Xu, Z. Zhang, Z. Bao, Y. Yang, Q. Ren and Q. Yang, Vertex Strategy in Layered 2D MOFs: Simultaneous Improvement of Thermodynamics and Kinetics for Record C_2H_2/CO_2 Separation Performance, *J. Am. Chem. Soc.*, 2023, **145**, 9254–9263.

99 R. Matsuda, R. Kitaura, S. Kitagawa, Y. Kubota, R. V. Belosludov, T. C. Kobayashi, H. Sakamoto, T. Chiba, M. Takata, Y. Kawazoe and Y. Mita, Highly controlled acetylene accommodation in a metal-organic microporous material, *Nature*, 2005, **436**, 238–241.

100 J. Gao, X. Qian, R.-B. Lin, R. Krishna, H. Wu, W. Zhou and B. Chen, Mixed Metal-Organic Framework with Multiple Binding Sites for Efficient C_2H_2/CO_2 Separation, *Angew. Chem., Int. Ed.*, 2020, **59**, 4396–4400.

101 F. Luo, C. Yan, L. Dang, R. Krishna, W. Zhou, H. Wu, X. Dong, Y. Han, T.-L. Hu, M. O'Keeffe, L. Wang, M. Luo, R.-B. Lin and B. Chen, UTSA-74: A MOF-74 Isomer with Two Accessible Binding Sites per Metal Center for Highly Selective Gas Separation, *J. Am. Chem. Soc.*, 2016, **138**, 5678–5684.

102 Z. Niu, X. Cui, T. Pham, G. Verma, P. C. Lan, C. Shan, H. Xing, K. A. Forrest, S. Suepaul, B. Space, A. Nafady, A. M. Al-Enizi and S. Ma, A MOF-based Ultra-Strong Acetylene Nano-trap for Highly Efficient C_2H_2/CO_2 Separation, *Angew. Chem., Int. Ed.*, 2021, **60**, 5283–5288.

103 J. Pei, K. Shao, J.-X. Wang, H.-M. Wen, Y. Yang, Y. Cui, R. Krishna, B. Li and G. Qian, A Chemically Stable Hofmann-Type Metal-Organic Framework with Sandwich-Like Binding Sites for Benchmark Acetylene Capture, *Adv. Mater.*, 2020, **32**, 1908275.

104 Y.-L. Peng, T. Pham, P. Li, T. Wang, Y. Chen, K.-J. Chen, K. A. Forrest, B. Space, P. Cheng, M. J. Zaworotko and Z. Zhang, Robust Ultramicroporous Metal-Organic Frameworks with Benchmark Affinity for Acetylene, *Angew. Chem., Int. Ed.*, 2018, **57**, 10971–10975.

105 K. Shao, H.-M. Wen, C.-C. Liang, X. Xiao, X.-W. Gu, B. Chen, G. Qian and B. Li, Engineering Supramolecular Binding Sites in a Chemically Stable Metal-Organic Framework for Simultaneous High C_2H_2 Storage and Separation, *Angew. Chem., Int. Ed.*, 2022, **61**, e202211523.

106 H. Zeng, M. Xie, Y.-L. Huang, Y. Zhao, X.-J. Xie, J.-P. Bai, M.-Y. Wan, R. Krishna, W. Lu and D. Li, Induced Fit of C_2H_2 in a Flexible MOF Through Cooperative Action of Open Metal Sites, *Angew. Chem., Int. Ed.*, 2019, **58**, 8515–8519.

107 L. Zhang, K. Jiang, L. Yang, L. Li, E. Hu, L. Yang, K. Shao, H. Xing, Y. Cui, Y. Yang, B. Li, B. Chen and G. Qian, Benchmark C_2H_2/CO_2 Separation in an Ultra-Microporous Metal-Organic Framework via Copper(I)-Alkynyl Chemistry, *Angew. Chem., Int. Ed.*, 2021, **60**, 15995–16002.

108 H. Zeng, X.-J. Xie, Y. Wang, D. Luo, R.-J. Wei, W. Lu and D. Li, Spatial disposition of square-planar mononuclear nodes in metal-organic frameworks for C_2H_2/CO_2 separation, *Chem. Sci.*, 2022, **13**, 12876–12882.

109 S. R. Caskey, A. G. Wong-Foy and A. J. Matzger, Dramatic Tuning of Carbon Dioxide Uptake via Metal Substitution in a Coordination Polymer with Cylindrical Pores, *J. Am. Chem. Soc.*, 2008, **130**, 10870–10871.

110 M. Fischer, F. Hoffmann and M. Fröba, New Microporous Materials for Acetylene Storage and C_2H_2/CO_2 Separation: Insights from Molecular Simulations, *ChemPhysChem*, 2010, **11**, 2220–2229.

111 S. Xiang, W. Zhou, J. M. Gallegos, Y. Liu and B. Chen, Exceptionally high acetylene uptake in a microporous metal-organic framework with open metal sites, *J. Am. Chem. Soc.*, 2009, **131**, 12415–12419.

112 Y.-P. Li, Y. Wang, Y.-Y. Xue, H.-P. Li, Q.-G. Zhai, S.-N. Li, Y.-C. Jiang, M.-C. Hu and X. Bu, Ultramicroporous Building Units as a Path to Bi-microporous Metal-Organic Frameworks with High Acetylene Storage and Separation Performance, *Angew. Chem., Int. Ed.*, 2019, **58**, 13590–13595.

113 W. Fan, S. Yuan, W. Wang, L. Feng, X. Liu, X. Zhang, X. Wang, Z. Kang, F. Dai, D. Yuan, D. Sun and H.-C. Zhou, Optimizing Multivariate Metal-Organic Frameworks for Efficient C_2H_2/CO_2 Separation, *J. Am. Chem. Soc.*, 2020, **142**, 8728–8737.

114 L. Yang, L. Yan, Y. Wang, Z. Liu, J. He, Q. Fu, D. Liu, X. Gu, P. Dai, L. Li and X. Zhao, Adsorption Site Selective Occupation Strategy within a Metal-Organic Framework for Highly Efficient Sieving Acetylene from Carbon Dioxide, *Angew. Chem., Int. Ed.*, 2021, **60**, 4570–4574.

115 J. Pei, H.-M. Wen, X.-W. Gu, Q.-L. Qian, Y. Yang, Y. Cui, B. Li, B. Chen and G. Qian, Dense Packing of Acetylene in a Stable and Low-Cost Metal-Organic Framework for Efficient C_2H_2/CO_2 Separation, *Angew. Chem., Int. Ed.*, 2021, **60**, 25068–25074.

116 X. Zhang, R.-B. Lin, H. Wu, Y. Huang, Y. Ye, J. Duan, W. Zhou, J.-R. Li and B. Chen, Maximizing acetylene packing density for highly efficient C_2H_2/CO_2 separation through immobilization of amine sites within a prototype MOF, *Chem. Eng. J.*, 2022, **431**, 134184.

117 Z. Di, C. Liu, J. Pang, C. Chen, F. Hu, D. Yuan, M. Wu and M. Hong, Cage-Like Porous Materials with Simultaneous High C_2H_2 Storage and Excellent C_2H_2/CO_2 Separation Performance, *Angew. Chem., Int. Ed.*, 2021, **60**, 10828–10832.

118 W. Gong, H. Cui, Y. Xie, Y. Li, X. Tang, Y. Liu, Y. Cui and B. Chen, Efficient C_2H_2/CO_2 Separation in Ultramicroporous Metal-Organic Frameworks with Record C_2H_2 Storage Density, *J. Am. Chem. Soc.*, 2021, **143**, 14869–14876.

119 J. Lee, C. Y. Chuah, J. Kim, Y. Kim, N. Ko, Y. Seo, K. Kim, T. H. Bae and E. Lee, Separation of Acetylene from Carbon Dioxide and Ethylene by a Water-Stable Microporous Metal-Organic Framework with Aligned Imidazolium Groups inside the Channels, *Angew. Chem., Int. Ed.*, 2018, **57**, 7869–7873.

120 L. Liu, Z. Yao, Y. Ye, Y. Yang, Q. Lin, Z. Zhang, M. O'Keeffe and S. Xiang, Integrating the Pillared-Layer Strategy and Pore-Space Partition Method to Construct Multicomponent MOFs for C_2H_2/CO_2 Separation, *J. Am. Chem. Soc.*, 2020, **142**, 9258–9266.

121 L. Wang, W. Sun, Y. Zhang, N. Xu, R. Krishna, J. Hu, Y. Jiang, Y. He and H. Xing, Interpenetration Symmetry Control Within Ultramicroporous Robust Boron Cluster Hybrid MOFs for Benchmark Purification of Acetylene from Carbon Dioxide, *Angew. Chem., Int. Ed.*, 2021, **60**, 22865–22870.

122 Y. Ye, Z. Ma, R.-B. Lin, R. Krishna, W. Zhou, Q. Lin, Z. Zhang, S. Xiang and B. Chen, Pore Space Partition within a Metal-Organic Framework for Highly Efficient C_2H_2/CO_2 Separation, *J. Am. Chem. Soc.*, 2019, **141**, 4130–4136.

123 Y. Ye, S. Xian, H. Cui, K. Tan, L. Gong, B. Liang, T. Pham, H. Pandey, R. Krishna, P. C. Lan, K. A. Forrest, B. Space, T. Thonhauser, J. Li and S. Ma, Metal-Organic Framework Based Hydrogen-Bonding Nanotrap for Efficient Acetylene Storage and Separation, *J. Am. Chem. Soc.*, 2022, **144**, 1681–1689.

124 Q.-G. Zhai, X. Bu, X. Zhao, D.-S. Li and P. Feng, Pore Space Partition in Metal-Organic Frameworks, *Acc. Chem. Res.*, 2017, **50**, 407–417.

125 J. Wang, Y. Zhang, Y. Su, X. Liu, P. Zhang, R.-B. Lin, S. Chen, Q. Deng, Z. Zeng, S. Deng and B. Chen, Fine pore engineering in a series of isoreticular metal-organic frameworks for efficient C_2H_2/CO_2 separation, *Nat. Commun.*, 2022, **13**, 200.

126 M. Shivanna, K.-i Otake, B.-Q. Song, L. M. van Wyk, Q.-Y. Yang, N. Kumar, W. K. Feldmann, T. Pham, S. Suepaul, B. Space, L. J. Barbour, S. Kitagawa and M. J. Zaworotko, Benchmark Acetylene Binding Affinity and Separation through Induced Fit in a Flexible Hybrid Ultramicroporous Material, *Angew. Chem., Int. Ed.*, 2021, **60**, 20383–20390.

127 J. Tian, Q. Chen, F. Jiang, D. Yuan and M. Hong, Optimizing Acetylene Sorption through Induced-fit Transformations in a Chemically Stable Microporous Framework, *Angew. Chem., Int. Ed.*, 2023, **62**, e202215253.

128 D. Sensharma, D. J. O'Hearn, A. Koochaki, A. A. Bezrukov, N. Kumar, B. H. Wilson, M. Vandichel and M. J. Zaworotko, The First Sulfate-Pillared Hybrid Ultramicroporous Material, SOFOUR-1-Zn, and Its Acetylene Capture Properties, *Angew. Chem., Int. Ed.*, 2022, **61**, e202116145.

129 L.-Z. Cai, Z.-Z. Yao, S.-J. Lin, M.-S. Wang and G.-C. Guo, Photoinduced Electron-Transfer (PIET) Strategy for Selective Adsorption of CO_2 over C_2H_2 in a MOF, *Angew. Chem., Int. Ed.*, 2021, **60**, 18223–18230.

130 K.-J. Chen, H. S. Scott, D. G. Madden, T. Pham, A. Kumar, A. Bajpai, M. Lusi, K. A. Forrest, B. Space, J. J. Perry and M. J. Zaworotko, Benchmark C2H2/CO2 and CO2/C2H2 Separation by Two Closely Related Hybrid Ultramicroporous Materials, *Chem*, 2016, **1**, 753–765.

131 D. S. Choi, D. W. Kim, D. W. Kang, M. Kang, Y. S. Chae and C. S. Hong, Highly selective CO_2 separation from a CO_2/C_2H_2 mixture using a diamine-appended metal-organic framework, *J. Mater. Chem. A*, 2021, **9**, 21424–21428.

132 J. Cui, Z. Qiu, L. Yang, Z. Zhang, X. Cui and H. Xing, Kinetic-Sieving of Carbon Dioxide from Acetylene through a Novel Sulfonic Ultramicroporous Material, *Angew. Chem., Int. Ed.*, 2022, **61**, e202208756.

133 M. L. Foo, R. Matsuda, Y. Hijikata, R. Krishna, H. Sato, S. Horike, A. Hori, J. Duan, Y. Sato, Y. Kubota, M. Takata and S. Kitagawa, An Adsorbate Discriminatory Gate Effect in a Flexible Porous Coordination Polymer for Selective Adsorption of CO_2 over C_2H_2, *J. Am. Chem. Soc.*, 2016, **138**, 3022–3030.

134 Y. Gu, J.-J. Zheng, K.-I. Otake, M. Shivanna, S. Sakaki, H. Yoshino, M. Ohba, S. Kawaguchi, Y. Wang, F. Li and

S. Kitagawa, Host-Guest Interaction Modulation in Porous Coordination Polymers for Inverse Selective CO_2/C_2H_2 Separation, *Angew. Chem., Int. Ed.*, 2021, **60**, 11688–11694.

135 C. Hao, H. Ren, H. Zhu, Y. Chi, W. Zhao, X. Liu and W. Guo, CO2-favored metal-organic frameworks SU-101(M) (M = Bi, In, Ga, and Al) with inverse and high selectivity of CO2 from C2H2 and C2H4, *Sep. Purif. Technol.*, 2022, **290**, 120804.

136 C. He, P. Zhang, Y. Wang, Y. Zhang, T. Hu, L. Li and J. Li, Thermodynamic and kinetic synergetic separation of CO_2/C_2H_2 in an ultramicroporous metal-organic framework, *Sep. Purif. Technol.*, 2023, **304**, 122318.

137 L. Li, J. Wang, Z. Zhang, Q. Yang, Y. Yang, B. Su, Z. Bao and Q. Ren, Inverse Adsorption Separation of CO_2/C_2H_2 Mixture in Cyclodextrin-Based Metal-Organic Frameworks, *ACS Appl. Mater. Interfaces*, 2019, **11**, 2543–2550.

138 X.-Y. Li, Y. Song, C.-X. Zhang, C.-X. Zhao and C. He, Inverse CO_2/C_2H_2 separation in a pillared-layer framework featuring a chlorine-modified channel by quadrupole-moment sieving, *Sep. Purif. Technol.*, 2021, **279**, 119608.

139 Q. Liu, S. G. Cho, J. Hilliard, T.-Y. Wang, S.-C. Chien, L.-C. Lin, A. C. Co and C. R. Wade, Inverse CO_2/C_2H_2 Separation with MFU-4 and Selectivity Reversal via Postsynthetic Ligand Exchange, *Angew. Chem., Int. Ed.*, 2023, **62**, e202218854.

140 B. Ma, D. Li, Q. Zhu, Y. Li, W. Ueda and Z. Zhang, A Zeolitic Octahedral Metal Oxide with Ultra-Microporosity for Inverse CO_2/C_2H_2 Separation at High Temperature and Humidity, *Angew. Chem., Int. Ed.*, 2022, **61**, e202209121.

141 D. Ma, Z. Li, J. Zhu, Y. Zhou, L. Chen, X. Mai, M. Liufu, Y. Wu and Y. Li, Inverse and highly selective separation of CO_2/C_2H_2 on a thulium-organic framework, *J. Mater. Chem. A*, 2020, **8**, 11933–11937.

142 O. T. Qazvini, R. Babarao and S. G. Telfer, Selective capture of carbon dioxide from hydrocarbons using a metal-organic framework, *Nat. Commun.*, 2021, **12**, 197.

143 Y. Shi, Y. Xie, H. Cui, Y. Ye, H. Wu, W. Zhou, H. Arman, R.-B. Lin and B. Chen, Highly Selective Adsorption of Carbon Dioxide over Acetylene in an Ultramicroporous Metal-Organic Framework, *Adv. Mater.*, 2021, **33**, 2105880.

144 Y. Xie, H. Cui, H. Wu, R.-B. Lin, W. Zhou and B. Chen, Electrostatically Driven Selective Adsorption of Carbon Dioxide over Acetylene in an Ultramicroporous Material, *Angew. Chem., Int. Ed.*, 2021, **60**, 9604–9609.

145 J. Yang, M. Tong, G. Han, M. Chang, T. Yan, Y. Ying, Q. Yang and D. Liu, Solubility-Boosted Molecular Sieving-Based Separation for Purification of Acetylene in Core–Shell IL@MOF Composites, *Adv. Funct. Mater.*, 2023, **33**, 2213743.

146 J. Yu, J. Zhang, P. Zhang, Y. Wang, S.-N. Li and Q.-G. Zhai, Controllable inverse C_2H_2/CO_2 separation in ultra-stable Zn-organic frameworks for efficient removal of trace CO_2 from acetylene, *J. Mater. Chem. A*, 2022, **10**, 23630–23638.

147 Z. Zhang, S. B. Peh, R. Krishna, C. Kang, K. Chai, Y. Wang, D. Shi and D. Zhao, Optimal Pore Chemistry in an Ultramicroporous Metal-Organic Framework for Benchmark Inverse CO_2/C_2H_2 Separation, *Angew. Chem., Int. Ed.*, 2021, **60**, 17198–17204.

148 Z. Zhang, Z. Deng, H. A. Evans, D. Mullangi, C. Kang, S. B. Peh, Y. Wang, C. M. Brown, J. Wang, P. Canepa, A. K. Cheetham and D. Zhao, Exclusive Recognition of CO_2 from Hydrocarbons by Aluminum Formate with Hydrogen-Confined Pore Cavities, *J. Am. Chem. Soc.*, 2023, **145**, 11643–11649.

149 Y. Wang, N.-Y. Huang, X.-W. Zhang, H. He, R.-K. Huang, Z.-M. Ye, Y. Li, D.-D. Zhou, P.-Q. Liao, X.-M. Chen and J.-P. Zhang, Selective Aerobic Oxidation of a Metal-Organic Framework Boosts Thermodynamic and Kinetic Propylene/Propane Selectivity, *Angew. Chem., Int. Ed.*, 2019, **58**, 7692–7696.

150 A. Cadiau, K. Adil, P. M. Bhatt, Y. Belmabkhout and M. Eddaoudi, A metal-organic framework-based splitter for separating propylene from propane, *Science*, 2016, **353**, 137–140.

151 Y. Xie, Y. Shi, E. M. Cedeño Morales, A. El Karch, B. Wang, H. Arman, K. Tan and B. Chen, Optimal Binding Affinity for Sieving Separation of Propylene from Propane in an Oxyfluoride Anion-Based Metal-Organic Framework, *J. Am. Chem. Soc.*, 2023, **145**, 2386–2394.

152 H. Wang, X. Dong, V. Colombo, Q. Wang, Y. Liu, W. Liu, X.-L. Wang, X.-Y. Huang, D. M. Proserpio, A. Sironi, Y. Han and J. Li, Tailor-Made Microporous Metal-Organic Frameworks for the Full Separation of Propane from Propylene Through Selective Size Exclusion, *Adv. Mater.*, 2018, **30**, 1805088.

153 L. Yu, X. Han, H. Wang, S. Ullah, Q. Xia, W. Li, J. Li, I. da Silva, P. Manuel, S. Rudić, Y. Cheng, S. Yang, T. Thonhauser and J. Li, Pore Distortion in a Metal-Organic Framework for Regulated Separation of Propane and Propylene, *J. Am. Chem. Soc.*, 2021, **143**, 19300–19305.

154 B. Liang, X. Zhang, Y. Xie, R.-B. Lin, R. Krishna, H. Cui, Z. Li, Y. Shi, H. Wu, W. Zhou and B. Chen, An Ultramicroporous Metal-Organic Framework for High Sieving Separation of Propylene from Propane, *J. Am. Chem. Soc.*, 2020, **142**, 17795–17801.

155 H. Zeng, M. Xie, T. Wang, R.-J. Wei, X.-J. Xie, Y. Zhao, W. Lu and D. Li, Orthogonal-array dynamic molecular sieving of propylene/propane mixtures, *Nature*, 2021, **595**, 542–548.

156 Q. Dong, Y. Huang, J. Wan, Z. Lu, Z. Wang, C. Gu, J. Duan and J. Bai, Confining Water Nanotubes in a $Cu_{10}O_{13}$-Based Metal-Organic Framework for Propylene/Propane Separation with Record-High Selectivity, *J. Am. Chem. Soc.*, 2023, **145**, 8043–8051.

157 D. Liu, J. Pei, X. Zhang, X.-W. Gu, H.-M. Wen, B. Chen, G. Qian and B. Li, Scalable Green Synthesis of Robust Ultra-Microporous Hofmann Clathrate Material with Record C_3H_6 Storage Density for Efficient C_3H_6/C_3H_8 Separation, *Angew. Chem., Int. Ed.*, 2023, **62**, e202218590.

158 M.-H. Yu, B. Space, D. Franz, W. Zhou, C. He, L. Li, R. Krishna, Z. Chang, W. Li, T.-L. Hu and X.-H. Bu, Enhanced Gas Uptake in a Microporous Metal-Organic Framework via a Sorbate Induced-Fit Mechanism, *J. Am. Chem. Soc.*, 2019, **141**, 17703–17712.

159 X. Wang, R. Krishna, L. Li, B. Wang, T. He, Y.-Z. Zhang, J.-R. Li and J. Li, Guest-dependent pressure induced gate-opening effect enables effective separation of propene and

propane in a flexible MOF, *Chem. Eng. J.*, 2018, **346**, 489–496.

160 S. Tu, L. Yu, Y. Wu, Y. Chen, H. Wu, L. Wang, B. Liu, X. Zhou, J. Xiao and Q. Xia, A new yttrium-based metal-organic framework for molecular sieving of propane from propylene with high propylene capacity, *AlChE J.*, 2022, **68**, e17551.

161 J. Peng, H. Wang, D. H. Olson, Z. Li and J. Li, Efficient kinetic separation of propene and propane using two microporous metal organic frameworks, *Chem. Commun.*, 2017, **53**, 9332–9335.

162 L. Li, R.-B. Lin, X. Wang, W. Zhou, L. Jia, J. Li and B. Chen, Kinetic separation of propylene over propane in a microporous metal-organic framework, *Chem. Eng. J.*, 2018, **354**, 977–982.

163 K. Li, D. H. Olson, J. Seidel, T. J. Emge, H. Gong, H. Zeng and J. Li, Zeolitic Imidazolate Frameworks for Kinetic Separation of Propane and Propene, *J. Am. Chem. Soc.*, 2009, **131**, 10368–10369.

164 C. Y. Lee, Y.-S. Bae, N. C. Jeong, O. K. Farha, A. A. Sarjeant, C. L. Stern, P. Nickias, R. Q. Snurr, J. T. Hupp and S. T. Nguyen, Kinetic Separation of Propene and Propane in Metal-Organic Frameworks: Controlling Diffusion Rates in Plate-Shaped Crystals via Tuning of Pore Apertures and Crystallite Aspect Ratios, *J. Am. Chem. Soc.*, 2011, **133**, 5228–5231.

165 N. Lamia, M. Jorge, M. A. Granato, F. A. Almeida Paz, H. Chevreau and A. E. Rodrigues, Adsorption of propane, propylene and isobutane on a metal-organic framework: Molecular simulation and experiment, *Chem. Eng. Sci.*, 2009, **64**, 3246–3259.

166 A. Knebel, B. Geppert, K. Volgmann, D. I. Kolokolov, A. G. Stepanov, J. Twiefel, P. Heitjans, D. Volkmer and J. Caro, Defibrillation of soft porous metal-organic frameworks with electric fields, *Science*, 2017, **358**, 347–351.

167 Q. Ding, Z. Zhang, C. Yu, P. Zhang, J. Wang, L. Kong, X. Cui, C.-H. He, S. Deng and H. Xing, Separation of propylene and propane with a microporous metal-organic framework via equilibrium-kinetic synergetic effect, *AlChE J.*, 2021, **67**, e17094.

168 Y. Chen, Z. Qiao, D. Lv, C. Duan, X. Sun, H. Wu, R. Shi, Q. Xia and Z. Li, Efficient adsorptive separation of C_3H_6 over C_3H_8 on flexible and thermoresponsive CPL-1, *Chem. Eng. J.*, 2017, **328**, 360–367.

169 P. Zhang, L. Yang, X. Liu, J. Wang, X. Suo, L. Chen, X. Cui and H. Xing, Ultramicroporous material based parallel and extended paraffin nano-trap for benchmark olefin purification, *Nat. Commun.*, 2022, **13**, 4928.

170 Y. Wang, T. Li, L. Li, R. B. Lin, X. Jia, Z. Chang, H. M. Wen, X. M. Chen and J. Li, Construction of Fluorinated Propane-Trap in Metal-Organic Frameworks for Record Polymer-Grade Propylene Production under High Humidity Conditions, *Adv. Mater.*, 2023, **35**, 2207955.

171 X. Li, J. Liu, K. Zhou, S. Ullah, H. Wang, J. Zou, T. Thonhauser and J. Li, Tuning Metal-Organic Framework (MOF) Topology by Regulating Ligand and Secondary Building Unit (SBU) Geometry: Structures Built on 8-Connected M_6 (M = Zr, Y) Clusters and a Flexible Tetracarboxylate for Propane-Selective Propane/Propylene Separation, *J. Am. Chem. Soc.*, 2022, **144**, 21702–21709.

172 S.-Q. Yang, F.-Z. Sun, R. Krishna, Q. Zhang, L. Zhou, Y.-H. Zhang and T.-L. Hu, Propane-Trapping Ultramicroporous Metal-Organic Framework in the Low-Pressure Area toward the Purification of Propylene, *ACS Appl. Mater. Interfaces*, 2021, **13**, 35990–35996.

173 A. N. Hong, H. Yang, T. Li, Y. Wang, Y. Wang, X. Jia, A. Zhou, E. Kusumoputro, J. Li, X. Bu and P. Feng, Pore-Space Partition and Optimization for Propane-Selective High-Performance Propane/Propylene Separation, *ACS Appl. Mater. Interfaces*, 2021, **13**, 52160–52166.

174 C. He, Y. Wang, Y. Chen, X. Wang, J. Yang, L. Li and J. Li, Modification of the pore environment in UiO-type metal-organic framework toward boosting the separation of propane/propylene, *Chem. Eng. J.*, 2021, **403**, 126428.

175 M. Chang, J. Ren, Y. Wei, J.-X. Wang, Q. Yang, D. Liu and J.-F. Chen, A robust metal-organic framework with guest molecules induced splint-like pore confinement to construct propane-trap for propylene purification, *Sep. Purif. Technol.*, 2021, **279**, 119656.

176 L. Yang, X. Cui, Q. Ding, Q. Wang, A. Jin, L. Ge and H. Xing, Polycatenated Molecular Cage-Based Propane Trap for Propylene Purification with Recorded Selectivity, *ACS Appl. Mater. Interfaces*, 2020, **12**, 2525–2530.

177 P. Iacomi, F. Formalik, J. Marreiros, J. Shang, J. Rogacka, A. Mohmeyer, P. Behrens, R. Ameloot, B. Kuchta and P. L. Llewellyn, Role of Structural Defects in the Adsorption and Separation of C_3 Hydrocarbons in Zr-Fumarate-MOF (MOF-801), *Chem. Mater.*, 2019, **31**, 8413–8423.

178 E. Andres-Garcia, L. Oar-Arteta, J. Gascon and F. Kapteijn, ZIF-67 as silver-bullet in adsorptive propane/propylene separation, *Chem. Eng. J.*, 2019, **360**, 10–14.

179 E. Andres-Garcia, J. López-Cabrelles, L. Oar-Arteta, B. Roldan-Martinez, M. Cano-Padilla, J. Gascon, G. Mínguez Espallargas and F. Kapteijn, Cation influence in adsorptive propane/propylene separation in ZIF-8 (SOD) topology, *Chem. Eng. J.*, 2019, **371**, 848–856.

180 U. Böhme, B. Barth, C. Paula, A. Kuhnt, W. Schwieger, A. Mundstock, J. Caro and M. Hartmann, Ethene/Ethane and Propene/Propane Separation via the Olefin and Paraffin Selective Metal-Organic Framework Adsorbents CPO-27 and ZIF-8, *Langmuir*, 2013, **29**, 8592–8600.

181 L. Li, R.-B. Lin, R. Krishna, X. Wang, B. Li, H. Wu, J. Li, W. Zhou and B. Chen, Flexible-Robust Metal-Organic Framework for Efficient Removal of Propyne from Propylene, *J. Am. Chem. Soc.*, 2017, **139**, 7733–7736.

182 L. Li, H.-M. Wen, C. He, R.-B. Lin, R. Krishna, H. Wu, W. Zhou, J. Li, B. Li and B. Chen, A Metal-Organic Framework with Suitable Pore Size and Specific Functional Sites for the Removal of Trace Propyne from Propylene, *Angew. Chem., Int. Ed.*, 2018, **57**, 15183–15188.

183 H.-M. Wen, L. Li, R.-B. Lin, B. Li, B. Hu, W. Zhou, J. Hu and B. Chen, Fine-tuning of nano-traps in a stable metal-organic framework for highly efficient removal of propyne from propylene, *J. Mater. Chem. A*, 2018, **6**, 6931–6937.

184 L. Yang, X. Cui, Q. Yang, S. Qian, H. Wu, Z. Bao, Z. Zhang, Q. Ren, W. Zhou, B. Chen and H. Xing, A Single-Molecule Propyne Trap: Highly Efficient Removal of Propyne from Propylene with Anion-Pillared Ultramicroporous Materials, *Adv. Mater.*, 2018, **30**, 1705374.

185 L. Yang, X. Cui, Z. Zhang, Q. Yang, Z. Bao, Q. Ren and H. Xing, An Asymmetric Anion-Pillared Metal-Organic Framework as a Multisite Adsorbent Enables Simultaneous Removal of Propyne and Propadiene from Propylene, *Angew. Chem., Int. Ed.*, 2018, **57**, 13145–13149.

186 Y.-L. Peng, C. He, T. Pham, T. Wang, P. Li, R. Krishna, K. A. Forrest, A. Hogan, S. Suepaul, B. Space, M. Fang, Y. Chen, M. J. Zaworotko, J. Li, L. Li, Z. Zhang, P. Cheng and B. Chen, Robust Microporous Metal-Organic Frameworks for Highly Efficient and Simultaneous Removal of Propyne and Propadiene from Propylene, *Angew. Chem., Int. Ed.*, 2019, **58**, 10209–10214.

187 Y. Jiang, J. Hu, L. Wang, W. Sun, N. Xu, R. Krishna, S. Duttwyler, X. Cui, H. Xing and Y. Zhang, Comprehensive Pore Tuning in an Ultrastable Fluorinated Anion Cross-Linked Cage-Like MOF for Simultaneous Benchmark Propyne Recovery and Propylene Purification, *Angew. Chem., Int. Ed.*, 2022, **61**, e202200947.

188 Q. Wang, J. Hu, L. Yang, Z. Zhang, T. Ke, X. Cui and H. Xing, One-step removal of alkynes and propadiene from cracking gases using a multi-functional molecular separator, *Nat. Commun.*, 2022, **13**, 2955.

189 M.-Y. Gao, A. A. Bezrukov, B.-Q. Song, M. He, S. J. Nikkhah, S.-Q. Wang, N. Kumar, S. Darwish, D. Sensharma, C. Deng, J. Li, L. Liu, R. Krishna, M. Vandichel, S. Yang and M. J. Zaworotko, Highly Productive C_3H_4/C_3H_6 Trace Separation by a Packing Polymorph of a Layered Hybrid Ultramicroporous Material, *J. Am. Chem. Soc.*, 2023, **145**, 11837–11845.

190 H. I. Mahdi and O. Muraza, An exciting opportunity for zeolite adsorbent design in separation of C_4 olefins through adsorptive separation, *Sep. Purif. Technol.*, 2019, **221**, 126–151.

191 E. V. Makshina, M. Dusselier, W. Janssens, J. Degrève, P. A. Jacobs, B. F. Sels and E. V. Makshina, Review of old chemistry and new catalytic advances in the on-purpose synthesis of butadiene, *Chem. Soc. Rev.*, 2014, **43**, 7917–7953.

192 Z. Zhang, Q. Yang, X. Cui, L. Yang, Z. Bao, Q. Ren and H. Xing, Sorting of C_4 Olefins with Interpenetrated Hybrid Ultramicroporous Materials by Combining Molecular Recognition and Size-Sieving, *Angew. Chem., Int. Ed.*, 2017, **56**, 16282–16287.

193 P.-Q. Liao, N.-Y. Huang, W.-X. Zhang, J.-P. Zhang and X.-M. Chen, Controlling guest conformation for efficient purification of butadiene, *Science*, 2017, **356**, 1193–1196.

194 J. Chen, J. Wang, L. Guo, L. Li, Q. Yang, Z. Zhang, Y. Yang, Z. Bao and Q. Ren, Adsorptive Separation of Geometric Isomers of 2-Butene on Gallate-Based Metal-Organic Frameworks, *ACS Appl. Mater. Interfaces*, 2020, **12**, 9609–9616.

195 L. Wang, W. Xue, H. Zhu, X. Guo, H. Huang and C. Zhong, Stepwise Engineering the Pore Aperture of a Cage-like MOF for the Efficient Separation of Isomeric C_4 Paraffins under Humid Conditions, *Angew. Chem., Int. Ed.*, 2023, **62**, e202218596.

196 A. H. Assen, Y. Belmabkhout, K. Adil, P. M. Bhatt, D.-X. Xue, H. Jiang and M. Eddaoudi, Ultra-Tuning of the Rare-Earth fcu-MOF Aperture Size for Selective Molecular Exclusion of Branched Paraffins, *Angew. Chem., Int. Ed.*, 2015, **54**, 14353–14358.

197 H. Wang, X. Dong, J. Lin, S. J. Teat, S. Jensen, J. Cure, E. V. Alexandrov, Q. Xia, K. Tan, Q. Wang, D. H. Olson, D. M. Proserpio, Y. J. Chabal, T. Thonhauser, J. Sun, Y. Han and J. Li, Topologically guided tuning of Zr-MOF pore structures for highly selective separation of C_6 alkane isomers, *Nat. Commun.*, 2018, **9**, 1745.

198 Y. Lin, L. Yu, S. Ullah, X. Li, H. Wang, Q. Xia, T. Thonhauser and J. Li, Temperature-Programmed Separation of Hexane Isomers by a Porous Calcium Chloranilate Metal-Organic Framework, *Angew. Chem., Int. Ed.*, 2022, **134**, e202214060.

199 F. Zheng, L. Guo, R. Chen, F. Zhou, Z. Zhang, Q. Yang, Y. Yang, Q. Ren and Z. Bao, Temperature-swing molecular exclusion separation of hexane isomers in robust MOFs with double-accessible open metal sites, *Chem. Eng. J.*, 2023, **460**, 141743.

200 K. Jie, Y. Zhou, E. Li, R. Zhao, M. Liu and F. Huang, Linear Positional Isomer Sorting in Nonporous Adaptive Crystals of a Pillar[5]arene, *J. Am. Chem. Soc.*, 2018, **140**, 3190–3193.

201 T. Wang, J. Gu, Q. Cui and H. Wang, Study on Adsorption and Desorption Performances of Trace C_4–C_6 Alkane Mixture on MIL-101(Cr) and WS-480, *Energy Fuels*, 2019, **33**, 7587–7594.

202 Y. Yu, L. Yang, B. Tan, J. Hu, Q. Wang, X. Cui and H. Xing, Remarkable separation of C_5 olefins in anion-pillared hybrid porous materials, *Nano Res.*, 2021, **14**, 541–545.

203 R. Lyndon, Y. Wang, I. M. Walton, Y. Ma, Y. Liu, Z. Yu, G. Zhu, S. Berens, Y. S. Chen, S. G. Wang, S. Vasenkov, D. S. Sholl, K. S. Walton, S. H. Pang and R. P. Lively, Unblocking a rigid purine MOF for kinetic separation of xylenes, *Chem. Commun.*, 2022, **58**, 12305–12308.

204 M. Shivanna, K.-I. Otake, J.-J. Zheng, S. Sakaki, S. Kitagawa and M. Shivanna, Control of local flexibility towards p-xylene sieving in Hofmann-type porous coordination polymers, *Chem. Commun.*, 2020, **56**, 9632–9635.

205 H. Wang, X. Dong, E. Velasco, D. H. Olson, Y. Han, J. Li and H. Wang, One-of-a-kind: a microporous metal–organic framework capable of adsorptive separation of linear, mono- and di-branched alkane isomers via temperature- and adsorbate-dependent molecular sieving, *Energy Environ. Sci.*, 2018, **11**, 1226–1231.

206 L. Li, L. Guo, D. H. Olson, S. Xian, Z. Zhang, Q. Yang, K. Wu, Y. Yang, Z. Bao, Q. Ren and J. Li, Discrimination of xylene isomers in a stacked coordination polymer, *Science*, 2022, **377**, 335–339.

207 X. Cui, Z. Niu, C. Shan, L. Yang, J. Hu, Q. Wang, P. C. Lan, Y. Li, L. Wojtas, S. Ma and H. Xing, Efficient separation of xylene isomers by a guest-responsive metal–organic framework with rotational anionic sites, *Nat. Commun.*, 2020, **11**, 5456.

208 J. Zhou, T. Ke, Y. Song, H. Cai, Z. A. Wang, L. Chen, Q. Xu, Z. Zhang, Z. Bao, Q. Ren and Q. Yang, Highly Efficient Separation of C_8 Aromatic Isomers by Rationally Designed Nonaromatic Metal-Organic Frameworks, *J. Am. Chem. Soc.*, 2022, **144**, 21417–21424.

209 D.-D. Zhou, P. Chen, C. Wang, S.-S. Wang, Y. Du, H. Yan, Z.-M. Ye, C.-T. He, R.-K. Huang, Z.-W. Mo, N.-Y. Huang and J.-P. Zhang, Intermediate-sized molecular sieving of styrene from larger and smaller analogues, *Nat. Mater.*, 2019, **18**, 994–998.

210 T. He, X.-J. Kong, Z.-X. Bian, Y.-Z. Zhang, G.-R. Si, L.-H. Xie, X.-Q. Wu, H. Huang, Z. Chang, X.-H. Bu, M. J. Zaworotko, Z.-R. Nie and J.-R. Li, Trace removal of benzene vapour using double-walled metal-dipyrazolate frameworks, *Nat. Mater.*, 2022, **21**, 689–695.

211 W.-B. Li, Y. Wu, X.-F. Zhong, X.-H. Chen, G. Liang, J.-W. Ye, Z.-W. Mo and X.-M. Chen, Fluorescence Enhancement of a Metal-Organic Framework for Ultra-Efficient Detection of Trace Benzene Vapor, *Angew. Chem., Int. Ed.*, 2023, **62**, e202303500.

212 R. Wei, X. Liu and Z. Lai, MOF or COF membranes for olefin/paraffin separation: Current status and future research directions, *Adv. Membr.*, 2022, **2**, 100035.

213 C. Zhang, Y. Dai, J. R. Johnson, O. Karvan and W. J. Koros, High performance ZIF-8/6FDA-DAM mixed matrix membrane for propylene/propane separations, *J. Membr. Sci.*, 2012, **389**, 34–42.

214 Y. Liu, Z. Chen, G. Liu, Y. Belmabkhout, K. Adil, M. Eddaoudi and W. Koros, Conformation-Controlled Molecular Sieving Effects for Membrane-Based Propylene/Propane Separation, *Adv. Mater.*, 2019, **31**, 1807513.

215 Y. Peng, Y. Li, Y. Ban, H. Jin, W. Jiao, X. Liu and W. Yang, Metal-organic framework nanosheets as building blocks for molecular sieving membranes, *Science*, 2014, **346**, 1356–1359.

216 K. Yang, Y. Ban, A. Guo, M. Zhao, Y. Zhou, N. Cao and W. Yang, *In situ* interfacial assembly of ultra-H_2-permeable metal-organic framework membranes for H_2/CO_2 separation, *J. Membr. Sci.*, 2020, **611**, 118419.

217 K. Yang, Y. Ban and W. Yang, Layered MOF membranes modified with ionic liquid/$AgBF_4$ composite for olefin/paraffin separation, *J. Membr. Sci.*, 2021, **639**, 119771.

218 H. Song, Y. Peng, C. Wang, L. Shu, C. Zhu, Y. Wang, H. He and W. Yang, Structure Regulation of MOF Nanosheet Membrane for Accurate H_2/CO_2 Separation, *Angew. Chem., Int. Ed.*, 2023, **62**, e202218472.

219 J. E. Bachman, Z. P. Smith, T. Li, T. Xu and J. R. Long, Enhanced ethylene separation and plasticization resistance in polymer membranes incorporating metal-organic framework nanocrystals, *Nat. Mater.*, 2016, **15**, 845–849.

220 Y. Sun, T. Ji, Y. Gao, J. Yan, Y. He, G. Xu, F. Yan, Q. Bian and Y. Liu, Freezing Contra-diffusion: A New Protocol for Synthesizing Co-Gallate MOF Membranes toward Superior Ethylene/Ethane Separation Performance, *ACS Mater. Lett.*, 2023, **5**, 558–564.

221 L. Liu, Y. Song, T. Ji, Y. Sun, D. He, H. Hu and Y. Liu, Beyond Solution-Based Protocols: MOF Membrane Synthesis in Supercritical Environments for an Elegant Sustainability Performance Balance, *ACS Mater. Lett.*, 2020, **2**, 1142–1147.

